THE UNIVERSITY OF CHICAGO

CYTOSKELETAL CONTROL OF TISSUE SHAPE CHANGES

A DISSERTATION SUBMITTED TO
THE FACULTY OF THE DIVISION OF THE BIOLOGICAL SCIENCES
AND THE PRITZKER SCHOOL OF MEDICINE
IN CANDIDACY FOR THE DEGREE OF
DOCTOR OF PHILOSOPHY

COMMITTEE ON CANCER BIOLOGY

BY
TIMOTHY B FESSENDEN

CHICAGO, ILLINOIS
JUNE 2017

For my mother Judith

Organic structure is then no longer an arrangement of self-existent material parts in an environment of similar character, but, along with its environments, the active expression of life; and organic activity is no longer the passage of self-existent energy from part to part, and between organism and environment, but simply another aspect of the expression of a life. We thus do not artificially separate in theory the structure from the activity, and we recognize the artificiality of separating them.

JS Haldane, *Materiality* 1932

TABLE OF CONTENTS

LIST OF FIGURES

ACKNOWLEDGMENTS

All of the accomplishments documented here, and many that were left out, were only possible because of the many wonderful people who surrounded me at the University of Chicago. My mentor, Margaret Gardel, has been an incredible teacher and friend to me. I have no doubt that the knowledge I gained in our many conversations will benefit me for the rest of my career. The members of Margaret's lab have been a steady source of graciousness and support. Above all I must recognize Yvonne Beckham for her constant generosity and unconditional friendship. Patrick Oakes and Guillermina Ramirez-San Juan have also been wonderful friends and invaluable collaborators.

Over the years, I have drawn great strength from the support of my family. Even across the country I was buoyed by them and the affection we share. My three sisters Rachel, Rebekah, and Leah, are my constant friends and guides, and have made me the person I am today. Finally I must recognize the steady support of my father Chris, who loved hearing about experiments or the strange and wonderful world of academia. Without his support I would be a worse student, and a worse scientist.

ABSTRACT

The collective actions of epithelial cells drive tissue shape changes, whether these are tightly organized during development or disorganized as during cancer invasion. In both cases, the motility of the bulk tissue is determined by the signaling and mechanical properties of its constituent cells. Decades of careful study have coalesced into detailed models that describe how individual cells move through their environment. Motility relies on the dynamics of filamentous actin, which cells use to maintain their shape and adhere to their surroundings during migration. Precisely connecting single cell properties with tissue behaviors to which they contribute would furnish critical advances to the understanding of of cancer invasion and tissue development. This thesis describes the application of model epithelial tissues toward bridging these scales, focusing on the formin family of actin filament nucleators. We employ Madin Darby Canine Kidney (MDCK) cells, as a model for tissue shape changes to study its requirements in a controlled 3D environment. Both MDCK cells and mouse tumor explants require the activity of formin proteins to undertake tissue migration into prepared collagen gels. We analyzed separately cell motility within the 2D plane of the epithelium from invasive motility into the collagen gel. These modes of cell motility are distinguished by the depletion of the formin protein Dia1. We show that invasive motility requires Dia1, which regulates cell adhesions to individual collagen fibrils. Finally, we capitalize on a simple mathematical model describing cell shape for epithelial monolayers. Applying this model to MDCK acini reveals that under quiescent conditions Dia1 enforces an immobile "jammed" state within epithelia. This immobile state is released upon growth factor stimulation or loss of Dia1. Overall this work forges novel connections between cytoskeletal regulators at the single- and multi-cell scales, and prompts new hypotheses to test how cell behaviors contribute to tissue functions in health and disease.

CHAPTER 1

INTRODUCTION

1.1 Breast Cancer Progression and Invasion

1.1.1 Mammary gland organization and tumor formation

Cancer is a complex biological state involving multiple cell types, biochemical signaling events, and genome-wide changes. The progression of tumors and their response to therapy is an outcome of dynamic relationships among the multiple cells types and the extracellular matrix that determine tissue biology [1, 2]. Given this complexity, it may be little surprise that direct relationships linking genetic drivers to patient outcomes been difficult to define for many cancer types. This section will explore the development and progression of tumors using breast cancer as a model.

Cancer has been recognized as a discrete medical condition for millennia, and schemes to classify its forms have been well-established for over a century [3]. However, a rigorous classification system based on empirical evidence was not proposed until 1958, by the experimental pathologist Leslie Foulds [4]. The advance that he formulated was "the demonstration that neoplasia is [sic] discontinuous in space and time; it is a dynamic process advancing through stages that are qualitatively different" (emphasis his) [4]. Foulds argued that tumors progress through irreversible changes and that this progression leads to the advance of the disease into its fatal forms. In his view, the alterations which tumors underwent as they progressed might not all be outwardly apparent to a clinician, but they could still determine its final outcome. His work synthesized histopathological observations under one rubric, and laid the groundwork for the later molecular definitions into which different tumor types could be functionally grouped. Following the advent of modern genetics and molecular biology, this concept was extended and clarified using genetic signatures. First among these was the revolutionary work in 1988 by Vogelstein and colleagues that linked the histopathology (i.e.

increasingly aberrant tissue organization) of colorectal cancers with specific genetic alterations [5]. This work established the preconditions for understanding the cellular behaviors shared by different tumor types.

Establishing a causal chain from genotype to a precise cellular behavior to patient outcome forms a premier goal of cancer research. This scheme may work for genes acting within the same signaling pathway (e.g. resistance to cell death signals) that give rise to one of the "hallmarks" of cancer as defined by Hanahan and Weinberg [6]. However, individual genes are rarely identified that control a histologically identifiable cell behavior, as well as a specific patient outcome, even when gene actions are well-established. This challenge motivates efforts to clarify and extend the explanatory power of gene expression data, as well as creative approaches to model the conserved features of tumor progression such as invasion.

The etiology of most tumors follows an established progression driven by abnormal cell proliferation, resulting in a primary tumor mass [6]. While it remains contained, the mass is defined as benign. The onset of invasion defines the transition from benign to malignant tumors, typified by egress of tumor cells singly or collectively from this primary lesion [7, 8]. In its most aggressive forms, cancer is thus a disease of aberrant cell movement as much as aberrant cell proliferation. Accordingly, a comprehensive understanding of the most deadly manifestations of cancer require that we understand the cell behaviors driving cancer spread. A proper description of this transition first necessitates an understanding of tissue organization prior to tumorigenesis.

Mature epithelial tissues such as the mammary gland comprise a few cell types organized into a typical tissue layout. Epithelial cells form a continuous layer surrounding a hollow lumen. Cell polarization causes the spatial segregation of intracellular components such that secretory (in the case of mammary epithelium) or absorptive (in the case of intestinal epithelium) functions are oriented toward the lumen, on the cells apical surface [9, 10]. The basal surface, oriented away from the lumen toward the stroma, is the site of cell interaction with the extracellular matrix. For epithelial tissues this matrix is the basement membrane,

a highly specialized 2-dimensional mesh of structural proteins that surrounds the epithelial layer [11]. These elements – a central lumen, one or multiple layers of polarized cells, and a surrounding basement membrane – are defining features of most epithelial tissues.

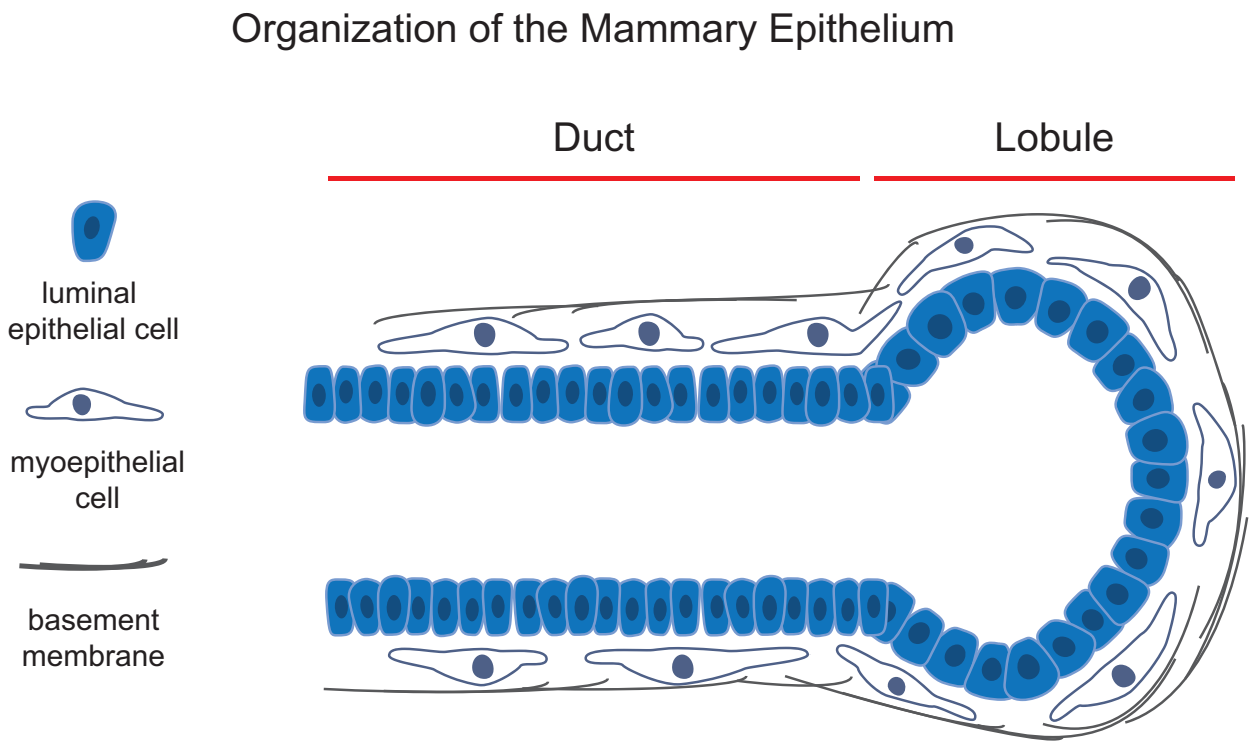

Figure 1.1. Luminal and myoepithelial cells derive from a common progenitor but differentiate to fulfill different roles in the mature tissue. Milk secretion is carried out in lobules by luminal epithelial cells, and is then transported via ducts. Tumors can arise in both ducts and lobules.

Different cell types within the epithelium further define mammary gland biology. Secretory functions are carried out by the luminal epithelium. These cells are sensitive to estrogen and progesterone and thereby respond to systemic hormone levels that orchestrate mammary function during puberty, pregnancy, and lactation [12, 13]. Joining luminal cells in the mammary epithelium are myoepithelial cells, residing between the luminal cells and the basement membrane (Figure 1.1). Myoepithelial cells share a common progenitor with luminal cells, and serve a contractile role to aid in lactation [14, 15]. In addition they secrete and maintain components of the basement membrane and are critical for maintenance of mammary gland homeostasis, albeit through unknown mechanisms [14].

1.1.2 Transition from Benign to Invasive Breast Cancer

The formation and progression of carcinomas, tumors derived from epithelial tissues, are defined by the organization of their native tissue. Mammary carcinomas offer an illustrative example of this principle as they are well-studied in both human observational studies as well as experimental models in animals. Primary ductal carcinomas begin as foci of hyperplastic cells within the plane of the epithelium. These foci may exhibit loss of cell polarity [16], increased proliferation along with increased apoptosis, and high levels of genotoxic stress markers [17]. The cell lineages that give rise to mammary duct constituents, basal and luminal, portend different courses of progression for breast lesions as indicated by gene expression profiling [18, 19]. Luminal-type breast tumors are more likely to be dependent on estrogen for their growth, in accordance with their origins. Meanwhile tumors termed basal-type resemble progenitor stem cells and the basal myoepithelium, lack hormone receptors for estrogen and progesterone and thus can proliferate in the absence of these hormones. These tend to be less differentiated and more likely to progress to metastasis.

The most common non-invasive form of breast cancer, Ductal Carcinoma *in situ* (DCIS), bears histological features determined by the normal mammary ductal structure in which it forms. Genetic signatures of DCIS include insertion or deletion of large genomic regions, overexpression of the growth factor receptor HER2/neu, and, less frequently, loss of the tumor suppressor p53 [20]. Together, these factors collaborate to permit ductal epithelial cells to persist in aberrant settings: in the luminal space or crowding their phenotypically normal neighbors. Invasive breast cancer typically presents histologically as clusters of tumor cells interspersed in the stroma surrounding the primary tumor site. These cells move singly or collectively through the stroma and eventually enter the vasculature or lymphatic system and spread to distant sites [21].

Of special interest are factors that contribute to the onset of invasion and metastatic spread, as these tumor behaviors prove deadly. Despite the wealth of clinical, histologic, and genetic data on breast tumor progression, identifying the mechanisms by which DCIS lesions

become invasive has eluded researchers [20, 22]. Several confounding factors contribute to this difficulty, perhaps reflecting many possible routes by which a tumor mass initiates spreading. First it is crucial to note that despite the gross genetic and morphological changes present in DCIS lesions, they often do not progress to malignancy. If untreated, around half of all DCIS lesions do not progress to invasive disease within 10 years [20]. A similar picture emerges when considering recurrence: 10 years following removal of a DCIS lesion, 70-85% of women remain disease-free [23]. Given this variation in the destinies of indolent lesions, researchers have sought the means to stratify DCIS patients as low or high risk for progression.

Tumor grading schemes separate DCIS lesions with some predictive power. Grading guidelines for DCIS characterize the profound changes to tissue architecture that anticipate features of invasive disease. Grading rests on three parameters: tissue organization (tubular or disorganized), frequency of proliferative cells (using markers for mitosis), and nuclear pleiomorphism [24].

Accompanying these progressive alterations to the carcinoma itself are a host of stromal changes that herald the breakdown of tissue homeostasis [2, 25]. Myoepithelial cells are generally absent in high-grade DCIS, along with a normal basement membrane, yet precisely how and why these disappear is unclear [26, 27, 12, 15]. It is known that they are lost during tumor progression, yet exactly how is not known [14]. Likewise, the direct impact of their loss is poorly understood. Lesions are often infiltrated by immune cells, and surrounding fibroblasts increase in number and change in morphology [28]. Finally, extracellular matrix (ECM) proteins are substantially altered from normal breast tissue, most notably by an increase in Collagen 1 fibril concentration and their arrangement into bundles [29, 25]. Collectively, these changes bear resemblance to sustained tissue injury as seen during fibrosis [1]. While this concept provides a compelling general framework, it leaves unclear the causal relationships between tumor cells, myoepithelial cells, immune cells, fibroblasts, and the ECM.

Attempts to classify gene expression changes that reliably track the transition to the

invasive state from DCIS have yielded widely varying results. This is not isolated to breast cancer, as attempts to predict metastasis have varied across tumor types [30]. The course for patients diagnosed with invasive disease correlates well with the distinct molecular subtypes luminal or basal that likely reflect the developmental lineage from which they arise [31, 32]. Applying the same classification scheme to stratify DCIS vs. invasive tumors has yielded mixed results [33, 22]. The basal and luminal subtypes that define invasive disease and predict their aggressiveness may not exist as stable categories for DCIS tumors. Indeed there is well-documented heterogeneity that characterizes cell populations in DCIS lesions [34, 35, 26]. In one study, high grade DCIS lesions were found to bear greater genetic resemblance to invasive tumors than to low-grade DCIS or benign hyperplastic disease [20]. Thus high-grade DCIS tumors appear as heterogeneous invasion-competent tumors which have yet to initiate invasion. Although the diversity of cell lineages and behaviors in preinvasive tumors explains their gene expression profiles, these do not capture the precise the mechanisms that drive invasion. This challenge might be more reasonably approached by focusing on the behaviors that cells acquire in order to invade, rather than molecular markers that would identify invasive cells.

1.1.3 Cancer invasion and tissue development

A phenotype-based approach to cancer invasion motivates experimental systems to analyze invasive behaviors using organotypic cell culture. With the benefit of directly observing cell invasion, inferences can be drawn about its origins and means of regulation [36]. The Ewald group has led efforts to dissect the mechanisms of tumor invasion by challenging tumor explants removed from humans or mice to migrate into a prepared collagen matrix [37]. Their findings have provided support for the multicellular nature of cancer invasion [38], and highlight the dominant role of the ECM [39], as suggested by others [40, 29].

In particular, the Ewald group has found that invasive cohorts of mouse or human tumors were organized into leading and following cells specified by their developmental lineage [41].

These findings identified basal-like carcinoma cells, which resemble myoepithelial cells and are marked by cytokeratin 14, that consistently led invasive cohorts from a mixed population of basal-like and luminal-like tumor cells. These findings were corroborated by gene expression data predicting poor outcomes for women whose tumors expressed high levels of this cytokeratin. Ewald and colleagues proposed that breast tumor invasion requires that epithelial tissues "reinvent" motility regimes present during mammary gland development [42]. This reinvention was directly observable by live imaging of luminal-like cells converting to basal-like cells upon contact with collagen fibrils that reside outside the basement membrane [41, 43]. These observations agree with the dire consequences of deregulation or loss of the basement membrane seen in high-grade DCIS lesions, which would expose tumor cells to collagen fibrils [20, 12]. Finally, fundamental features of this model were confirmed by later work that established the necessity of collective migration via cell-cell junctions for efficient tumor spread [38]. More recently, work by the Sahai and Trepat groups has extended studies of collective invasion *in vitro* to include associated fibroblasts [44]. These can form cell-cell adhesions with tumor cells and subsequently lead their invasion. The set of immune cells surrounding and infiltrating tumors can also direct their local spread. The Condeelis group has analyzed invasion using intravital imaging of mouse tumors and immune cells [45]. Their work showed that immune cells secrete signaling proteins that promote tumor cell migration from the tumor towards nearby vasculature [46].

Overall these findings encourage a holistic perspective of breast tumor progression from the standpoints, first, of an aberrant tissue comprising multiple cell types and ECM components [25, 1], and second as a resurgence of multicellular motility exhibited during development [42]. Invasion via multicellular clusters is a common means of tumor spread [47, 48]. Mounting data suggests a close collaboration between distinct cell subpopulations, as proposed by Ewald et al, and the arrangement of thick collagen bundles, as explored by Keely and colleagues [49]. These thick bundles are stiffer than normal breast stroma, and concentrate the adhesive ligands by which cells migrate in 3D [50, 51]. Presumably, cohorts of cells

encountering these fibrils could extend along them, led by basal-type epithelial cells. Multicellular invasion also offers a plausible mechanism by which heterogeneous cell populations cooperate during tumor spreading [8]. Finally, multicellular clusters are better able to form distant metastases following transit through the bloodstream [52, 53, 54].

The transformation over years of a normal epithelium to an invasive tumor is a context-dependent and highly variable process. The complexities of tumor formation and progression described here prompt an evaluation of the conserved properties that enable tumor cell spreading. Fundamental physical properties governing tumor cells interactions with each other and their surrounding matrix remain incompletely understood, despite recent interest in mechanical descriptions of cancer progression and metastasis [55]. Building a sufficiently detailed understanding of cancer cell motility and invasion *in situ* would therefore be aided by a better grasp of the means by which cells interact with their matrix and how these interactions are integrated across cell collectives. Detailed cell invasion studies using experimental systems may open new perspectives on how tissues either prevent or permit aberrant cell motility.

1.2 The cellular basis of tissue shape changes

1.2.1 Branching morphogenesis generates the final shape of many organs

The primary function of a tissue necessitates that it acquires the appropriate form during organismal development, as captured by the aphorism that form follows function throughout biology. This is as true for the brain as the small intestine. Specificity of form and organization was a feature of tissues recognized as early as 1822 by Bichat, in his work classifying tissue types [56]. The lens exhibits a geometry that quite directly impacts its role in the visual system, but even the expansive, complex, and intricate shapes adopted by the vasculature or the skin must equally contribute to their respective functions [57]. The conserved means by which tissues assume their shapes during development, and general principles they

share, have been the objects of study for generations of biologists.

With some variation, most epithelial tissues adopt shapes that aid in the transport, secretion, or absorption of solutes [58]. These include the lung, gut, and mammary tissues in mammals. In these cases, tissues with very different roles acquire a highly stereotyped final form. The final shape of the lung epithelium optimizes airflow and surface area for gas exchange [59], epithelial tubules of the kidney collecting system mediate water resorption [60], and the ductal tree of the mammary gland transports milk secreted by lobules [61]. These tissues vary widely in complexity and size, but they have in common a geometry of iteratively branched tubules [9, 62, 63]. Proper function for all of these tissues, whether as selective barriers or transport routes, requires this highly stereotyped layout of hollow, interconnected networks [63].

Branching morphogenesis refers to a broadly conserved strategy of tissue expansion and remodeling that generates branched tissues [62, 63]. During their development, most such tissues start as small, contained masses of precursor cells. The constituent cells of these nascent tissues generate the final dendritic structure often through a combination of collective motility and proliferation [9, 64]. The elaboration of the mammary ductal tree [65] or formation of the *Drosophila* tracheal system [66] are classic examples of branching morphogenesis. However, each of these organs develop in their own specific milieu within the embryonic or post-natal animal. Further, the actions taken by each tissue are directed by distinct signaling molecules. Thus a perfect comparison across all tissues whose development requires branching morphogenesis is impossible. Nonetheless, branching morphogenesis is represents a conserved strategy observed throughout biology, owing to its adherence to certain hallmarks [9, 64, 67, 68]. These include the maintenance of cell-cell adhesions, self-organization into migratory and non-migratory cohorts, regularly spaced and iterative generation of new branches, and resolution into hollow tubules.

Branching morphogenesis begins when a few individual cells within an immature tissue become motile and move with their neighbors into the surrounding Extracellular Matrix

(ECM). They lead a cohort of cells through their surroundings, elaborating multiple branches to form a characteristic dendritic structure [69, 64, 62]. Depending on the tissue type, new branches can be formed by bifurcation of the leading edge, or by cell extensions emanating from the sides of an elongating branch, which then grow into a new branch (Figure 1.2) [67]. Finally, cell fusion or rearrangement events form a contiguous lumen during or after the full extension of branches, depending on the tissue type [70].

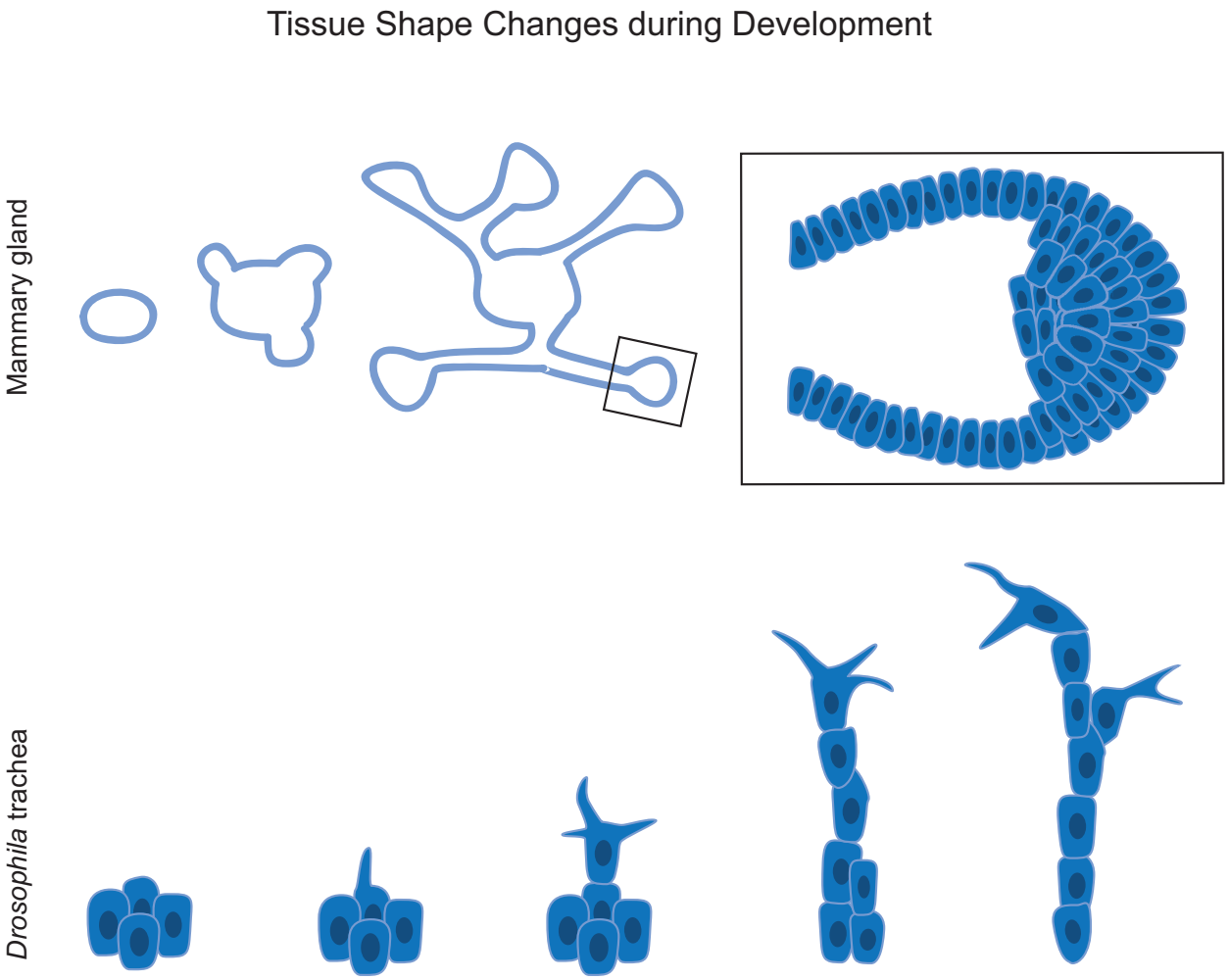

Figure 1.2. Branching morphogenesis describes the development of the mammary ductal tree, above, as well as the *Drosophila* tracheal system, below. Mammary ductal elongation is achieved by a cohort of rapidly rearranging cells that do not exhibit cell extensions into the ECM. Meanwhile, *Drosophila* tracheal development is led by a single cell that leads its neighbors and makes extensive protrusions into its surroundings.

1.2.2 Mechanisms of collective cell motility during branching morphogenesis

Collective cell motility is a highly conserved phenomenon seen across organisms and in both physiologic and pathologic contexts [71, 48, 64]. To translocate through a tissue or across a surface, individual cells must control their shape and regulate adhesions to their surroundings. Single mesenchymal cells such as fibroblasts move by extending processes from the cell body which adhere to ligands in the ECM, and use this adhesion to pull the cell body forward. However, studies of cell movements in living organisms and in various 3D environments *in vitro* have identified a range of strategies used by cells for locomotion [72]. Cells of epithelial or mesenchymal origin readily migrate without the use of specific adhesion sites to the ECM, termed ameoboid migration [73]. This involves controlled contraction of the cell rear to squeeze the cell body forward through a porous matrix, and does not require strong cell-ECM adhesion.

These motility behaviors are also coordinated by groups of cells during tissue morphogenesis [69]. A hallmark of branching morphogenesis is the organization of cells into motile or invasive behaviors at the tissue's leading edge. The motile cell front leads the cells following behind and determines the direction taken by the cohort [72, 64]. In many cases leader cells at the front exhibit a polarized morphology resembling single mesenchymal cells, while maintaining adhesion to their neighbors that follow [74, 75]. These leader cells protrude, adhere, and contract against the Extracellular Matrix (ECM) as do single cells. However, specific behaviors that propel the leading edge differ according to the tissue type and environment [63].

With some variation, there are two strategies to accomplish elongation of cell collectives. During puberty in mammals, elaboration of branches by mammary ducts is carried out through dynamic, nonprotrusive motility localized to the front of the elongating tissue. The leading edge in these tissues is composed of a rapidly rearranging cohort of cells [65, 76, 77]. Elongation of the tissue branch is independent of cell proliferation, and instead relies on

dynamic cell shape changes and rearrangements. In this case, the leading edge is properly described as a localized cell behavior rather than as a stable lineage- or signaling-specified population. In contrast, branching morphogenesis during development of the *Drosophila* tracheal system and vascular sprouting during mammalian angiogenesis begins when individual cells extend protrusions from the initial cohort, commonly known as the tissue rudiment, into the ECM [62]. These protrusions form adhesions to the ECM. Individual leader cells use these protrusions and adhesions to pull themselves forward and drag their neighbors with them.

The differences between the strategies of ductal elongation described above may not run so deep. Organotypic assays examining mammary duct morphogenesis *in vitro* demonstrated that these tissues migrate via protrusive or nonprotrusive collective cell motility according to the 3D matrix. In the soft, meshlike matrices formed from basement membrane proteins, branch elongation was nonprotrusive, while in fibrillar matrices of collagen 1, branch elongation was accomplished by protrusive cells at the leading edge, reminiscent of those described for *Drosophila* tracheal development or vascular sprouting [39]. As branch elongation in collagen proceeded, protrusive fronts resolving into nonprotruding end buds or lobules over tens of hours. Thus these apparently opposed phenotypes may simply be manifestations of a conserved collective behavior dependent on the extracellular environment [40].

Many developing tissues are patterned by soluble factors known as morphogens whose spatial distribution dictates tissue geometry [67]. Individual cells in a tissue sense the local concentration of a morphogen through specific cell surface receptors, in a dose-dependent manner. This patterning strategy has been intimately linked with tissue morphogenesis by a broad array of *in vivo* and *in vitro* experiments [78, 79, 80]. In the well-defined case of *Drosophila* tracheal development, Branchless (ortholog of mammalian Fibroblast Growth Factor), the morphogen that cues branching, bathes equally the ˜80 cells of the nascent tissue. Only a minority of these cells form protrusions and become leader cells during branching morphogenesis. These differential cell fates are determined through cells unequal expression

of the Branchless receptor Breathless (ortholog of Fibroblast Growth Factor Receptor 2) [74]. Specification of leader cells can thus arise deterministically through this or similar mechanisms, but many tissues such as the mammary epithelium undergo branching initiation in a stochastic manner [42, 63]. These cases challenge biologists to devise and interpret experimental systems that can uncover the causative factors, such as mechanical properties, that determine branch initiation.

1.2.3 MDCK cells as an in vitro model to explore the regulation branching morphogenesis

Few cell culture models exist to explore complex rearrangements such as branching morphogenesis in a reproducible fashion [79, 75, 36]. These models are valuable because they permit testing for the requirements of branching morphogenesis with a wider range of perturbations and measurements than is possible when studying intact organisms. Below is a brief history of one such model, the Madin Darby Canine Kidney (MDCK) cell line.

Following the initial isolation in 1958 of epithelial cells from the renal tubule of an adult Cocker Spaniel by S. H. Madin and N. B. Darby, the cell line bearing their name was employed primarily as a model for viral infection of mammalian cells. It was not until 1970 that the laboratory of Zbynek Brada published work describing MDCK cells as a representative cell line bearing hallmarks of renal tubule epithelial cells [81]. They based this conclusion on the fluid transport activities of cell monolayers, the presence of microvilli on their apical surface, and their multicellular organization into tubules and cysts (a phenotype that required multiple weeks of culture). In their report, the authors speculated that the "histotypic expression" by which MDCK cells formed structures reminiscent of their tissue of origin might be fruitfully applied to the study of other tissues. The following decades have proved them largely right, although the repertoire for studying tissue morphogenesis has vastly expanded [36]. After this point, the MDCK cell line found new use as a model for mammalian epithelia. In 1982 Mina Bissell and colleagues demonstrated that MDCK

monolayers responded to the addition of a collagen overlay, generating a sandwich culture, by forming a lumen [82]. This hinted for the first time that the cell line would respond to 3D environments *in vitro* by self-organizing into the appropriate 3D structure. In the following years, the culture of MDCK cells embedded fully in collagen was shown to yield hollow cysts, or acini [83]. These were spherical epithelial monolayers with a defined interior and exterior. However, the fact that MDCK cells did not form tubules under these conditions remained unexplained until later.

Over the same period, biologists studying cell motility had hit upon an interesting and reproducible phenotype of cells: the scattering response. Epithelial cell clusters could be induced to break cell-cell contacts and become elongated and motile, after exposure to a "scatter factor" that was secreted by mesenchymal cells such as Swiss 3T3 fibroblasts [84, 85]. This was best described by Julia Grays group in 1987 [86]. During the same period in the mid 1980's, a monoclonal antibody published by the group of Walter Birchmeier was described to disrupt cell-cell contacts and alter the front-rear polarity of cells in culture [87, 88]. The target of this antibody was later identified as the adherens junction component E-cadherin [89]. These concepts eventually coalesced into a paradigm for cell motility and cell polarity.

In 1991, the response of MDCK acini in 3D culture to this factor was first reported by Lelio Orci and colleagues. They cultured acini of MDCK cells in collagen gels with or without Swiss 3T3 fibroblasts, in which media could exchange but the cell types were not in direct contact [90]. Coculture with fibroblasts induced MDCK acini to undergo branching and elongation to yield a network of tubules. In the same year, the paracrine-acting "scatter factor" was shown to be a previously described protein secreted by fibroblasts, Hepatocyte Growth Factor (HGF) [91]. This work solved an outstanding mystery of MDCK culture, as the tissue from which these cells derived is tubular, and thus not reminiscent of spherical acini. Beyond that immediate paradox, a crucial connection was forged between the acute induction of cell motility in 2D by the "scatter factor," and its impact on the spatial organization adopted by tissues in 3D. This connection remains significant as a link

between precisely defined mechanisms of cell motility in 2D and complex rearrangements in 3D whose regulation is yet to be understood fully.

In the last 20 years, understanding of MDCK cell biology in 3D culture has been advanced largely by the laboratory of Keith Mostov. This group has focused on the regulation of cell polarity and its downstream effects on branching morphogenesis [92, 75]. Indeed the body of work generated by the Mostov group has successfully synthesized decades of knowledge about the spatial segregation of intracellular functions, and their molecular markers, into a remarkable model for the generation and homeostasis of cell polarity in tissues [93, 92, 94]. In 2003, Yu et al reported the first comprehensive account linking branching morphogenesis with hallmarks of apical-basal polarity [95]. This work established that MDCK cells do not loose contacts with neighbors during the onset of branching, but that canonical markers of polarity are transiently lost. One outcome of this shift in polarity signaling is the reorientation of cell division along a newly growing branch of cells, in order to correctly position daughter cells to continue branch extension. Cell motility by which MDCK cells produce and elongate branches was linked with these polarity phenotypes. Specifically, they showed enrichment of phosphoinoside-3-phosphate at the leading edge of elongating branches, and that reduction of cell contractility resulted in overabundant and disorganized cell protrusions at the outset of branching.

These findings were integrated into a model for branching morphogenesis that focused on the transient rearrangement of cell polarity signaling. This allows normally nonmotile cells to generate protrusions and migrate collectively, followed by redifferentiation and formation of hollow tubules [96]. In support of this model, Mostov and colleagues have identified the effects of HGF on MDCK acini as eliciting a partial transition from epithelial to mesenchymal cell phenotypes [96]. This argument marshals an established signaling program termed the epithelial to mesenchymal transition (EMT), by which sessile epithelial cells become motile and break cell-cell contacts [97]. EMT has been proposed as the transcriptional signaling cascade that drives cell scattering, although previously researchers did not conflate the two

[98, 99]. Given the distinction that, for acini in 3D, cell-cell junctions do not rupture, it is unclear how to precisely relate the EMT concept with branching morphogenesis.

The Mostov group has also investigated the means by which HGF activates cell motility during MDCK branching morphogenesis [100, 101]. Their studies have shown that branching morphogenesis requires the Erk transcription factor, downstream of the Mitogen Activated Protein Kinase cascade, a well-defined signal transduction pathway implicated in cell motility and proliferation [102]. The cell motility machinery responsible for branching morphogenesis has not been specified by the Mostov group, beyond the requirement for a signaling protein involved in regulating the small GTPase Rho [100, 101]. A few reports have linked ECM receptor family of integrins to MDCK acinar polarity. These have not focused the ability of cells to maintain integrin-based adhesions, but have documented profound polarity defects when β-1 integrin function is blocked [95, 103].

Meanwhile, other groups have demonstrated the requirement for cell-ECM adhesion proteins or their regulators in MDCK branching morphogenesis [104, 105, 106]. These have not yielded mechanistic insights that show precisely how HGF changes cell behavior to drive branching morphogenesis. They have, however, correlated cell adhesions to the ECM with the ability to undergo branching. Using a modified model for MDCK cell culture and branching morphogenesis, Gierke and Wittman established the requirement for microtubule dynamics in regulating the early steps in branching [107]. They observed deficient cell adhesive coupling to the collagen matrix when microtubules were deregulated. This phenotype indicated the importance of trafficking the appropriate cell adhesion and protrusion proteins to the cell front as branching morphogenesis was initiated. Combined with observations from the Mostov group, this work confirmed that cell polarity is indispensable for MDCK acinar homeostasis as well as migratory behaviors during branching.

1.3 The molecular basis of directed cell motility

1.3.1 Cell motility

The study of directed motion by single cells developed alongside advances in the study of morphogenesis and cancer biology discussed above. This section addresses the intracellular mechanisms that enable cells, and the tissues they compose, to change shape and move.

Migration of adherent cells integrates three fundamental properties: Protrusion, adhesion, and contraction [108, 109]. While these are somewhat separable functions and can be ascribed to related groups of proteins, their functions are interdependent and tightly co-regulated. However, at initial glance, cell migratory behavior in many different contexts can be reduced to these three properties. For an adherent cell on a flat substrate, the direction of motion is determined by a protrusive front. A broad, constantly ruffling cell edge is formed by lamellipodia [110], while filopodia are slender, spike-like extensions that rapidly emerge from the cell body. The cell front may exhibit a combination of these mechanisms [111], but both can serve to advance the cell membrane in the direction of migration. Following protrusion, cells form adhesions at or near the cell edge. These take the form of focal adhesions, dense subcellular plaques of proteins that make strong yet dynamic attachments to proteins on the substrate [112]. Anchored by focal adhesions at the cell front, the cell contracts across its trailing edge in order to retract its rear and move the cell body forward [113]. Retraction is dominated by contractile actomyosin networks, which are distinct in form and regulation from protrusive networks. This step highlights the importance of spatial organization of protrusion and retraction, through which sustained front-rear polarity is established [114, 113].

As noted in previously, differing cell shapes and environments impose specific constraints on the above process. Notably, cells moving through 3D matrices can move with a wide array of protrusive structures, and do not always form focal adhesions [115]. However, these fundamental elements still describe the vast majority of cell motility processes [116].

1.3.2 The actomyosin cytoskeleton

Cell migration relies on conserved dynamics of the actomyosin cytoskeleton, which is organized in space and time into protrusive and adhesive organelles [109]. The primary structural material with which cells maintain their shape, exert forces, and migrate is the actin cytoskeleton. Across a migrating cell, actin monomers are continuously polymerized into networks, which continuously undergo depolymerization on timescales of seconds to minutes [117]. Through the combined activities of a panoply of actin nucleation and elongation factors, actin bundling proteins, and filament severing proteins, different networks are spatially segregated into organelles, each with specific mechanical properties [118, 119]. These networks are both crosslinked and contracted by myosin motor proteins [120]. Together these networks, and the mechanical properties they confer, permit cells to execute a wide range of motility behaviors and shape changes [121].

Actin is one of the most abundant proteins in eukaryotic cells. Assembly of monomers into filaments generates a helical, semiflexible polymer with an intrinsic polarity [119]. Monomer addition is favored at the barbed end, with intrinsic polymer activity under most purified conditions. Depolymerization dominates at the pointed end, the other end of filaments, which is accelerated by hydrolysis of a bound ATP molecule as monomers age within the filament [122]. These rates of filament assembly and disassembly are dominated by a rich diversity of actin regulatory proteins discussed below.

At the leading edge of a migrating cell, lamellipodia drive protrusion of the cell edge. These organelles are rapidly advancing and retracting broad extensions whose defining feature is an extensively branched meshwork of actin filaments [123, 110, 124]. Lamellipodia are nucleated by Arp2/3, a complex of 7 proteins whose conformation allows it to both bind to the side of an existing actin filament and nucleate a new filament. Arp2/3 activity thereby generates a dense meshwork of actin filaments, joined to each other at a 70 degree angle [125]. Critical to the function of Arp2/3 networks within lamellipodia are capping and severing proteins. Capping protein binds to the growing end of actin filaments, ensuring

filament length is kept short [119]. A complementary function is played by severing proteins, such as ADF/cofilin, which bind along the length of filaments and sever them. Severing events recuperate monomeric actin for recycling into new filaments and maintain a short average filament length [126]. Together these confer to Arp2/3 networks the density and turnover rate necessary for efficient advance of the cell edge. Indeed, the collective actions of lamellipodia components are sufficiently robust to retain their morphology, motility, and directional persistence, even when isolated from intact cells [127].

On the other hand, experiments to test the central role of Arp2/3 in lamellipodia have used both genetic ablation of Arp2/3 complex components, as well as more recent pharmacologic approaches [128]. Collectively, these studies established that cells can indeed migrate, albeit inefficiently, with the total loss or instability of lamellipodia, although they become insensitive to the changes in their physical environment [129, 130].

Complementing the Arp2/3 network at the cell's leading edge are an array of linear networks maintained by Diaphanous-related formins, a diverse family of actin nucleators and elongators. These linear networks assemble into stress fibers within the lamellum, spike-like filopodia at the cell edge, and the cytokinetic ring following mitosis [131]. The protein domains that define the formin family and carry out actin filament assembly, Formin Homology (FH) 1 and 2, are highly conserved from yeast to humans. In humans the 15 family members show considerable variation outside of these domains [132, 133]. Catalytic activity of formins is carried out by homodimers of the FH2 domain, which constitute a ring structure that associates with and continuously elongates the barbed end of an actin filament [131]. Formin-nucleated actin filaments are thus unbranched and tend to be longer than Arp2/3-nucleated filaments. Adjacent to the FH2 domains are flexible FH1 domains, which bind actin via the small actin monomer-binding protein profilin [134]. Thanks to the high affinity of profilin for the FH1 domain, monomers of actin can be continuously associated with the formin dimer. These interactions combine to enable the rapid yet controllable generation of linear actin filaments.

Besides the FH1 and FH2 domains, the other domains are less conserved across the formin family. They are responsible for dimerization and regulatory functions critical for controlling formin activity in space and time [135, 131]. Most important are the Diaphanous Inhibitory Domain (DID) and Diaphanous Autoregulatory Domain (DAD), located at either end of the protein. Binding of the DAD to the DID prevents formin activity and must be displaced by binding of the small GTPase Rho in order to relieve inhibition [133]. Through this mechanism, formin activity is regulated tightly by Rho. Further regulation is mediated through the FH1 domain, which can bind to Src homology domains whose activity links formins to upstream tyrosine kinase signaling pathways [136]. This domain organization is representative of diaphanous related formins Dia1 and Dia2 [131]. Another formin, Formin Homology 2 Domain Containing 1 (FHOD1) retains actin polymerization activity of Dia1 and Dia2 but interacts with different regulatory partners [137].

The emergence of dynamic networks from the simple filaments generated by formins and Arp2/3 requires the actions of two broad classes of proteins: actin-crosslinking proteins and myosins [118]. Non-muscle myosins were one of the first motor proteins to be described in detail and their functions as contractile elements were surmised early on thanks to the study of muscle physiology [138]. Yet it took a set of nontrivial conceptual leaps, such as by Huxley in 1973, to describe cytoskeletal function in nonmuscle cells lacking the organization of muscle fibers [139]. In most cells, Non-muscle Myosin II forms small bipolar oligomers termed minifilaments, that bind to and contract against actin filaments at either end [140, 120]. Their activity is regulated directly through Myosin Light Chain (MLC), which binds and releases head-tail interactions that otherwise lock Myosin II into an inactive state. Two isoforms of Myosin II, A and B, are highly expressed in most cell types, and exert dominant effects on cell shape and motility. With some variation, Myosin IIA is found predominantly near the leading edge of migrating cells, and is abundant throughout the lamellum. Meanwhile Myosin IIB accumulates at the cell rear and nonprotrusive regions of the cell body [141]. Together Myosins IIA and IIB generate virtually all of a cell's contractile force, and the spatial control

of their activity is essential to generate the wide diversity of cell shapes observed throughout biology [109, 142, 121].

Rapid assembly, reinforcement, and disassembly of the above actin networks are achieved by signaling pathways converging on the small GTPases Rac, Rho, and Cdc42 [143, 114]. These membrane-bound, switch-like proteins integrate biochemical signaling inputs from cell receptors or gene expression and govern the activation of the Arp2/3 complex and formins, via direct and indirect mechanisms. Rac is active primarily at the leading edge of a migrating cell, where it activates Arp2/3 through adaptor proteins such as Neural Wiskott-Aldrich Syndrome Protein (nWASP). Rac also activates the formin family protein FHOD1, which assembles stress fibers near the leading edge [137, 144]. Cdc42 activation is also polarized toward the cell front, and primarily directs formation of filopodia [145]. Rho promotes the assembly of contractile actomyosin arrays and is associated with contraction of the cell rear and maintenance of front-rear polarity in migrating cells [143]. Activation of myosin contractility is controlled by Rho primarily through its activation of Rho Kinase (ROCK) [146]. Like Rac and Cdc42, the effects of Rho are integrated across the whole cell for efficient migration [147]. Indeed, the use of optical probes has suggested that Rho is recruited to the leading edge of migrating cells, although these claims have yet to be broadly confirmed [148, 149].

1.3.3 Formation and regulation of cell adhesions

During migration along planar surfaces cells form focal adhesions, complexes 1-2 um in length comprising hundreds of proteins that bind to extracellular proteins on the cell exterior, and interact extensively with the actin cytoskeleton on the cell interior [112]. Focal adhesions were identified as early as 1976 by Izzard and Lochner as discrete subcellular points of adhesion, via the careful use of interference microscopy on migrating chick cardiac fibroblasts [150]. This technique achieved exquisite resolution of the cell membrane's proximity to a glass coverslip, from which the authors correctly reported their size and shape, and their

integration into the cell's cytoskeleton. Later work using the same technique permitted them to form early conclusions regarding the formation of focal adhesions within protrusive, actin-rich structures, from which stress fibers emanated [151]. These conclusions have been borne out by later studies using an array of genetic, optical, and computational techniques through which focal adhesion structure and dynamics have been comprehensively detailed [118, 112, 152].

The features of focal adhesions which permitted their visualization by Izzard and Lochner reflect their underlying structure and integration into the actin cytoskeleton. The nanoscale organization of a focal adhesion originates with small clusters of integrins, a family of transmembrane receptor proteins [153]. These clusters bind to extracellular proteins such as fibronectin or collagen [154, 155]. Initial binding by integrins occurs at the cell's periphery in association with the actin pool within the lamellipodia. In this way, lamellipodia test their environment for ECM proteins as integrins make initial contacts with ECM proteins [156]. More integrins are recuited upon initial engagement with the ECM, as well as focal adhesion proteins such as Paxillin, Talin and Vinculin, forming a nascent focal adhesion [157, 158]. This small complex is immobilized with respect to the ECM. Over a period of minutes, focal adhesions then undergo a structural and biochemical maturation process that integrates them with the cells contractile actomyosin networks [118, 112]. The complex remains associated with actin filaments, and recruits the actin bundling protein alpha-actinin as well as actin nucleators and elongators [157, 159, 160]. During this process the adhesion grows in length perpendicular to the cell edge and its protein constituents are modified by phosphorylation. These include modification sites on Paxillin and Focal Adhesion Kinase (FAK) that are associated with focal adhesion maturation and participate in biochemical signaling through Src kinase [161, 162]. Eventually, mature focal adhesions are disassembled in concert with cell motility.

The orderly picture for focal adhesion assembly and maturation described here falls far short of capturing the tight integration of these processes with the actomyosin networks

in which focal adhesions exist. Focal adhesions initially assemble within Arp2/3-generated networks that are largely free of myosins. During and after initial integrin engagement with the ECM and clustering, nascent adhesions must contend with rapid flow of the bulk actin network toward the cell center, termed retrograde flow [163, 164]. This centripetal flow was recognized long ago as a conserved feature of migrating cells, and reflects rates of Arp2/3 network assembly at the cell front coupled with myosin activity within the cell body [165, 166, 119]. Nascent adhesions are dragged rearward with this flow and are either disassembled in the contractile lamellum, or are stabilized in concert with focal adhesion protein assembly [167, 168]. Myosin activity is required for focal adhesion maturation but not their formation, indicating that nascent adhesion formation within lamellipodia is a spatially and mechanically separate process [118, 158].

Nascent focal adhesions are, however, sites of actin polymerization through Arp2/3 [169], formins [157, 170], and the actin filament elongation factor Vasodilater Stimulated Phosphoprotein (VASP) [171]. Formins and VASP colocalize with maturing and mature focal adhesions, from which they generate stress fibers [172, 159]. Cells lacking formins [160, 170] or the actin crosslinking protein alpha-actinin [157] show impaired focal adhesion maturation. Septins, which can bind to and stabilize stress fibers, also promote focal adhesion maturation [173]. These observations suggest that rather than passive linkages, focal adhesions are active players in the actomyosin network organization in cells. Moreover, focal adhesion properties require regulators of the actin cytoskeleton directly, making them acute sensors of the actin network dynamics in a migrating cell.

As initially observed over 20 years ago, the direct consequences of Rho activity include myosin contractility and the formation and growth of focal adhesions [174]. This observation has evolved into a model of myosin-dependent maturation of focal adhesions. Myosin contractility translated through the actin cytoskeleton applies tension to focal adhesion plaques, which respond by undergoing maturation and transmitting increased tension to the cells substrate [175]. Other experiments have detailed how cells respond to substrate stiffness,

showing that increased stiffness correlates with increased focal adhesion size and maturation [176, 177]. In this way, the maturation of focal adhesions appears to furnish a mechanic signal to the cell, governing cellular responses to the physical environment [175]. This concept has stimulated a range of hypotheses for the precise mechanisms, as well as proposed outcomes, of how cells sense mechanical forces at focal adhesions [178, 50, 179, 180]. Many putative sensing mechanisms involve tension-dependent conformational changes in focal adhesion proteins such as integrins, talin, and vinculin [154, 181].

Complicating these results are observations that refute the correlation established between focal adhesion maturation and mechanical force. First, nascent focal adhesions can bear substantial tension and their size is not sensitive to increases intracellular tension [170, 182]. Second, measures of the stress exerted by a cell, via its focal adhesions, have consistently scaled with the area of the cell, rather than the number or composition of its focal adhesions [167, 121]. Moreover, most experimental evidence for mechanical maturation of focal adhesions use approaches that reduce myosin contractility [174, 175]. Such perturbations necessarily impair the actin network rearrangements inherent to normal focal adhesion maturation. Thus structural defects in actin network organization are difficult to separate from defects in myosin contractility [157, 160].

Furthermore, mutations in or depletion of individual focal adhesion components have resulted in a wide range of cell motility defects [183, 184, 185]. These effects appear to be highly context-dependent, which has made it difficult to parse the consistent, general properties of the focal adhesion functions. A recent study found that pharmacologic inhibition of FAK, a central regulator and signaling protein at focal adhesions, rendered few measurable effects on focal adhesion morphology or maturation [186]. Rather, these authors observed a slight but consistent reduction in the turnover of FAK at focal adhesions. Results such as these indicate either that focal adhesion structure and signaling is unimportant for their functions (which seems unlikely), or that cell biologists may not yet know the salient features of focal adhesions that link their functions to cell biology.

1.3.4 Cell motility through 3D environments

The detailed understanding of cell migration described above need not be limited to cells crawling on flat substrates. As fluorescence imaging has improved, cell biologists have looked to cell culture models using biopolymer gels in order to analyze cell motility in 3D.

The key parameters distinguishing 3D from 2D cell motility are clearly not the cytoskeletal proteins involved nor their molecular functions, but rather 1) the physical properties of the environment and 2) the arrangement of cytoskeletal proteins across the cell [115, 187]. Cells such as fibroblasts adopt a flattened shape and protrude via broad lamellipodia in 2D, whereas in 3D, identical cells tend to be much more elongated with a narrow cross section [187]. As they move through 3D environments, cells often protrude via narrow extensions, with active ruffling reminiscent of lamellipodia only at the narrow tips of these extensions (Figure 1.3) [116]. Across the cell, the signaling proteins that govern actomyosin architecture and dynamics are spatially segregated as in cells on 2D surfaces [188, 116].

Focal adhesions and their regulators control cell adhesion and migration in 3D matrices just as on 2D substrates. In fibrillar 3D environments, components of focal adhesions are known to be required for migration, but their composition and formation dynamics are poorly defined [189, 190]. The laboratory of Kenneth Yamada has made considerable contributions to a general understanding of cell motility regimes and requirements in 3D. Kutys et al showed reciprocal interactions between collagen fibril adhesion, focal adhesions, and polarized cell protrusion that brought considerable detail to cell migration and agreed with 2D migration modes [187, 191]. As in 2D, myosin plays a critical role in enforcing cell shape, and contributes to focal adhesion size and stability [192, 193]. Yet some aspects of focal adhesion morphology remain unclear in 3D. A recent report documented variations in focal adhesion size of over an order of magnitude [185]. Another report claimed that focal adhesion proteins regulate cell migration but do not form dense plaques as in 2D [189]. In other cases, however, cells exhibit migration strategies in 3D using blebbing or amoeboid migration that are independent of focal adhesions [73]. These widely varying reports made

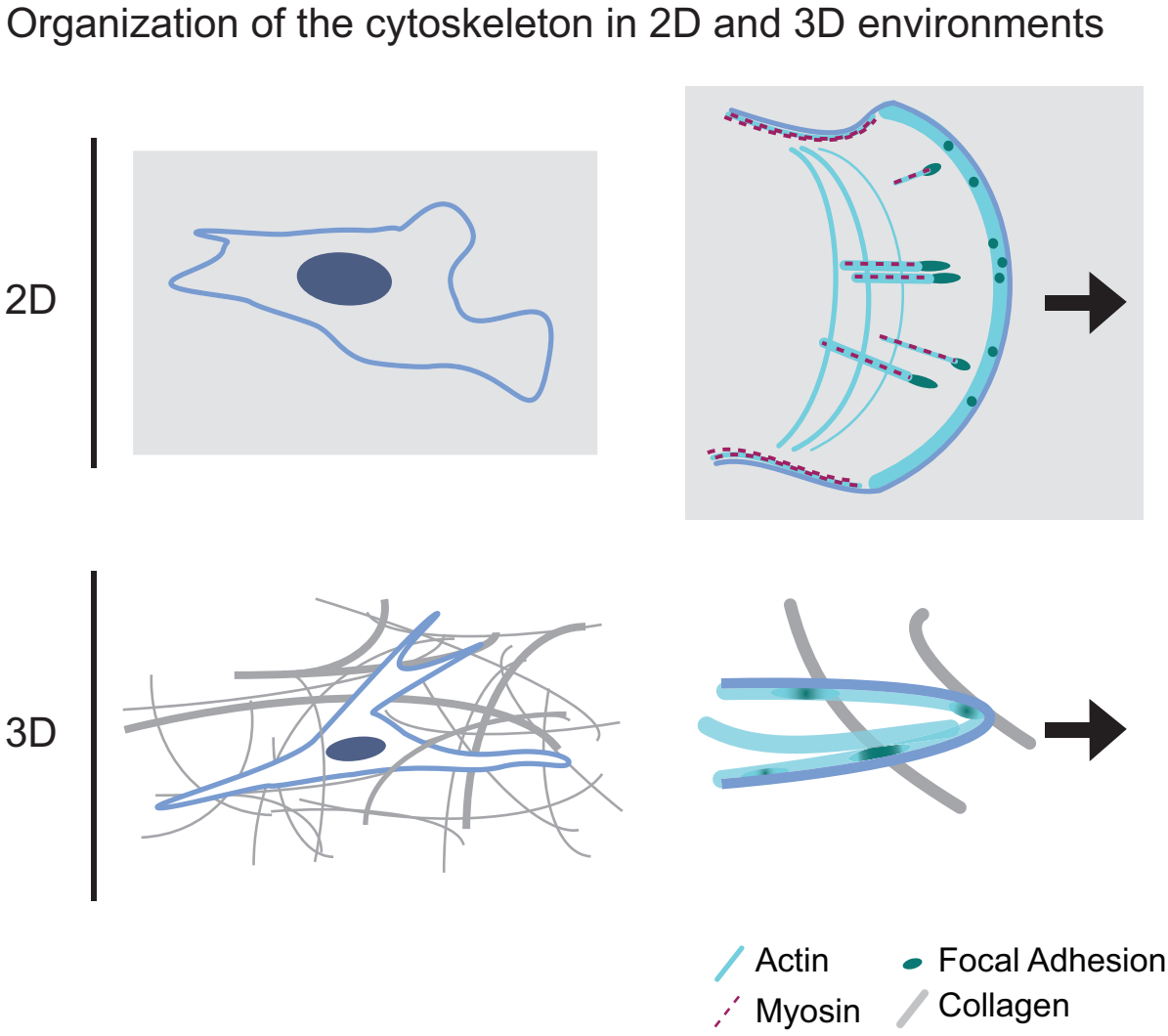

Figure 1.3. Similarities and differences between cell migration through 2D and 3D environments. To move in a directed manner, cells on 2D surfaces form broad lamellipodia where many discrete adhesions are formed. These adhesions undergo maturation and are integrated into the cells contractile actomyosin networks. In contrast, 3D migration typically involves long extensions in which adhesions form but their maturation and integration inot the cytoskeleton are not well understood. Notably the spatial organization of myosin in 3D is less well defined than for cells on 2D surfaces.

a broad consensus difficult to formulate for 3D migration, owing in part to variations in culture techniques, imaging capabilities, ect.

However, physical parameters necessarily circumscribe the possible mechanisms of 3D migration [115]. When using focal adhesions to migrate, cells must form adhesions at ECM fibrils. These offer much smaller adhesive area than a cell on a 2D surface, and can resemble 1-dimensional migration along lines [194, 193]. Moreover, even if their precise organization into puncta is not obvious under all conditions, cell movements still depend on focal adhesion proteins to translocate under many conditions [192, 189, 195]. Cell movement without focal adhesions appears to be controlled by upstream signaling through GTPases signaling and may set the range of movement possibilities for a given cell [116, 196, 197]. Thus while much of the existing literature highlights a wide variety of cell motility strategies, some key features can be extracted that help advance a broad knowledge base.

The impacts of different actin regulatory GTPases and myosin activity have been studied in detail for cells migrating in 3D [188, 116]. For the case of 2D migration, the roles played by these regulators have been linked intimately with actin architectures and dynamics, connecting Rho activation, for instance, with stress fiber formation [174]. Yet the actin architecture of cells in 3D has been more difficult to identify and parse between different subcellular organelles. Rather, actin is almost exclusively cortical and rarely shows a particular network organization. Stress fibers, for instance, are less abundant and difficult to resolve in 3D [198]. This missing link between biochemical signaling and cell migration has forestalled efforts to build a unified view of cytoskeletal function for cells in 3D environments.

Fortunately, the range of motility phenotypes in 3D can be narrowed to those that operate during development and cancer invasion. Interestingly, branching morphogenesis and tumor invasion have been shown to require specific focal adhesion components, suggesting that focal adhesions may play a role in regulating tissue shape changes [199, 200, 162, 201]. These observations suggest that despite the relative variation in cell motility for individual cells in 3D compared with 2D, complex biological processes rely on these components for

motility. It remains to be seen what specific cellular behaviors lie between the molecular details of focal adhesion proteins and the final tissue shape changes they appear to control.

CHAPTER 2

METHODS FOR 3D CULTURE AND IMAGING OF MULTICELLULAR STRUCTURES

2.1 Introduction

The study of tissue morphogenesis concerns how the basic plans of tissues are generated during development. Microscopic examination the conserved geometries exhibited by tissues during morphogenesis has spanned at least a century. Biologists have enjoyed three primary methodologies to investigate morphogenesis [202]. First is histology of chemically fixed and sectioned tissues from developing or mature animals [203]. The second is the analysis of development, whether fixed or in real time, of small and transparent organisms serving as model species [204, 205]. Finally, isolated primary or immortalized cells can be cultured in 3D environments, known as organotypic culture [75, 36**?**]. When carried out under the correct conditions, organotypic culture permits cells to recapitulate self-organization behaviors of their representative tissues. This offers the chance to introduce genetic or pharmacologic perturbations while observing cell behaviors that can be reliably compared across conditions [206, 37]. This section will describe organotypic culture techniques and technical considerations for exploring cell behaviors that contribute to morphogenesis.

The cell culture techniques described below utilized mouse mammary carcinomas, and immortalized cells were from the Madin Darby Canine Kidney (MDCK) line. The culture of these cell types focused on growth and morphogenesis in organotypic conditions and their imaging by immunofluorescence and live microscopy.

2.2 3D culture of cells and tissues

2.2.1 General principles and strategies

Epithelial tissues are defined by distinct spatial relationships that dictate cell orientation. As barrier tissues organized into planes or hollow tubes, epithelial cells must recognize "inside" and "outside" environments and organize their behaviors accordingly. Taking the example of a tube, its outside is surrounded by the basement membrane, a tightly woven tapestry of extracellular proteins that form a physical and signaling barrier [92, 207]. Epithelial cells line the inside of the basement membrane and orient secretory or absorptive activity into the middle of the tube. Experimental systems to approximate this environment for cell propagation have focused on providing basement membrane mimics that form a supportive hydrogel [206]. Two parameters, appropriate protein cues and appropriate material properties, collaborate to support the growth and organization of epithelial cells into 3D structures that recapitulate key properties of epithelial tissues [11, 208]. With some caveats, these parameters are provided by Matrigel. Matrigel is inexpensive, easy to manipulate, and contains a variety of basement membrane proteins in roughly stoichiometric ratios[209]. The reproducible culture of epithelial cells in Matrigel mandates that the same production lot is used across experiments. This ensures that the variability inherent to the extraction and purification of basement membrane proteins from mice is minimized.

MDCK cells, however, can secrete and assemble a basement membrane autonomously [210, 75]. Because of this, MDCK cells can be cultured in gels of the fibrillar extracellular matrix Collagen 1 [83]. Collagen is the most abundant protein by weight in the human body, and forms scaffolds for interstitial as well as glandular tissues throughout the body [211]. As such, its polymerization and use as a 3D hydrogel support more closely resembles interstitial mammalian tissue than does Matrigel. Unlike Matrigel, the 3D networks formed by collagen fibrils *in vitro* resemble stromal collagen *in vivo*. Single MDCK cells grown in collagen 1 gels of 2-3 mg per ml proliferate and organize into acini over 10 days [75]. Their

growth in Matrigel is accelerated, and they form equivalent structures as those in Collagen 1. However, cell motility and response to mechanical properties are acutely impacted by Collagen 1 compared with Matrigel [39, 212].

Matrigel liquefies at temperatures near 0 C. Briefly lowering the temperature facilitates the extraction of intact cell ensembles from liquefied Matrigel and obviates the use of enzymes such as collagenase or trypsin. Cell ensembles may then be replated into collagen or other extracellular matrices. This technique was modified from a protocol developed by Yoshihiro Yui in the laboratory of Valerie Weaver. The primary benefit of this method is that it permits the separation of cell growth and polarization from cell motility and dissemination. Isolating multicellular structures in this manner also allows their exposure to low titer virus for the introduction of transgenes into a subpopulation of cells. This method enables labeling or genetic manipulation in a mosaic manner, as described by Cheung and Brugge [213].

Finally this method has proven a useful strategy for maintaining primary tumor explants from mice. Matrigel supports their growth while preventing their dissolution into single cells, prior to their isolation and plating for invasion studies using Collagen gels. Below we document procedures that capitalize on these two extracellular matrix gels for studying MDCK cells and mouse tumor explants. These offer a generalized protocol to be adapted to suit the needs of a particular experiment. The cell culture strategies used throughout this thesis are diagrammed in Figure 2.1.

2.2.2 A general protocol for the culture and isolation of MDCK acini

Epithelial cells can be extremely sensitive to high concentrations of basement membrane proteins, which in Matrigel may greatly exceed physiological concentrations. This, as well as variations in pH, makes pure Matrigel toxic for some cells. Mixing Matrigel with cell culture media proved the optimum for cell proliferation and morphogenesis of 3D structures. A 1:1 ratio of Matrigel and cell culture media provided the most robust support for cell growth and morphogenesis.

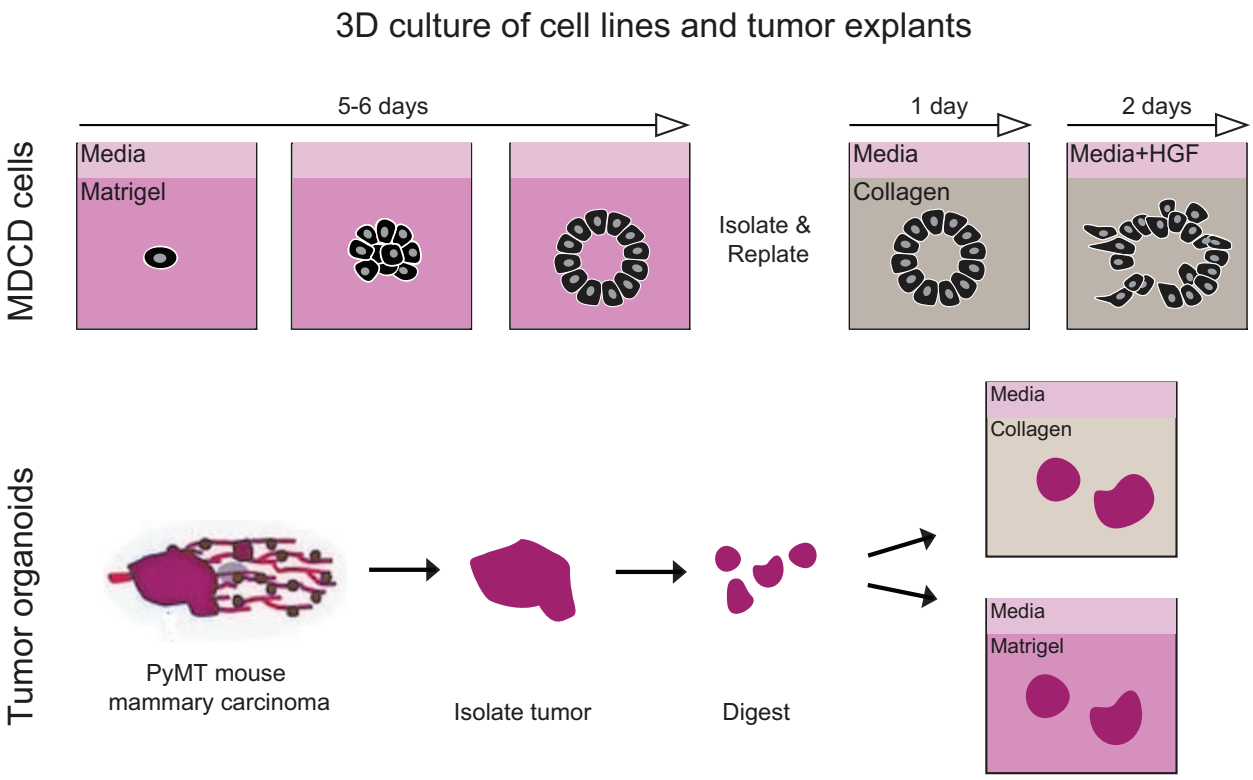

Figure 2.1. Matrigel promotes the self-organization of cells to form model tissues. It can be removed at low temperatures to isolate intact multicellular structures. This strategy works for immortalized cell lines as well as primary tumor explants. Below, tumor explants can be maintained in Matrigel for propagation, or plated directly into collagen gels for invasion studies.

From a confluent 10 cm tissue culture dish, MDCK cells were trypsinized and resuspended in 6-8 ml of media. During trypsinization, a solution of equal parts Matrigel and media was prepared on ice to a final volume of 500-800 μl. 30-50 μl pure Matrigel was pipetted into a well of a 24-well plate, and spread evenly across the bottom with the pipette tip. The 24-well plate was then placed in the incubator. Once cells were trypsinized and resuspended, cell clustering was disrupted by pipetting with a narrow (p1000) pipette tip. From this suspension, 8-20 μl were transferred to the cold Matrigel solution. Cells were mixed within the Matrigel solution and plated in the 24-well plate over the layer of pure Matrigel. The 24-well plate was placed immediately in the incubator for 30-60 minutes before 800 μl warm media was added. Cells left in Matrigel were viable overnight without added media, but not longer.

MDCK cells grow into multicellular acini usually of clonal origin over 5-7 days following initial plating. Cells in these contexts require fewer media exchanges, usually only twice over the course of their growth. When viewed through a typical tissue culture microscope, acini appear as semi-transparent spheres. A clear lumen becomes visible by around day 4 as an inner circle that is less optically dense than the ring of cells surrounding it. MDCK cells eventually slow but do not completely stop their growth after reaching maturity. Once mature, acini can be stained by immunofluorescence in Matrigel, or transferred to Collagen 1 gels.

To isolate mature acini from Matrigel for replating, a bucket of ice was prepared by sprinkling salt generously on it and the ice was shaken to mix the salt. The salted ice was left at 4 C. Media was aspirated from the wells containing acini to be islated. From a 15 ml conical tube containing 10 ml warm Phosphate Buffered Saline (PBS) with Ca/Mg, 5 ml were used to disrupt Matrigel with a 5 ml pipette. PBS was pipetted vigorously up and down while moving the tip around the bottom of the well in circles. All visible Matrigel was removed from the well, with special attention paid to the bottom and sides. This PBS-Matrigel solution was added to the remaining 5 ml of PBS. The tube was inverted rapidly

to thoroughly mix the solution. The PBS-Matrigel solution was centrifuged at low speed (1000 RPM) for 3 minutes. This step helped remove excess Matrigel.

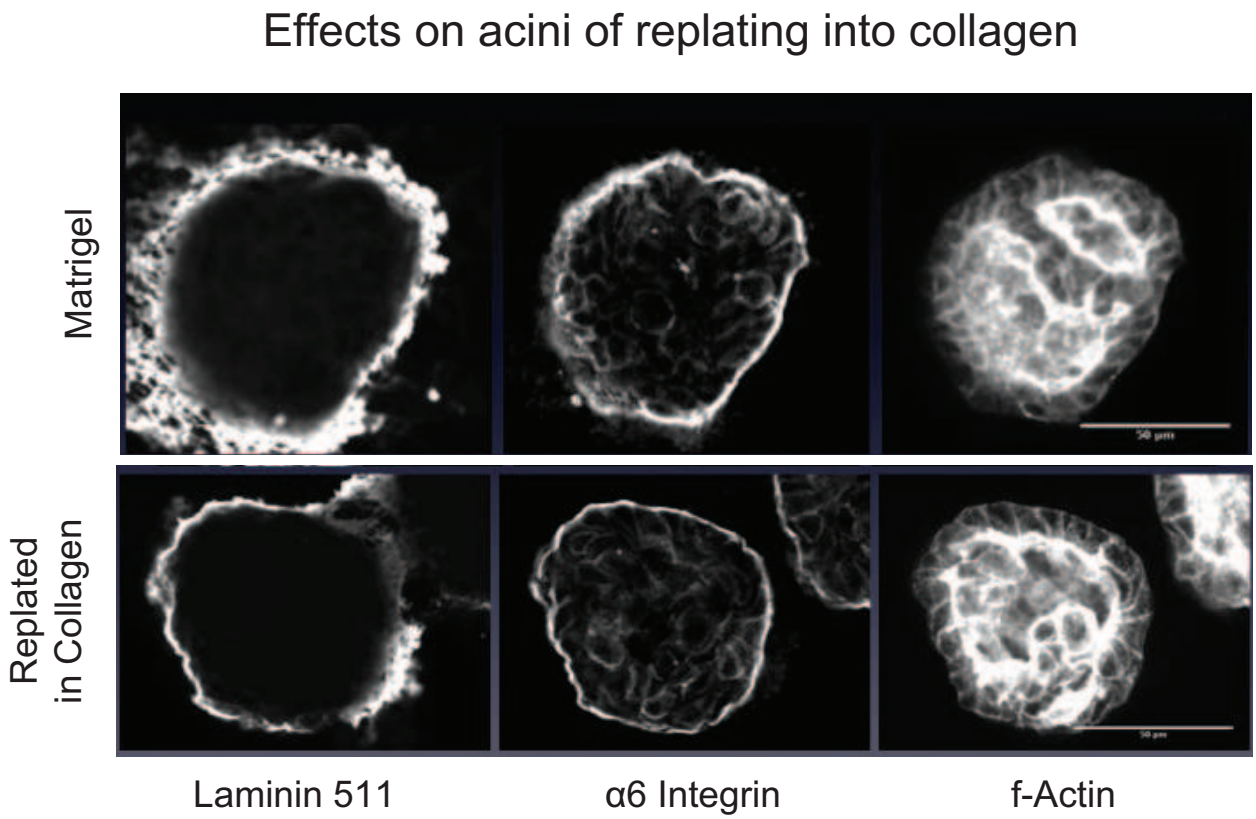

Figure 2.2. Immunofluorescence analysis of MDCK acini cultured in Matrigel (top) or cultured in Matrigel before isolation and replating into a collagen gel (bottom). Overall multicellular organization is retained. Acini retain peripheral Laminin 511 in collagen gels along with the Laminin-specific α6 integrin. Scale bars, 50μm.

The Matrigel, with acini still embedded in it, was visible as a large pellet. The supernatant was discarded and another 10 ml of PBS was added, pipetting up and down to disrupt the Matrigel pellet. This tube was embedded in the bucket of salted ice and the bucket was placed on a rocker at 4 C. The rocker was set to maximize the fluid displacement within the conical tube. After 30-45 minutes, the tube was removed from the ice and immediately centrifuge at low speed as above. Following this centrifugation the liquid supernatant was discarded and the remaining gelatinous pellet contained acini in small but variable volume (30-150 μl) of residual Matrigel. Acini were visible as small specks in a dense suspension at the bottom of the tube. The size of this pellet served as a good indication of the efficacy

of the isolation: A large pellet indicated that much of the Matrigel remained, while a small pellet indicated less Matrigel remained around acini. However, we have found that the total removal of Matrigel was not feasible.

Collagen gels were prepared prior to the start of isolation and allowed to incubate on ice. This incubation time was varied in some cases to form preferentially more or less bundled collagen gels, as discussed below. We made collagen gels from Rat Tail Collagen 1, which is stored in acetic acid to prevent polymerization. Collagen 1 was neutralized in a base such as sodium bicarbonate, and diluted in buffered cell culture media to a final concentration of 2 mg/ml. The volume of media was reduced to accommodate the 30-150 μl of acini concentrated in Matrigel following isolation. Following preparation of liquid collagen gels, the slurry of acini in suspension was added to collagen gels, mixed gently, and allowed to solidify at 37 C. Mixing is critical to ensure a homogenous gel and prevent pockets of acini trapped in large regions of residual Matrigel.

To test the effects of this replating procedure on acini, we performed immunofluorescence staining to visualize the basement membrane component Laminin 511, the Laminin-specific cell surface receptor integrin α6, and filamentous actin [210, 214]. We compared images acquired by confocal microscopy between acini replated into collagen gels and those left in Matrigel (Figure 2.2). Acini replated into Collagen 1 gels showed little disruption of acinar morphology or integrin expression. Most important, a layer of Laminin remained surrounding replated acini. It should be noted that the Laminin 511 antibody recognizes both Matrigel Laminin (of mouse origin) as well as canine Laminin and thus does not distinguish cell-derived Laminin from that in the Matrigel. Hallmarks of the larger Matrigel meshwork are visible by this staining. These images document changes in Laminin organization between these conditions, and confirm that multicellular organization is robust the isolation and replating of acini.

2.2.3 Tuning matrix properties to control collective cell motility

Matrix properties such as local ligand density, pore size, and stiffness can exert dominant effects on cell motility and invasion [40, 55, 25]. However these properties simultaneously alter gene expression and proliferation of cell and tissues [49, 179, 215]. Thus testing cell motility in a controlled manner, without altering cell proliferation, necessitates the separation of multicellular growth from cell motility and invasion. We therefore used the protocol above to isolate acini in conjunction with strategies to tune Collagen 1 gelation and the properties of the resulting gel.

Collagen gels of identical concentration were prepared to form dense bundles or an isotropic mesh of fibrils by incubating collagen solutions on ice for varying times before polymerization. This property of collagen has been described in detail, and its use for 3D cell culture has been explored by others [39, 195]. We found that varying the incubation time between 0 and 2 hours resulted in robust changes to the resulting collagen matrix. We then placed acini cultured together in Matrigel into these differing collagen gels. We used Collagen 1 conjugated to Alexa fluorophores to confirm that gels varied in apparent bundle thickness and pore size.

When acini plated in these two collagen gels were stimulated to undertake cell motility using Hepatocyte Growth Factor (HGF) [95], we observe profound effects of collagen matrix bundling on cell behavior, as shown in Figure 2.3. Bundled collagen gels promoted multicellular movement into the matrix, while meshwork gels prevented large-scale invasion. These could be explained by differing stiffness or pore size of the collagen gels, and can be further utilized to dissect cell-matrix interactions during morphogenesis.

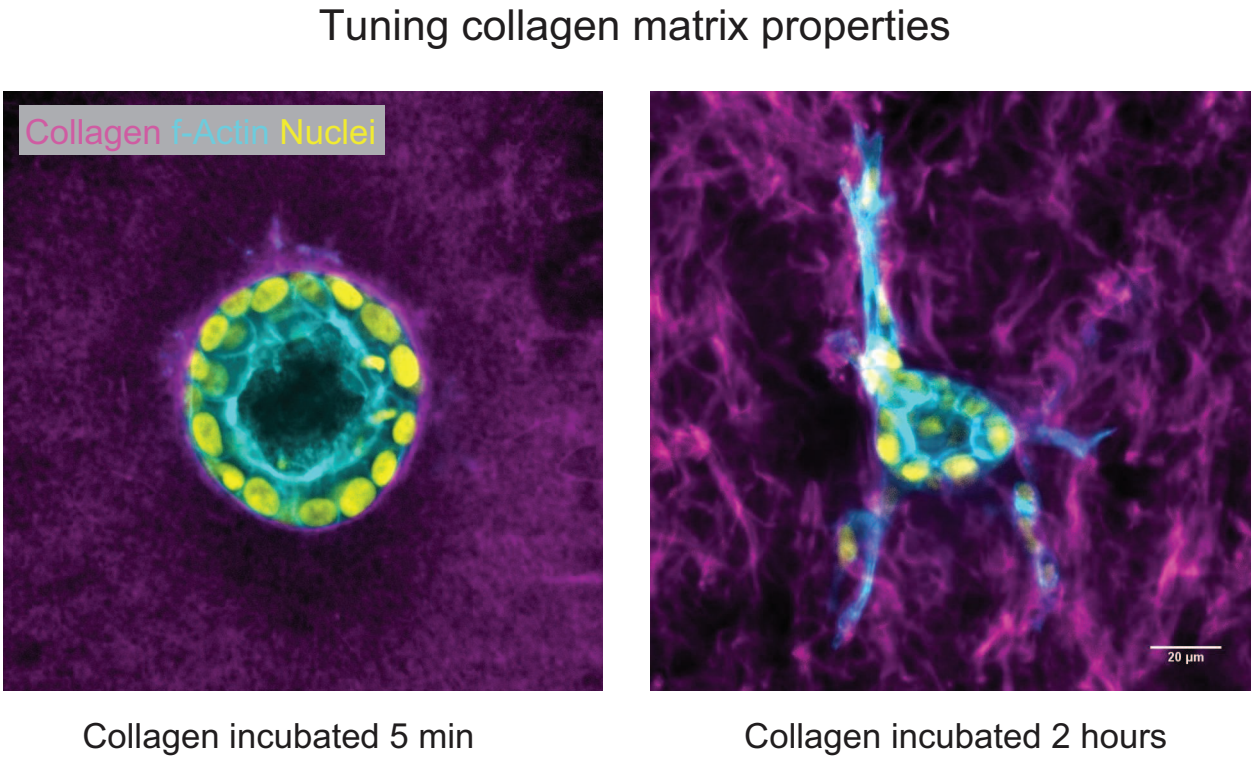

Figure 2.3. MDCK cells were cultured to form acini, which were isolated and plated in fluorophore-labeled collagen gels that had been prepared with or without a 2 hour incubation. After 24 hours acini were stimulated with Hepatocyte Growth Factor (HGF) to induce collective cell motility. Following 48 hours in HGF, acini were fixed and stained to visualize f-actin, cell nuclei, and Collagen 1.

2.2.4 Conclusion

Together these methods build upon and expand established strategies for organotypic cell culture and imaging. These techniques are premised on matching the cells physical environment to relevant cell behaviors under study: either polarized growth and self-organization in Matrigel or invasion and cell motility through collagen gels. Leveraging the strategic and creative use of these extracellular matrix proteins allowed us to both observe and modify multicellular behaviors.

We were especially encouraged by the ease with which intact acini could be isolated and manipulated without compromising cell organization. Thus the effects of different extracellular matrix properties can be tested in a controlled manner, by replating subsets from the same initial population of acini. We also expect that lentiviral infection of individual cells within acini can be employed to generate mosaic populations within acini. Overall these observations promote the creative use of 3D culture techniques to suit the experimental question at hand, and we expect future advances will lower the cost and improve the reproducibility of 3D culture techniques. The methods described here emphasize the careful consideration of cells' physical context to match the experimental question at hand. This is an overlooked priority that requires time and creativity, but permits unprecedented control and measurements of multicellular behaviors.

2.3 Lattice light sheet microscopy

2.3.1 Introduction

The many rich descriptions of living cells using confocal fluorescence microscopy have been circumscribed by its technical limitations [37, 216, 217]. These include, among others, the diffraction limit of light, as well as the effects on living cells rendered by intense laser illumination. Imaging the full 3 dimensional volumes of cells or tissues is limited by the z-resolution of conventional laser scanning or spinning disk confocal techniques. Compound-

ing this problem, imaging too frequently risks damaging cells due to the ionizing effects of laser light. Together, these obstacles enact a boundary on the spatial and temporal resolution with which images of living cells can reasonably be captured. These boundaries necessarily propagate into the working models put forth by cell biologists using knowledge gleaned from live imaging data. For example, widely accepted models for organelles have been upturned by improved imaging techniques that revealed the dynamic movements of mitochondria [218**?**] and the endoplasmic reticulum [219].

These challenges have been confronted by a variety of methods to improve microscopy of living cells. Chief among these are means of illuminating samples using light sheets, rather than point sources of laser light [220]. Light sheet illumination strategies encompass a range of modifications to light that result in a plane of light passing through the sample. This strategy derives from optical techniques initially described 100 years ago, which were repurposed for bioimaging starting in 1993. In that year, Voie et al described a fluorescent light sheet imaging strategy [221]. Selective Plane Illumination Microscopy (SPIM), described some ten years later, featured improvements on light sheet imaging and demonstrated its utility for capturing embryonic development. In contrast to SPIM, digitally scanned light sheet microscopy (DLSM) uses a rapidly dithered laser beam to illuminate the sample in a single plane [222]. Whether using SPIM or DLSM, the maximum axial resolution and imaging depth achievable by a light sheet are determined by the light sheets properties. Most of all, the beam waist, its thinnest point, sets the axial resolution. However, thinner waists reduce the penetrating depth over which the light sheet is effective.

The DLSM technique was adapted and improved by Eric Betzig and colleagues using a hollow cylinder of light known as a Bessel beam, created by passing light through an annulus. When dithered rapidly over the sample, constructive and destructive interference of the ring structure conferred superior resolution to the resulting plane. This permitted impressive imaging of cell rearrangements in living embryos [223]. Later, the same group developed lattice light sheet microscopy (LLSM), in which the annulus of the Bessel beam was replaced

with six points arrayed in a hexagon [224]. The resulting lattice produced a thinner plane and thereby improved z resolution. LLSM and other light sheet techniques require lower excitation light intensity relative to confocal microscopy to achieve comparable signal to noise ratios. Thus overall, LLSM yields improved spatial resolution while also permitting increased temporal resolution thanks to its lower light intensity.

While the speed and sensitivity of LLSM is a great improvement over conventional confocal microscopy, it requires a very tight arrangement of the objectives over the sample. LLSM mandates that two objectives (for separately illuminating the sample and recording emission) are placed within a few hundred microns of the sample, at oblique angles. This eliminates the possibility of using conventional coverslips or imaging chambers. The sample must instead be mounted on 5 mm diameter coverslips, which poses strict limitations on sample preparation and cell culture. The sample and the objectives are all immersed in a large bath of imaging media. Once the cellular environment is optimized in this bath by temperature and media buffers, imaging MDCK acini within collagen 'pillows' on 5 mm coverslip is feasible. The results of this imaging are presented below.

2.3.2 Visualization of single cells within acini by lattice light sheet microscopy

We used LLSM to investigate the dynamics of the actin cytoskeleton at the basal surface of MDCK acini expressing the fluorescent actin marker GFP-Lifeact [225]. Live imaging of acini expressing GFP-Lifeact portends multiple advantages and disadvantages. A limitation of expressing exogenous proteins such as GFP-Lifeact is that their expression can vary from cell to cell. In MDCK cells, this variation resulted in a mosaic pattern of expression in mature acini. This variation in expression precluded studies of actin dynamics across the basal cortex of an acinus in its entirety, which can be properly explored only through analysis of fixed samples. However, these acini often contained one or a few cells expressing GFP-Lifeact at levels much higher than their neighbors, and could be isolated visually by thresholding

(Figure 2.4). This approach permitted imaging of single cells within acini. A possible confounding factor is the selection of cells expressing the highest levels of GFP-Lifeact, which risks analyzing artifacts induced by its overexpression. While such artifacts have been documented for yeast [226], it is unclear whether Lifeact alters MDCK cell behavior.

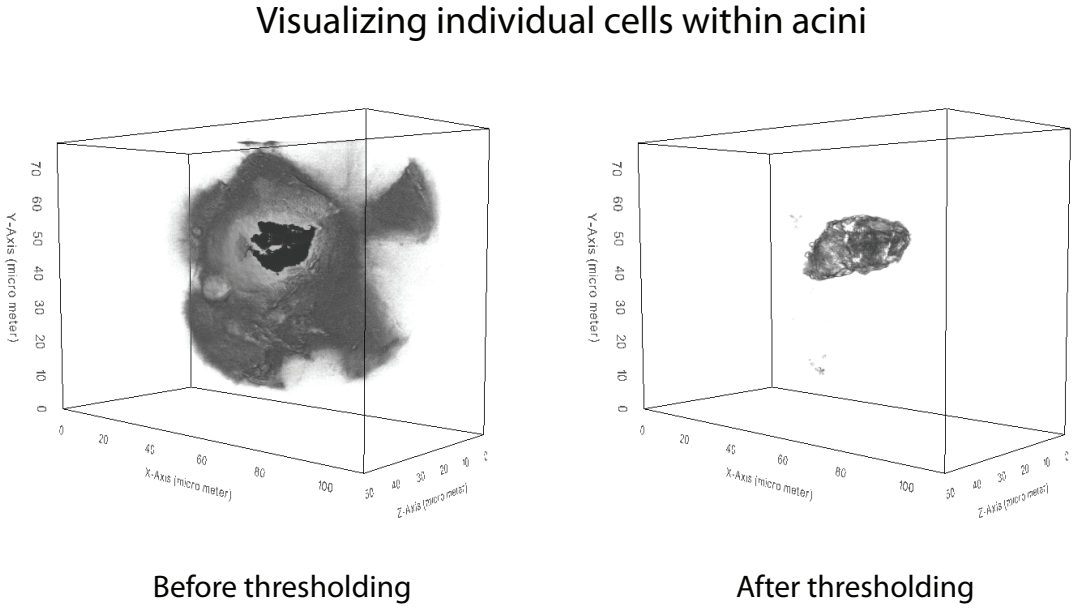

Figure 2.4. MDCK cells expressing the actin marker GFP-Lifeact were plated in collagen and imaged by time lapse lattice light sheet microscopy. Shown are two renderings of an acinus with different threshold settings to highlight the shape an individual cell.

2.3.3 Subcellular actin dynamics in acini

We next compared acini from MDCK cells depleted of a key regulator of the actin cytoskeleton, Dia1 (discussed in Chapters 3 and 4). Analysis of representative single shControl and shDia1 cells revealed stark differences in GFP-Lifeact dynamics (Figure 2.5). Regions of dense actin accumulation in shControl cells appeared to grow and shrink in a continuous manner. In shDia1 cells, in contrast, small puncta of Lifeact appeared and disappeared more rapidly. These puncta showed reduced apparent correlation between frames, suggesting faster turnover. The distribution of Lifeact into discrete puncta also contrasted with shControl cells, which showed larger continuous regions of bright Lifeact. These images suggest that cells within intact tissues exhibit increased turnover dynamics and reduced spatial

correlation of the actin cytoskeleton upon depletion of Dia1. LLSM enables resolution of these fine details of the cytoskeleton within multicellular structures.

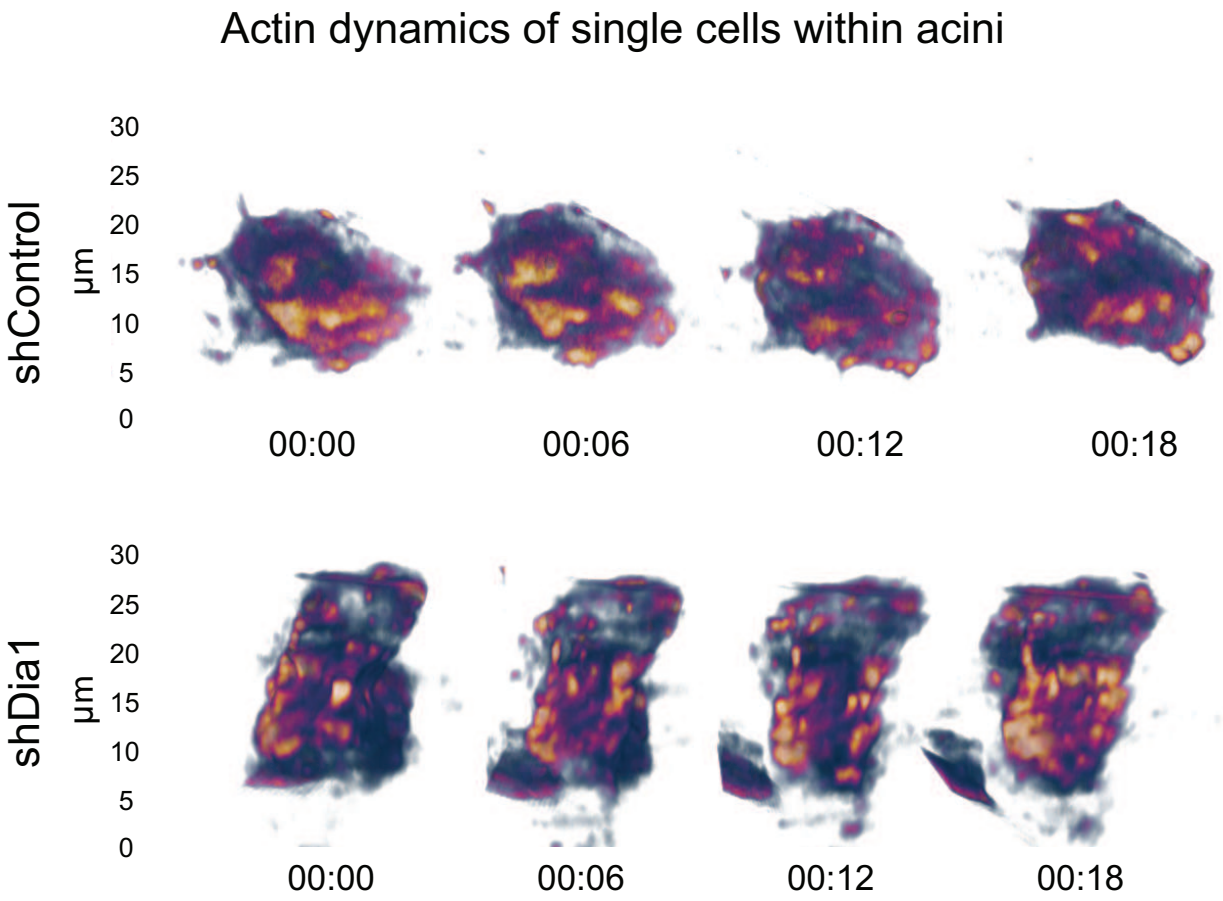

Figure 2.5. 3D rendering of a time-lapse comparing individual MDCK cells within acini expressing GFP-Lifeact and a control shRNA (top) or an shRNA targeting the cytoskeleton regulator Dia1 (bottom). Each cell is oriented to show its basal surface, in contact with the collagen gel. Representative renderings are shown for 4 time points out of 40 total taken. GFP-Lifeact intensity is scaled to show bright patches in yellow/orange and dimmer areas in magenta/purple. Images were collected at 3 minute intervals.

2.3.4 Monitoring cell deformations of collagen fibrils

Beyond imaging fluorescent proteins expressed by cells, LLSM is well-suited to capture fluorescent dyes conjugated to proteins. Its low power and high sensitivity aid in reducing bleaching of these dyes, which are not continuously expressed by cells and therefore have a limited lifetime. We used Collagen 1 conjugated with Alexa fluorophores to monitor the interactions between MDCK acini and their surrounding collagen gel. We plated wild type MDCK acini expressing GFP-Lifeact in labeled collagen and stimulated acini with HGF to

induce collective cell motility. LLSM was able to resolve individual collagen fibrils, and capture their deformations as cells moved within the acinus (Figure 2.6). These images reveal the range of complex deformations in the collagen matrix in response to cell movements.

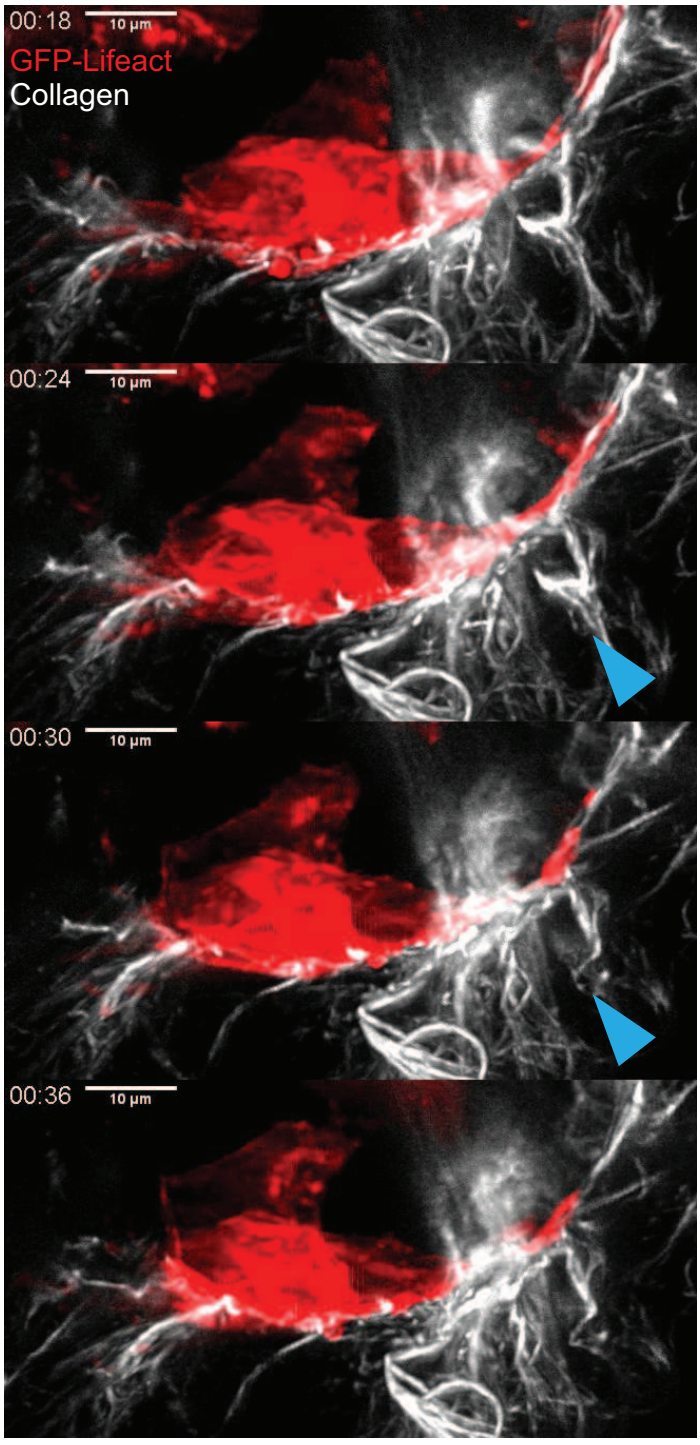

Figure 2.6. Montage showing time lapse imaging of an MDCK cell within an acinus and Collagen 1 at 6 minute intervals. Image z-stacks are shown in maximum projections. GFP-Lifeact is shown in red, Collagen 1 is in white. As the cell moves toward the left, its adhesion to the collagen gel causes deformations and rearrangements. Arrowheads show areas of the collagen gel altered as the cell moves.

2.3.5 Comparison of confocal and lattice light sheet microscopy

Finally we imaged a regulatory component of myosin, myosin light chain (MLC), fused to the fluorescent protein mCherry. We compared live imaging of MLC using LLSM and conventional spinning disk confocal imaging. Our results show that MLC undergoes clustering dynamics at the basal cortex of MDCK acini stimulated with HGF. As shown in Figure 2.7, subcellular patches of MLC grow over minutes in size and intensity, before their eventual disassembly. Using confocal microscopy to image acini in the same conditions, we could resolve small puncta of MLC and track their location. However, the spatial dynamics of MLC clusters were less easily resolved. These images suggest that the increased sensitivity of LLSM enables finer resolution of the true shape of subcellular structures. With higher sensitivity, complex shapes can be readily resolved over time. Meanwhile, confocal microscopy captures a bright spot of MLC and can track its lifetime, but does not resolve its true shape.

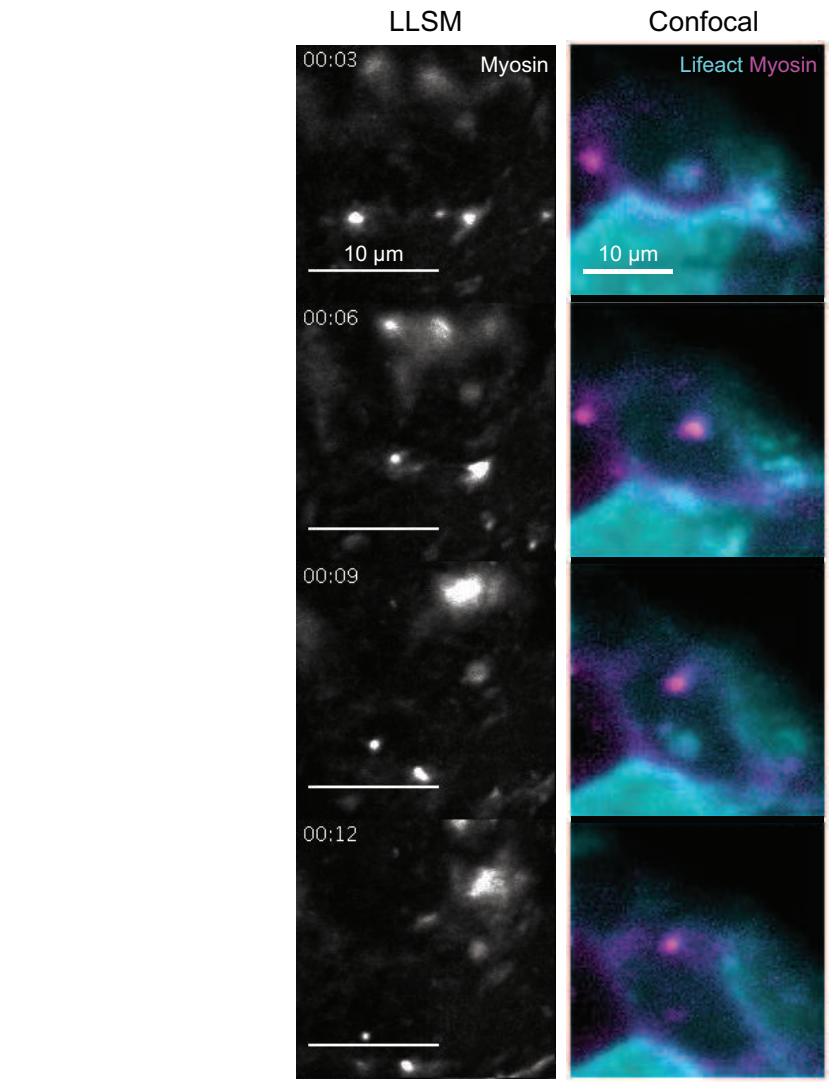

Figure 2.7. Time-lapse montage using LLSM and confocal microscopy to image myosin in MDCK cells expressing Myosin Light Chain tagged with mCherry. Acini of wt MDCK cells were plated in collagen gels and stimulated with HGF before imaging. LLSM imaging shows large, dim areas that coalesce into a bright, dense cluster at the top of the frame. Confocal imaging shows the appearance and location of a similarly sized spot of myosin. For the confocal microscopy montage, GFP-Lifeact was imaged simultaneously (in cyan) to highlight colocalization with myosin. Images for both were collected at 3 minute intervals.

2.3.6 Conclusion

Together these data point to the benefits of advanced imaging modes developed to improve spatial resolution and phototoxicity limitations that limit confocal microscopy. LLSM images shown here demonstrate its advantages in resolving individual cell shapes within acini, spatiotemporal dynamics of subcellular actin and myosin pools, and deformations across complex collagen structures occurring during cell motility. Each of these offers helpful lessons for the study of cell motility within complex 3D environments.

Despite these gains, the practical uses of LLSM are limited. Namely, the technique produces many terabytes of data per imaging experiment. Thus the imaging advantages it offers come a high cost, ensuring that cannot easily supplant conventional confocal imaging. The specific advantages of LLSM can help resolve otherwise intractable issues in imaging, but are not undertaken lightly. As a complement to confocal imaging, however, the selective use of LLSM allows greater insight into subcellular mechanisms that underlie multicellular behaviors. As such, its strategic use can directly address outstanding questions that confocal imaging leaves unexplored.

CHAPTER 3
FORMIN-DEPENDENT ADHESIONS ARE REQUIRED FOR INVASION BY EPITHELIAL TISSUES

3.1 Abstract

Developing tissues change shape, and tumors initiate spreading, through collective cell motility. Conserved mechanisms by which tissues initiate motility into their surroundings are not known. We investigated cytoskeletal regulators during collective invasion by mouse tumor organoids and epithelial Madin Darby Canine Kidney (MDCK) acini undergoing branching morphogenesis. Inhibition of formins, but not Arp2/3, prevented the formation of migrating cell fronts in both cell types. MDCK cells depleted of the formin protein Dia1 formed polarized acini and could execute planar cell motility, either within the acinus or in 2D scattering assays. However, Dia1 was required to form protrusions into the collagen matrix. Live imaging of actin, myosin, and collagen in control acini revealed adhesions that deformed individual collagen fibrils, while Dia1-depleted acini exhibited unstable adhesions with minimal collagen deformation. This work identifies Dia1-mediated adhesions as essential regulators of tissue shape changes, through their role in focal adhesion maturation.

3.2 Introduction

Tissue shape changes encompass multiple developmental and pathological processes. In order to form branched tubular networks, developing tissues such as mammalian vasculature or the *Drosophila* trachea undergo extensive elongation and remodeling known as branching morphogenesis [64, 62, 63]. In many cases, branching morphogenesis is initiated when growth factors stimulate a few individual cells within the developing tissue to extend protrusions that adhere to the surrounding extracellular matrix (ECM). These cells subsequently lead cohorts of their neighbors out of their initial site, migrating collectively through the ECM

to form extensively branched tubules [9, 75]. Malignant tissue can exhibit similar, if deregulated, shape changes during local invasion from the site of tumor formation [48]. Invasion by tumors is often accomplished by collective cell migration, in a manner that frequently mimics development [199, 69]. In both developmental and pathological contexts, shape changes undertaken by tissues rely on the coordination of cell motility and cell adhesions to neighboring cells and the ECM.

An outstanding question is how tissues transition from compact structures dominated by cell-cell adhesions to invading cohorts of cells that interact extensively with their ECM. A well-established framework describing the acquisition of invasive behaviors is the epithelial-mesenchymal transition (EMT) [97]. EMT comprises a gene regulatory program that simultaneously suppresses cells epithelial traits while activating mesenchymal traits, thereby stimulating invasion. However, EMT does not adequately describe tissue shape changes when epithelial traits such as cell-cell adhesion are maintained [9, 227, 38]. In these cases, a partial or transient EMT has been proffered to account for invasive behaviors exhibited by intact tissues [228, 48, 7, 75, 229]. But this model leaves unclear how the partial loss or gain of epithelial or mesenchymal traits, respectively, can orchestrate collective cell invasion [76, 101]. For example, cell movements within tissues are required in some cases to maintain epithelial homeostasis, [230, 231, 63] but in other cases to drive branching morphogenesis [65]. Thus we lack precise mechanisms to describe how motility and adhesions to the ECM are shifted in individual cells to accomplish tissue shape changes.

Cell motility and adhesions rely on the actin cytoskeleton, which is organized in space and time into protrusive, contractile and adhesive organelles [109]. Protrusion of the cells leading edge is typically driven by Arp2/3mediated lamellipodia [118, 119]. Proximal to the lamellipodia, within a RhoA-dependent lamella, actomyosin networks construct actin bundles and generate contractile forces. Coordinated with the actin cytoskeleton is the assembly and modification of focal adhesions, which serve as sites of biochemical signaling and as mechanical linkages between the cell and its surroundings [118, 112]. Focal adhe-

sions assemble within the lamellipodia [158], but undergo increases in size and changes in composition in a maturation process that relies on Rho effectors Myosin II [176] and Dia1 [174, 170]. Focal adhesion maturation has been extensively studied in cells on 2D planar surfaces, and exerts context-dependent effects on matrix deposition, front-rear polarity, and migration speed [183, 186, 170, 185, 184]. In fibrillar 3D environments, focal adhesion morphology is significantly altered and the role of focal adhesion maturation is less well-defined [192, 189, 190, 193]. While branching morphogenesis and tumor invasion require canonical focal adhesion components, [48, 104, 105, 106], the mechanism underlying their regulation is not known.

We used 3D culture and organotypic models to dissect the contributions of cytoskeletal organelles to tissue shape changes. A tractable *in vitro* model to study the regulation of tissue remodeling is provided by Manin Darby Canine Kidney (MDCK) cells undergoing branching morphogenesis. MDCK cells cultured in 3D matrices form hollow acini that resemble simple cuboidal epithelial tissues [92]. These undergo robust and well-described branching morphogenesis in response to Hepatocyte Growth Factor (HGF) [95]. Using pharmacological inhibitors, we found that branching morphogenesis requires the activity of formins but not Arp2/3. Tumor explants from mice confirmed that formins were also required for multicellular invasion. We found that the formin isoform Dia1 was dispensable for growth and polarization of MDCK acini and, interestingly, Dia1 depletion did not affect HGF-mediated planar cell motility in either cell scattering assays or cell motility within acini. Rather, Dia1 was selectively required for cells to form stable, mature adhesions and deform collagen fibrils during the initiation of branching morphogenesis. Interestingly, we found that adhesion sites to collagen fibrils contained both actin and myosin II, whose accumulation coincided with force generation on collagen fibrils. Dia1-depleted cells exhibited unstable myosin-rich adhesions, coincident with the loss of dense puncta and linear bundles of actin at the basal cortex. Thus, Dia1 conditions tissue shape changes by controlling the stabilization of cell-collagen adhesions.

3.3 Results

3.3.1 Formin activity is required for invasion and branching morphogenesis

To explore the roles of Arp2/3 and formins in tissue shape changes, we used two cell models: Manin-Darby Canine Kidney (MDCK) acini undergoing branching morphogenesis, and invasive motility by murine tumor explants. Single MDCK cells embedded in Matrigel grew into polarized acini with clear lumens over 4-5 days. Using a protocol modified from Rubashkin et al, we isolated acini and plated them intact into 2 mg/ml collagen gels [181]. Once plated in collagen, acini remained quiescent for at least 1 week or could be induced to undergo branching morphogenesis by the addition of 20 ng/ml Hepatocyte Growth Factor (HGF) (Materials and Methods). After 48 hours, branching morphogenesis resulted in multiple protrusive fronts extending into the collagen gel from each acinus. These protrusions started as extensions by single cells which then lengthened to form chains and tubules of cells, as shown by phalloidin staining for actin (Figure 3.1). The size and growth rate of protrusions we observed agreed with the stages of branching morphogenesis described previously[95, 96].

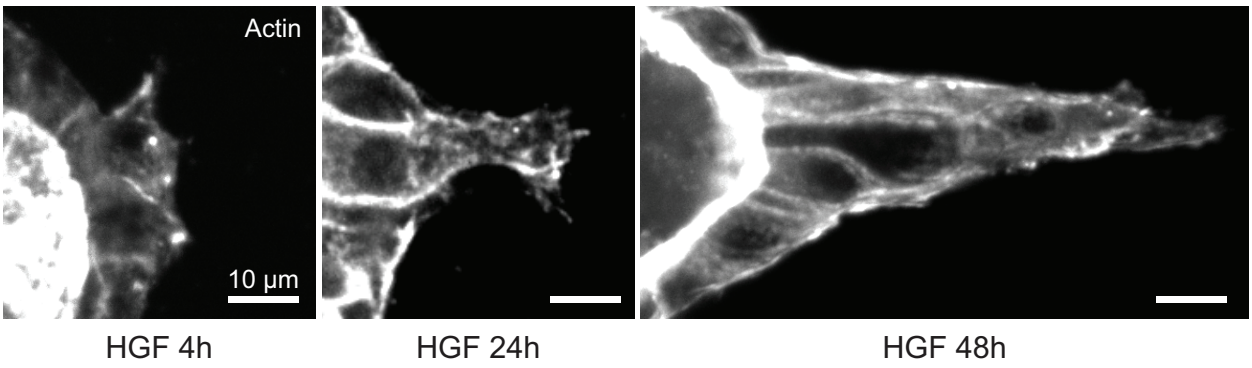

Figure 3.1. Growth of protrusions during branching morphogenesis. MDCK acini plated in collagen were stimulated with 20ng/ml Hepatocyte Growth Factor (HGF) for the durations indicated. Acini were fixed and stained with phalloidin. Shown are representative images of cell protrusions into the collagen gel at 4, 24, and 48 hrs following HGF addition.

To explore the role of Arp2/3 and formins in regulating branching morphogenesis, we treated acini with the Arp2/3 inhibitor CK666 [128] or the pan-formin inhibitor SMIFH2 [232]. Phalloidin staining in control acini, prior to branching morphogenesis, revealed that

F-actin was localized exclusively to the cell membranes. The apical surface was marked by a dense band of actin, due to the presence of microvilli as previously reported [83] (Figure 3.2B, i). Addition of 20 ng/ml HGF resulted in prototypical branching morphogenesis (Figure 3.2B, iv). Treatment with 50 μM CK666 in the absence of HGF caused individual cells to bulge within acini, as evidenced by convex curvature at the apical membrane (Figure 3.2B, ii). This suggested an acute polarity defect, consistent with reported roles for Arp2/3 in forming polarized membrane domains [93]. However, stimulating acini with HGF in the presence of CK666 did not prevent acini from forming multiple protrusions into the collagen gel even as cell morphology remained perturbed (Fig 3.2B, v). In contrast to Arp2/3 inhibition, treating acini with 30 μM SMIFH2 did not appreciably alter acinar morphology relative to controls (Figure 3.2B, iii). When stimulated HGF, however, SMIFH2-treated acini did not form any discernable protrusions into the collagen gel. Rather, these acini were indistinguishable from untreated controls (Figure 3.2B, vi).

We scored the ability of cells to respond to HGF in the above conditions by counting protrusive structures, whether by single cells or multicellular chains or branches invading into the collagen gel. This confirmed that SMIFH2, but not CK666, prevented protrusion formation in response to HGF (Figure 3.2C). Together, these data demonstrate that Arp2/3 activity is dispensable for invasion during branching morphogenesis, despite its role in polarity signaling. Meanwhile, formin activity is dispensable for acinar morphology, but required for formation of HGF-mediated invasion into the surrounding collagen matrix.

To confirm the generality of these results, we performed invasion assays with primary tumor organoids from mice. Tumors from the Murine Mammary Tumor Virus-Polyoma Middle-T (MMTV-PyMT) mouse strain comprise heterogeneous cell populations, do not form a basement membrane, and do not require a defined signal to stimulate invasion into collagen gels [41, 233]. Mice with advanced tumors were sacrificed and tumor tissue was harvested and digested into multicellular organoids. Organoids were first cultured in Matrigel for 48 hours in low-serum media, then replated intact into collagen gels. To stimulate

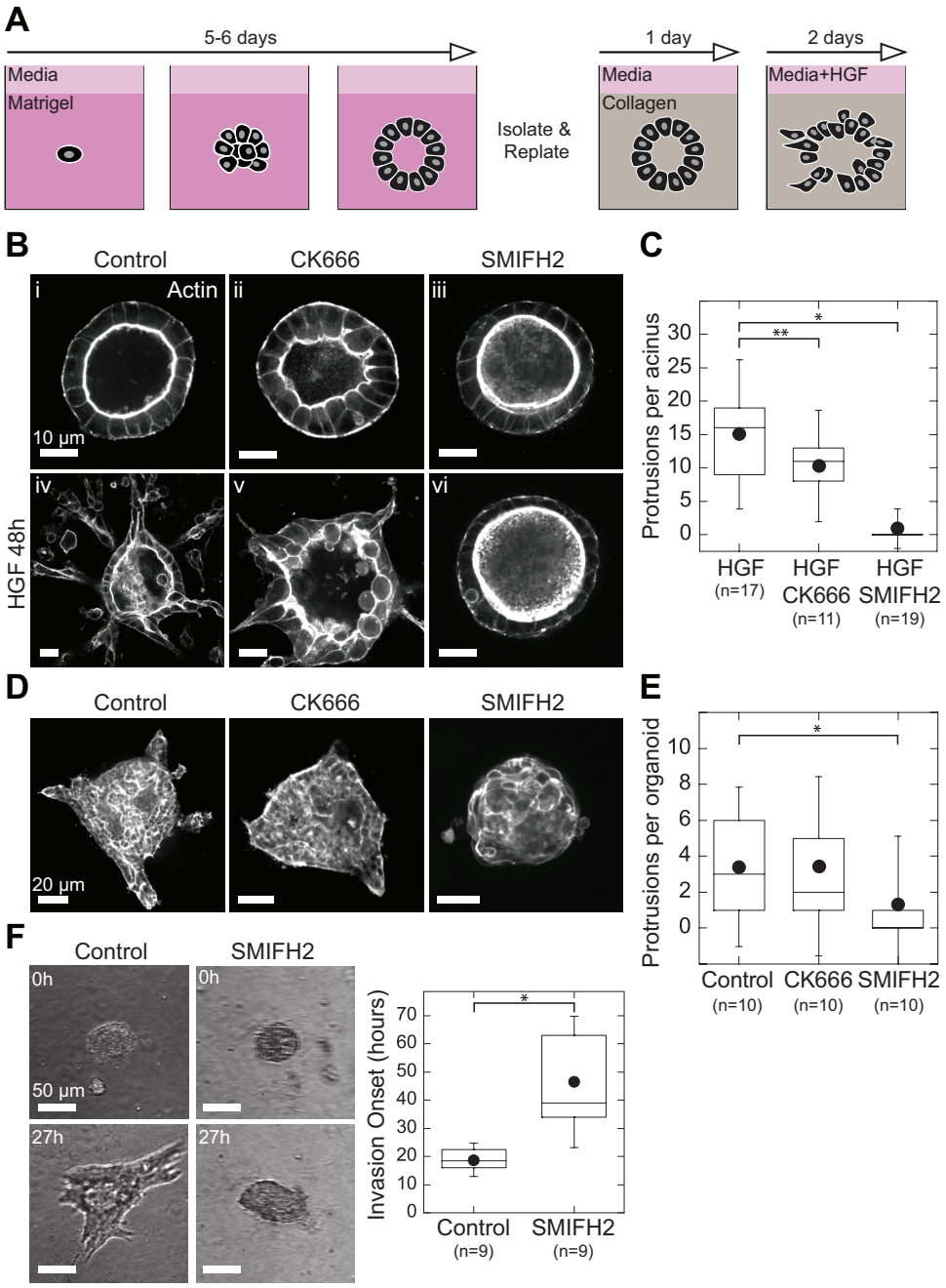

Figure 3.2. Formin activity is required for invasion and branching morphogenesis. Strategy for 3D culture and branching morphogenesis of Manin Darby Canine Kidney (MDCK) acini. Bi-iii, Equatorial confocal sections of MDCK acini showing phalloidin stain for f-actin. Acini were plated in collagen and treated with 50 μM CK666 or 30 μM SMIFH2 for 48 hrs. Biv-vi, F-actin in acini treated for 48 hrs with 20 ng/ml Hepatocyte Growth Factor (HGF) with or without the indicated inhibitors. C, Box plot of protrusions formed per acinus in each condition. D, Mouse mammary tumors from MMTV/PyMT mice. Tumors were harvested and digested, and resulting organoids were plated directly in collagen gels and treated with serum alone or with 50 μM CK666 or 30 μM SMIFH2, then fixed after 24 hrs. Shown are equatorial confocal sections of phalloidin stain for f-actin. E, Box plot of protrusions per organoid, with number of organoids scored indicated below. F, Organoids were plated in collagen, treated with serum alone or with 30 μM SMIFH2, and imaged in brightfield for 72 hrs by time lapse microscopy. Invasion onset was scored as the time of initial extension into collagen gel and plotted in box plot with number of organoids scored indicated below. Box plots show the 25th and 75th percentiles and the median, circle indicates mean, and whiskers mark 1.5 standard deviations. Single asterisk indicates $p<0.01$, double asterisk indicates $p<0.05$, by a Student's two tailed t-test assuming unequal variance.

invasion, media containing serum was added and after 24 hours tumor organoids were fixed to visualize the actin cytoskeleton. Control organoids were uniformly invasive, extending multicellular fronts into the collagen matrix (Figure 3.2D). Inhibition of Arp2/3 did not affect the total number of fronts per organoid. However, SMIFH2-treated organoids did not form invasive fronts after 24 hours (Figure 3.2E). To clarify the motility defects rendered by formin inhibition, we analyzed invasion in tumor organoids via time-lapse imaging. Cells in control and SMIFH2-treated tumor organoids appeared to actively rearrange over 48 hours. However, by 20 hours after plating, control organoids had formed subcellular extensions from which collective invasion proceeded. Formin inhibition prevented organoids from generating such extensions until ˜40 hours following plating (Figure 3.2F).

Collectively, these data implicate formin activity as a previously unappreciated determinant of both branching morphogenesis by MDCK acini and collective invasion by mouse tumor organoids. In MDCK acini, formin activity appears to be dispensable for cell shape and acinar homeostasis prior to HGF stimulation. However, in both acini and tumor organoids, formin inhibition blocked tissue shape changes by preventing the formation of the invasive fronts into the surrounding collagen matrix.

3.3.2 Dia1 and FHOD1 are required for branching morphogenesis

Because SMIFH2 is a pleiotropic inhibitor of formins [232], we sought to identify formin family members required for invasion. We initially chose to explore the roles of three formin family members: Diaphanous 1 (Dia1), Diaphanous 2 (Dia2), and Formin Homology 2 Domain Containing 1 (FHOD1). We and others have previously established roles for Dia1 in cell motility and focal adhesion maturation [170, 176]. Like Dia1, Dia2 is activated by Rho and participates in stress fiber formation but is also implicated in cytokinetic ring formation [172, 234]. FHOD1 is a noncanonical formin activated through Rac that has been shown to bind ROCK and participates in focal adhesion maturation ([160, 144]. shRNA constructs targeting these genes reduced the expression to 45-50% of control levels (Figure 3.3A).

Stable cell lines expressing each of these shRNA constructs could proliferate in 2D culture and in Matrigel. After replating acini from each into collagen gels, we fixed and stained them to analyze acinar morphology and actin architecture. While shDia1 and shFHOD1 cells could form acini with cleared lumens, shDia2 cells formed acini of aberrant shapes without clear lumens (Figure 3.4A, top row).

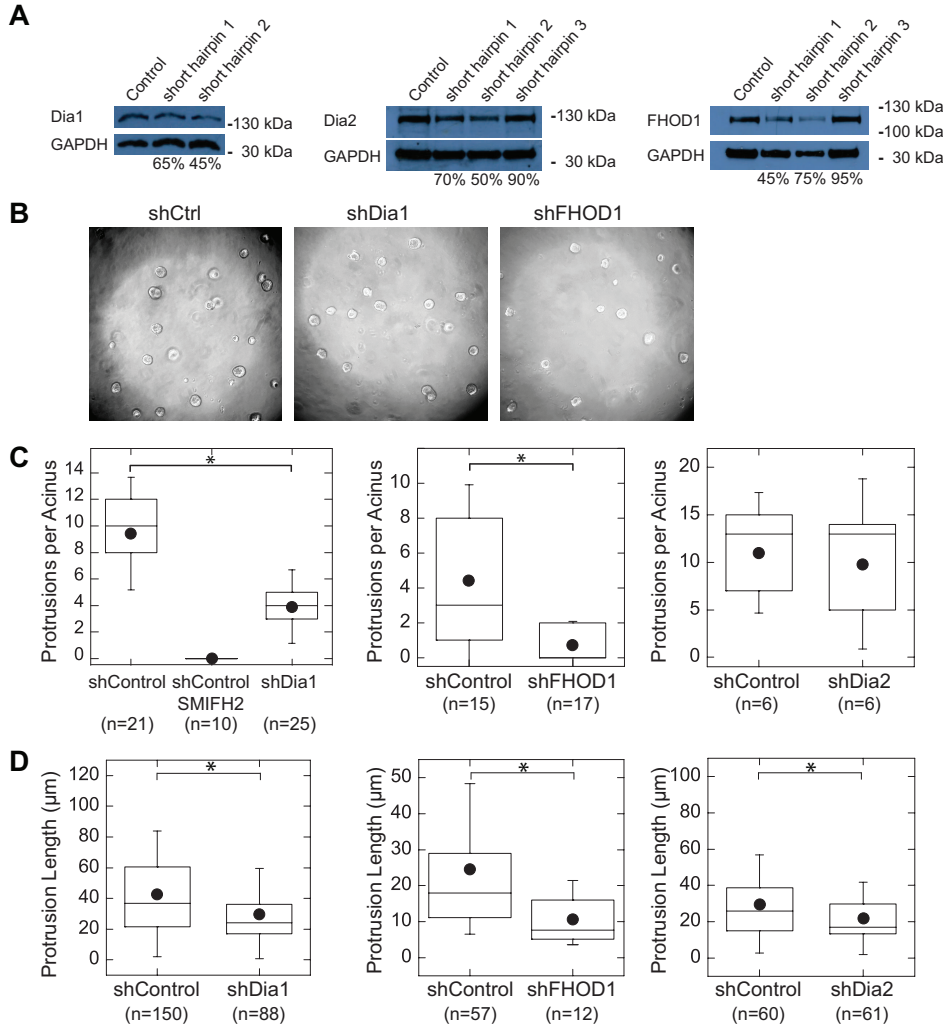

Figure 3.3. Knockdown of formin genes by shRNA. A, Western blots for the indicated proteins after knockdown. Percentages indicate protein remaining relative to Control, calculated by densitometry. B, Sample images of acinar growth after 6 days in Matrigel. C, Box plots showing protrusions per acinus for each knockdown and its matched control, following treatment with 20 ng/ml HGF for 48 hrs. Protrusions were scored as cell extensions greater than 5 μm. D, Box plots of protrusion length for each knockdown and its matched control. Box plots show the 25th and 75th percentiles and the median, circle indicates mean, and whiskers mark 1.5 standard deviations. Single asterisk indicates $p<0.01$ by a Student's two tailed t-test assuming unequal variance.

To test their capacity to undergo branching morphogenesis, we treated acini from each cell type with 20 ng/ml HGF. After 48 hours, shDia1 and shFHOD1 acini formed signifi-

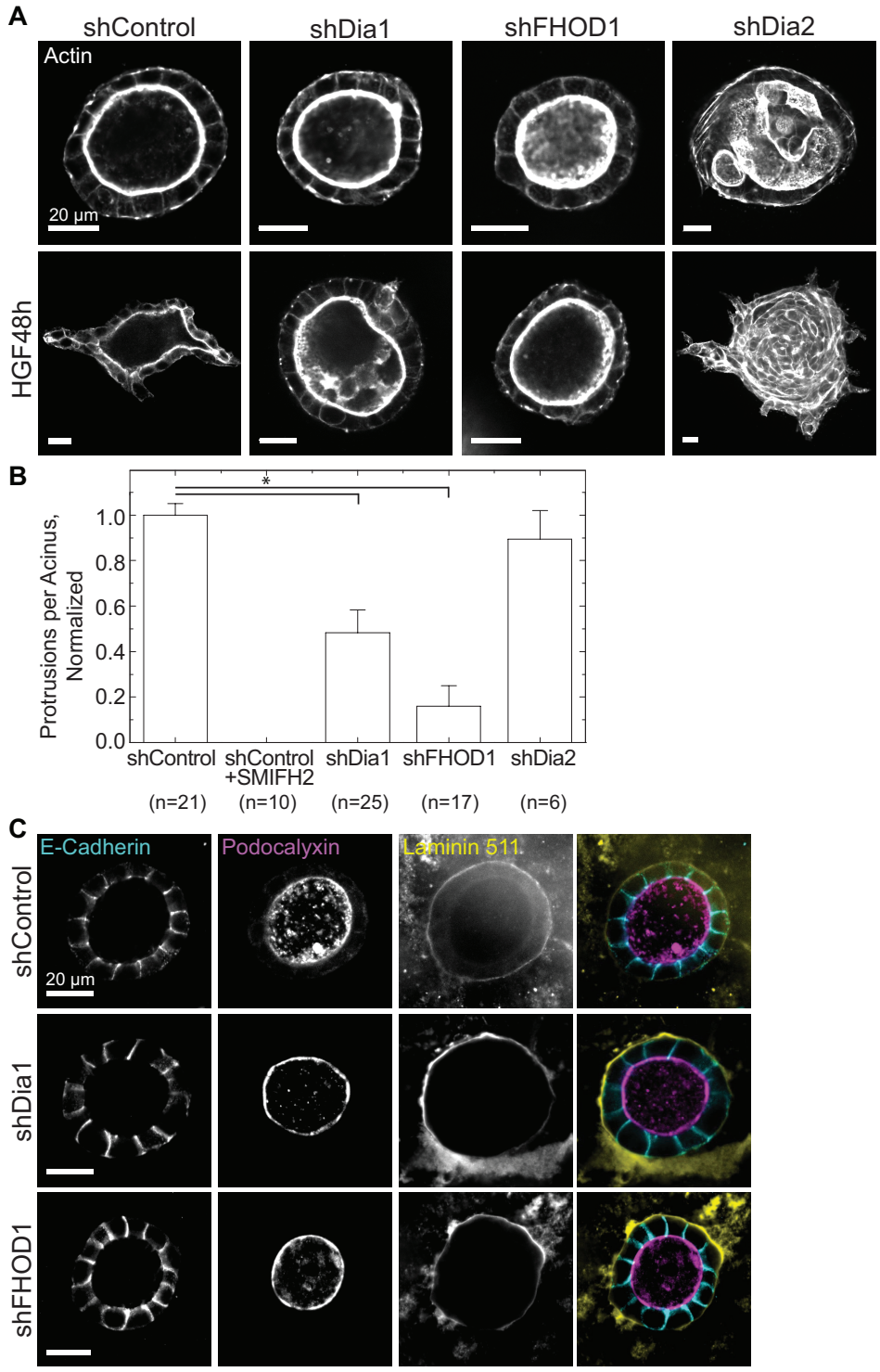

Figure 3.4. Dia1 and FHOD1 are required for branching morphogenesis Equatorial confocal sections of actin stain in acini of each genotype prior to (top) and following stimulation with HGF for 48 hrs (bottom). B, The number of protrusions per acinus relative to matched shControl acini; number of acini scored indicated below. SMIFH2 treatment serves as a negative control. C, Equatorial confocal sections of acini stained for E-cadherin to mark cell-cell junctions, podocalyxin to mark the apical surface, and the basement membrane component Laminin 511 in acini generated from control (top), shDia1 (middle) and shFHOD1 (bottom) cells. Asterisk indicates $p<0.01$ by a Student's two tailed t-test assuming unequal variance.

cantly fewer invasive protrusions relative to shControl acini (Figure 3.4A, bottom row). We analyzed protrusions as above and compared the average number of protrusions formed per acinus in each genotype. Combining data from all acini showed a significant decrease in protrusions formed by shDia1 and shFHOD1 acini, but not shDia2 acini, relative to matched controls (Figure 3.4B). When protrusion lengths were measured across these conditions, we found that the protrusions formed by shDia1 and shFHOD1 acini were shorter on average than matched controls (Figure 3.3D).

Although they appeared morphologically similar to controls, knockdown of Dia1 and FHOD1 may still alter cell polarity within the acini. To test for polarity defects in shDia1 and shFHOD1 acini we stained for E-cadherin, Podocalyxin, and Laminin 511 by immunofluorescence. Localization of these proteins to lateral, apical, and basal surfaces, respectively, resembled that in control acini (Figure 3.4C). These results suggest that as they develop and polarize, shDia1 and shFHOD1 acini could generate and orient an apical domain, marked by podocalyxin, and form adherens junctions, marked by E-cadherin. After replating in collagen, these acini also deposited basement membrane laminins similar to their control counterparts.

We conclude from these data that depletion of Dia1 and FHOD1 does not impair the growth and polarization of acini. These formins are, however, required to initiate branching morphogenesis by establishing and elongating protrusions into the collagen gel. In contrast, Dia2 is required for normal acinar development but is dispensable for generating invasive protrusions in response to HGF. Dia1 and FHOD1 appear to play nonoverlapping roles, perhaps due to their differing upstream activators. We were interested in the role played by Dia1 because another RhoA effector, ROCK, is known to restrict rather than promote protrusions in response to HGF [95]. This suggests that these two RhoA effectors may play competing roles in controlling branching morphogenesis. We therefore sought to clarify the role of Dia1.

3.3.3 Dia1 is dispensable for HGF-mediated planar motility in 2D and within acini

Branching morphogenesis requires that cells migrate into the surrounding collagen matrix [95]. Previous work has shown the importance of Dia1 in establishment of a polarized leading edge for motility on 2D substrates [**?** 235]. Thus, one possibility is that a cell migration defect underlies the role of Dia1 in branching morphogenesis.

To test this hypothesis, we first used a cell scattering assay, in which HGF drives the dissociation of cell islands on glass coverslips into individual, highly motile cells [86]. We plated shControl and shDia1 MDCK cells on glass coverslips and serum starved them for 24 hours before adding 20 ng/ml HGF to stimulate scattering. Timelapse microscopy revealed that shDia1 cells could break cell-cell contacts and migrate as single cells similarly to shControl cells (Figure 3.5A). We tracked individual cells (Figure 3.5B) and found a modest reduction in the mean instantaneous speed of shDia1 cells, but no change in their persistence (Figure 3.5C). Thus, Dia1 may contribute to the ability to initiate scattering, but is dispensable for HGF-mediated motility in Figure 3.2D.

We next explored cell motility within acini. Cell rearrangements and rotation within 3D tissues have been reported *in vitro* [236], and can contribute to tissue morphogenesis [65, 237] and ECM deposition [231, 63]. We speculated that MDCK cells may exhibit similar in-plane motility prior to and, perhaps, during branching morphogenesis. To track cell motility within acini, we generated Dia1 knockdown cell lines and matched controls expressing the nuclear marker H2B-mCherry. Immediately after stimulating with HGF, we imaged acini from these cell lines via time-lapse confocal microscopy. Shortly after the start of imaging, shControl cells began moving within the acinus (Figure 3.5D). This motility resulted in rotation of the entire acinus, with occasional cell rearrangements and rare single cells moving independently of their neighbors. The cell motility within shDia1 acini was virtually indistinguishable from that of control acini (Figs. 3.5D). Analysis of individual cell tracks (Figure 3.5E) showed a decline in average instantaneous speed of shDia1 cells from 0.3 μm/min to 0.2 μm/min,

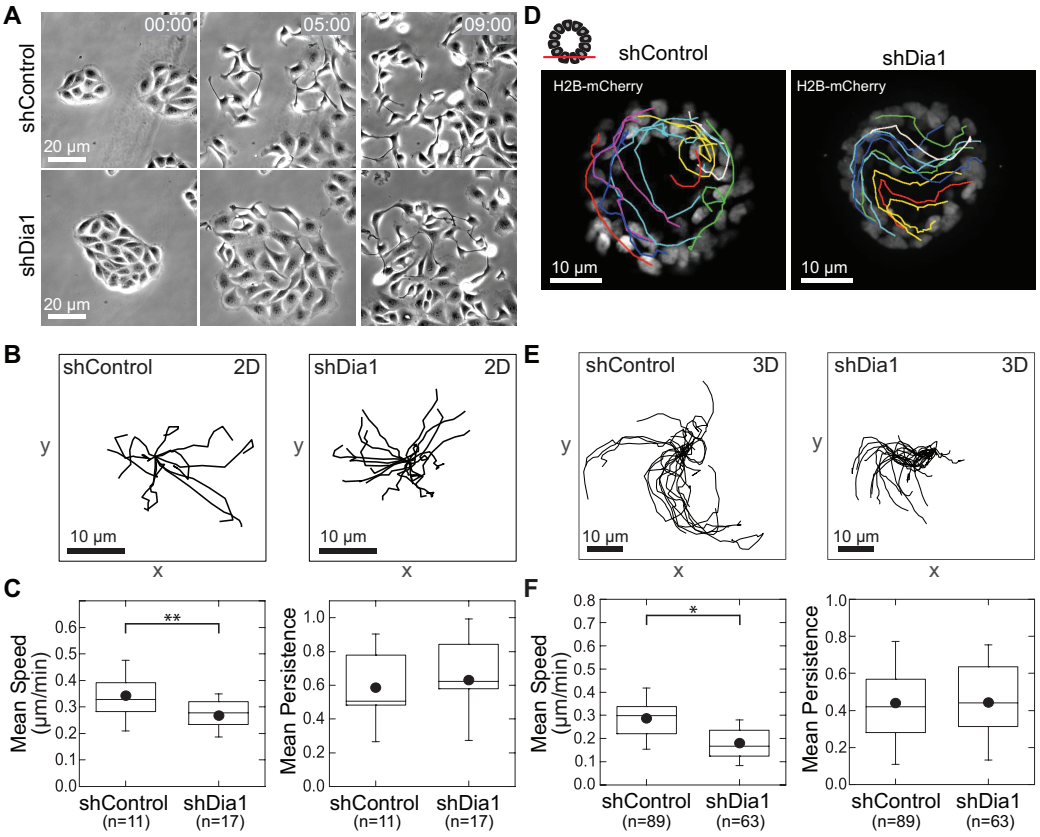

Figure 3.5. Dia1 is dispensable for HGF-mediated planar motility in 2D and within acini. Brightfield images at 0, 5, and 9 hrs of shControl and shDia1 cell islands scattering following 20ng/ml HGF addition at 0 hrs. Time is indicated in hr:min. B, Rose plots of 10 cell trajectories from the cell islands scattering in panel A and Video 2 over 9 hr. Initial location of each trajectory was positioned at (0,0). C, Box plots of instantaneous speed and persistence for shControl and shDia1 cells. D, Acini of shControl and shDia1 expressing H2B-mCherry. Acini were stimulated with 20 ng/ml HGF and imaged by timelapse fluorescence microscopy for 12 hrs. Shown are stills with individual tracks overlaid. E, Rose plots from cell trajectories obtained from panel D. F, Box plots of instantaneous speed and persistence to characterize cell motility, with number of cell trajectories obtained from at least 5 acini per condition indicated below. Box plots show the 25th and 75th percentiles and the median, circle indicates mean, and whiskers mark 1.5 standard deviations. Single asterisk indicates $p<0.01$, double asterisk indicates $p<0.05$ by a Student's two tailed t-test assuming unequal variance.

while average persistence did not change relative to shControl cells (Figure 3.5F).

These data show that in-plane cell motility driven by HGF, encompassing both scattering of small islands on 2D substrates and motility within acini, does not require Dia1. This suggests that HGF-mediated motility within the plane of a tissue or on 2D substrata is largely independent of Dia1. We next explored whether Dia1 regulates protrusions extending from acini into the surrounding collagen matrix.

3.3.4 Dia1 is required to stabilize protrusions into the collagen matrix

Defects in branching morphogenesis rendered by Dia1 depletion could arise from reduced formation of protrusions into the collagen matrix. Alternatively, reduced focal adhesion maturation could impair protrusion stability due to reduced adhesion to collagen fibrils.

To adjudicate between these hypotheses, we turned to time-lapse imaging in transmitted light and analyzed protrusive activity at the onset of branching morphogenesis. Following HGF stimulation, shControl acini extended narrow protrusions into the collagen gel over a period of tens of minutes (Figure 3.6A). All shControl acini imaged formed protrusions over 12 hours of imaging (Figure 3.6B). We analyzed protrusion lifetimes by measuring the duration over which protrusions remained before they underwent retraction. This analysis revealed that 60% of all protrusions retracted partially or completely within one hour (Figure 3.6C). A smaller proportion were stable for up to two hours, and 20% of protrusions were stable over several hours. These long-lived protrusions eventually mediated cell egress from control acini into the collagen matrix. Comparing the lifetime of each protrusion to its maximum length confirmed that the subpopulation of most stable protrusions grew to the greatest lengths of >20 microns (Figure3. 6D).

In contrast to control acini, shDia1 acini exhibited impaired protrusion stability (Fig 3.6A). While 50% of shDia1 acini formed protrusions, the distribution of protrusion lifetimes was weighted towards short protrusions lasting less than 90 minutes (Figure 3.6B and 3.4C). The loss of stable protrusions lasting >2 hours in shDia1 acini was matched by a reduction

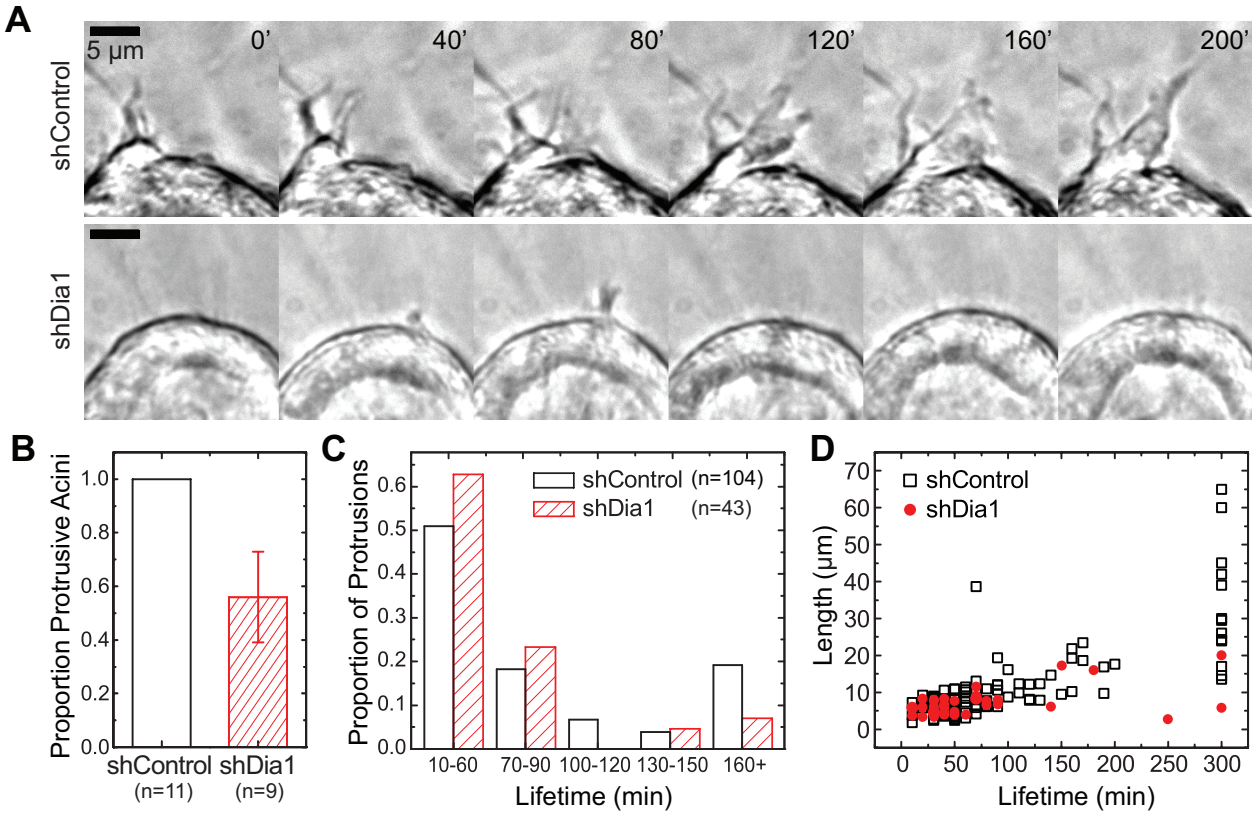

Figure 3.6. Dia1 is required to stabilize protrusions into the collagen matrix. Timelapse imaging in brightfield during initiation of branching morphogenesis, showing formation and growth of protrusions in shControl and shDia1 acini over a period of 200 min. Images were obtained starting 3 hrs after addition of 20 ng/ml HGF. B, The proportion of acini from each cell type that formed any protrusions over 12 hrs of imaging, with number of acini scored indicated below. C, Histogram summarizing the distribution of protrusion lifetimes from acini for each cell type, from movies obtained 1 hr after HGF addition. Number of protrusions scored indicated in legend. D, Plot of protrusion lifetime as a function of its maximal length for protrusions obtained in panel C.

in the maximum length they reached (Figure 3.6D). Meanwhile, protrusions lasting less than 90 minutes were indistinguishable between shDia1 and shControl acini (Figure 3.7A). To test whether this failure of protrusion stability caused motility defects that were cell-autonomous, we performed time-lapse imaging of single MDCK cells in collagen gels. This revealed a significant decrease in the motility of single shDia1 cells relative to their shControl counterparts following stimulation with HGF (Figure 3.7B and 3.7C).

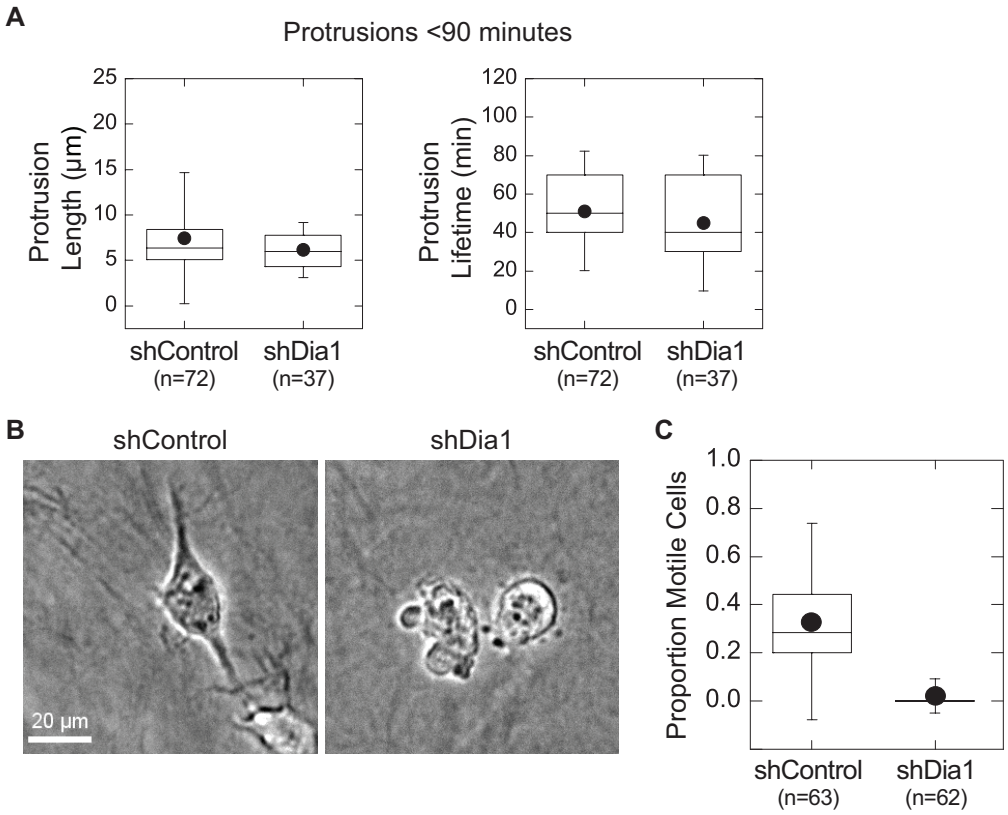

Figure 3.7. HGF-stimulated protrusions in collagen matrices. A, Box plots comparing only protrusions lasting less than 90 mins in shControl and shDia1 acini, taken from the data shown in Figure 3.6B-D. B, Brightfield images showing single MDCK cells in collagen gels and stimulated with 20 ng/ml Hepatocyte Growth Factor (HGF). Images were obtained 5 h after addition of HGF. C, Box plot of cell displacements over 8 hrs, with displacements exceeding 20 μm scored as motile. Number of cells scored indicated in legend. Box plots show the 25th and 75th percentiles and the median, circle indicates mean, and whiskers mark 1.5 standard deviations.

These data show that, under normal conditions, the early stages of branching morphogenesis are characterized by numerous small protrusions extending from the acinus into the surrounding collagen matrix. While a majority of these protrusions are unstable and retract within 90 minutes, a minority of protrusions adhere stably and extend into the collagen ma-

trix. The correlation observed between protrusion lifetime and maximum length indicates that protrusion growth depends acutely on their ability to adhere stably to collagen. Dia1 knockdown did not abolish protrusions, nor did it alter lifetimes and sizes of the short-lived protrusions relative to controls. Rather, Dia1 was required for protrusions to stably adhere to collagen matrix and subsequently elongate. These data therefore strongly suggest that Dia1 conditions branching morphogenesis through its role in focal adhesion maturation and stability.

3.3.5 Dia1 is required to adhere to and displace individual collagen fibrils

To test whether unstable protrusions observed in shDia1 acini resulted from an underlying adhesion defect, we used fluorescence live cell imaging to examine actin, myosin and collagen fibrils during cell protrusion. We imaged shControl and shDia1 acini coexpressing GFP-Lifeact and mCherry-tagged myosin light chain (MLC) plated in collagen matrices labeled with Alexa-647. After incubating acini for 4 hours in HGF, we captured fluorescence confocal images at the lower surface of acini juxtaposed to the collagen matrix. To better capture dynamic cell adhesions to collagen, we acquired images at 3 minute intervals for 3 hours. We noted passive responses of the collagen matrix as cells moved within acini. However we also observed shControl cells deforming single collagen fibrils at discrete points with displacements of ˜2 μm while leaving surrounding fibrils undisturbed (Figure 3.8A). We captured deformations within each field of view and found an average rate of one per hour per acinus (Figure 3.8C). Interestingly, we observed dense MLC puncta and increased actin intensity at sites of fibril deformation, which tracked the collagen fibril as it deformed over tens of minutes (Figure 3.8A).

We observed substantially fewer instances of acute collagen deformations in shDia1 acini, although nonspecific movements of the collagen matrix occurred as with controls (Figure 3.8B and). On average, we observed a three-fold decrease in collagen fibril deformations by shDia1 acini relative to controls (Figure 3.8C, left). When we scored only those deformations

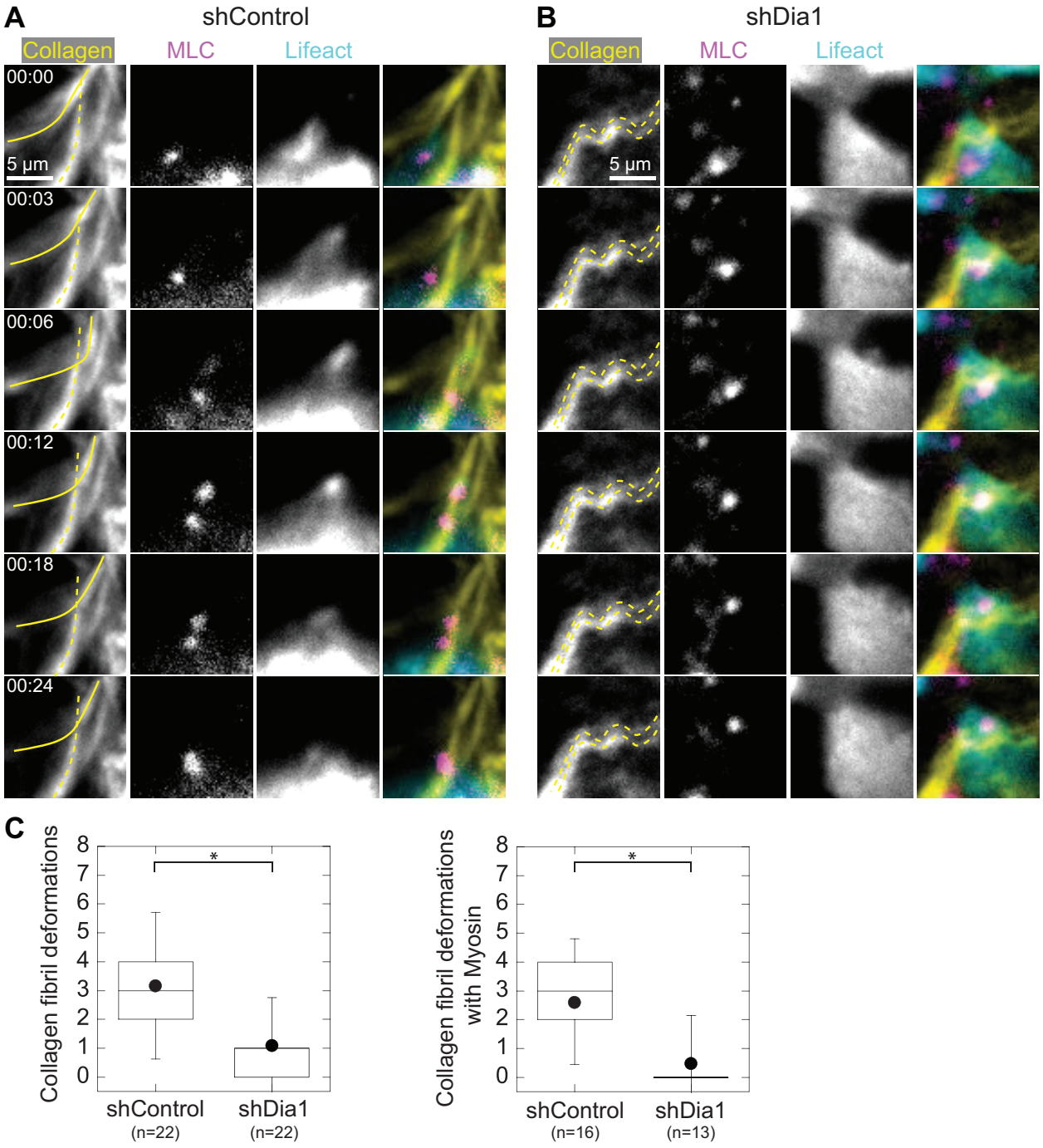

Figure 3.8. Dia1 is required to adhere to and displace individual collagen fibrils. A and B, Images at the basal acinar surface of GFP-Lifeact (cyan), mCherry-Myosin Light Chain (MLC, magenta) and Alexa-647 labelled collagen (yellow) obtained 4 hrs after addition of 20 ng/ml Hepatocyte Growth Factor (HGF) in (A) shControl acini and (B) shDia1 acini. Montage in (A) shows an example of shControl cell deforming a single collagen fibril, outlined in solid yellow line, over a period of 24 min. An unaffected fibril is outlined with a dashed line. B, Example of shDia1 cell showing collagen fibrils that remain immobile as a cell moves over them. C, Box plot indicating frequency of collagen fibril deformations, with number of acini scored indicated below. D, Collagen deformations at which MLC appeared or was recruited. Box plots show the 25th and 75th percentiles and the median, circle indicates mean, and whiskers mark 1.5 standard deviations. Asterisk indicates $p<0.01$ by a Student's two tailed t-test assuming unequal variance.

with coincident MLC puncta, these were even more suppressed in shDia1 acini relative to controls (Figure 3.8C, right).

These data identify Dia1-dependent interactions between cells and the collagen matrix during the earliest stages of HGF-stimulated protrusion. Adhesions to collagen are marked by dense myosin puncta through which cells deform single collagen fibrils while leaving surrounding fibrils unaffected. The planar motility observed in shDia1 acini suggests that Dia1 is not necessary for weak adhesion to collagen fibrils that can support planar motility and rotation, but is required specifically for adhesion to and contraction against collagen fibrils during the onset of branching morphogenesis.

3.3.6 Myosin colocalizes with Dia1-dependent adhesions

The observation that MLC accumulates into discrete puncta at sites of adhesion to collagen suggested that myosin-rich puncta are sites of focal adhesions. To confirm this, we imaged actin, myosin and collagen as leader cells protruded away from acini into the surrounding collagen 24 hours after stimulation with HGF. Leader cells advanced via bursts of actin, followed by the accumulation of MLC in puncta at the cell front (Figure 3.9A). MLC puncta at the cell front coincided with points of collagen fibril deformation.

To confirm these myosin-rich sites contained canonical focal adhesion proteins, we performed immunofluorescence staining for actin, myosin IIA, and either paxillin or phospho-tyrosine. These images revealed that actin and myosin-rich puncta within leader cells also contained paxillin and phospho-tyrosine (Figure 3.9B). We found that around half (0.48 $\pm$0.16, n=283) of all phospho-tyrosine positive puncta were also enriched in myosin IIA (Figure 3.10A). These observations confirm that focal adhesions along collagen fibrils retain a punctuate appearance and a subpopulation of them are rich in actin and myosin. While the myosin localization we observed contrasts with canonical descriptions of myosin exclusion from focal adhesions on planar 2D surfaces [120], our observations agree with reports identifying myosin recruitment at leading edge adhesions in some 2D and 3D contexts

[238, 239].

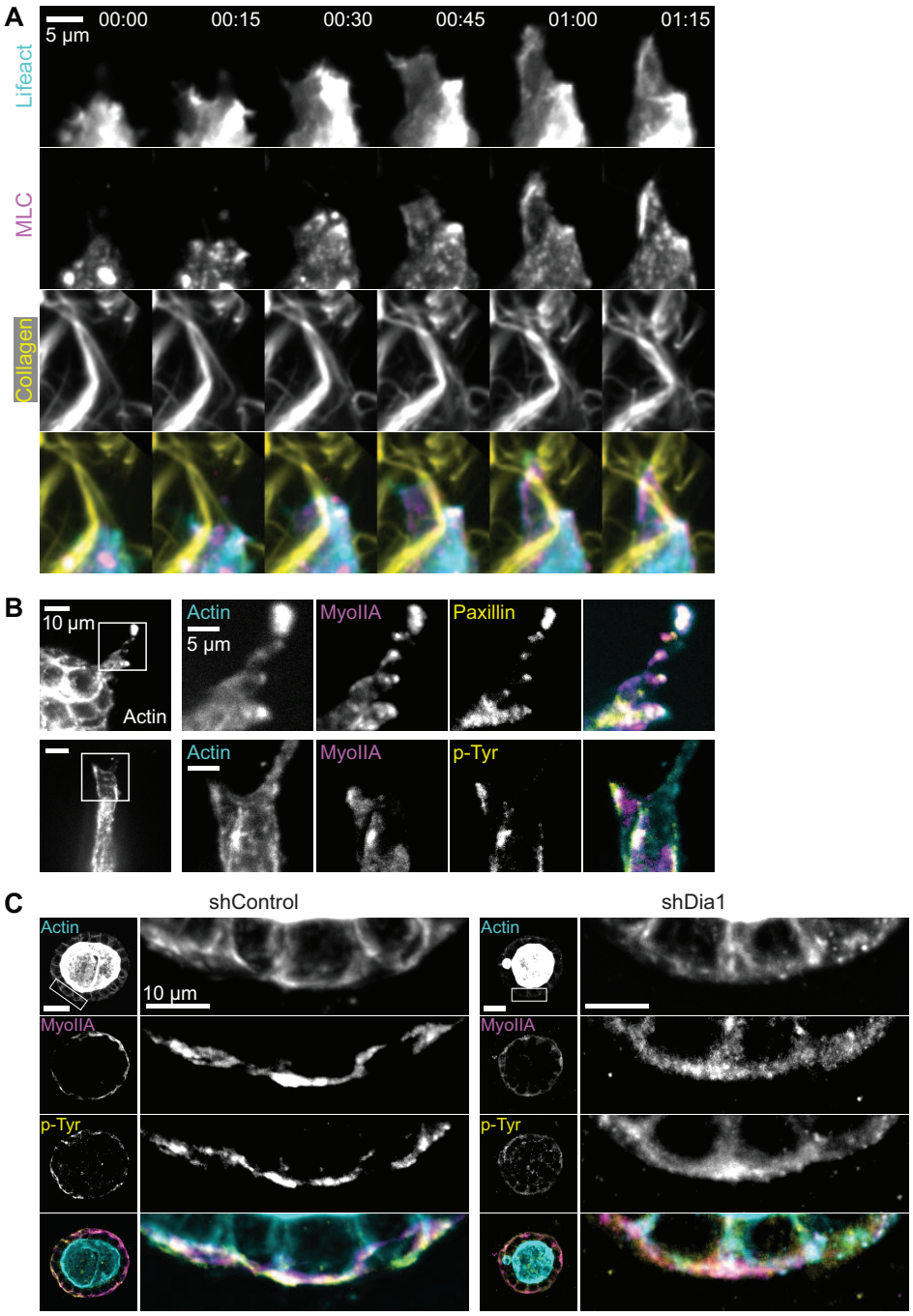

Figure 3.9. Myosin colocalizes with Dia1-dependent adhesions. A, Timelapse images of a leader cell protruding into the surrounding collagen matrix from an shControl acinus stimulated with HGF for 24 hrs. Images of GFP-Lifeact (cyan), mCherry-MLC (magenta) and Alexa-647 labelled collagen (yellow) are shown. Time is indicated in hrs:min. B, Immunofluorescence images of f-actin (cyan), Myosin IIA (magenta) and phospho-tyrosine (top row) or paxillin (bottom row), shown in yellow, in leader cells extending from shControl acini following stimulation with HGF for 48 hrs. C, Immunofluorescence images of f-actin (cyan), Myosin IIA (magenta) and phospho-tyrosine acini 4 hrs following stimulation with HGF, combined into maximum intensity projections spanning 3μm. Insets of the indicated boxed regions are shown at right. Scale bars, 10 μm.

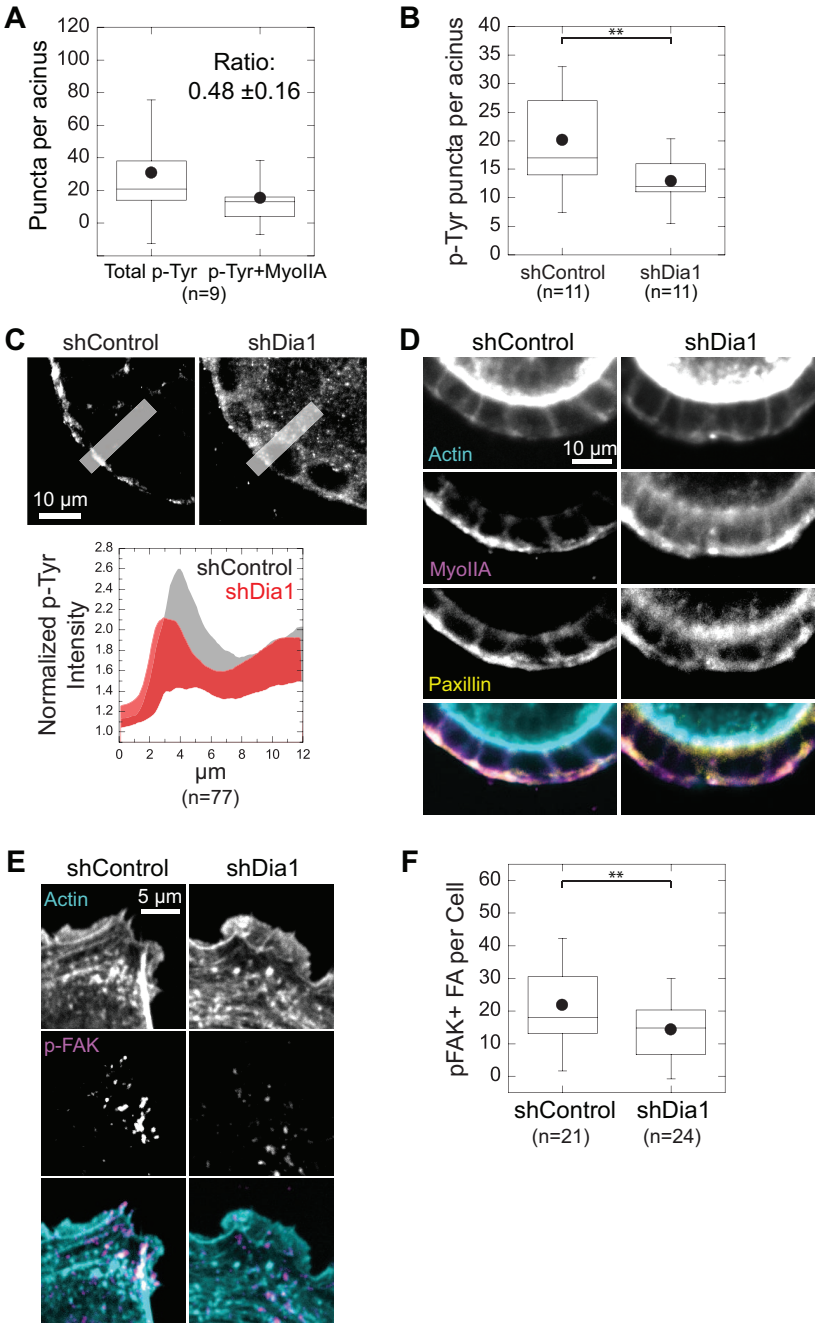

Figure 3.10. Analysis of focal adhesion components during branching morphogenesis. Box plots of total and myosin IIA-positive focal adhesions in n=9 acini, 48h following addition of 20 ng/ml Hepatocyte Growth Factor (HGF). B, Box plots comparing phospho-tyrosine-positive focal adhesions in shControl and shDia1 acini, 4 hrs following addition of HGF. Number of acini scored indicated in legend. C, Immunofluorescence images of phospho-tyrosine in shControl and shDia1 acini 4 hrs following addition of HGF, with red line indicating the regions measured by linescans. Plot shows the minima and maxima of 77 linescans in 11 acini per condition. D, Immunofluorescence images of shControl and shDia1 acini stained for f-actin (cyan), Myosin IIA (magenta), and Paxillin (yellow) at equatorial sections in shControl and shDia1 acini 4 hrs following addition of HGF. E, Immunofluorescence staining for f-actin (cyan) and p-FAK (magenta), in shControl and shDia1 cells undergoing scattering 6 hrs following addition of HGF. F, Box plot of p-FAK+ focal adhesions per cell, calculated from thresholded images of the cells shown in E. Number of cells indicated in legend. Box plots show the 25th and 75th percentiles and the median, circle indicates mean, and whiskers mark 1.5 standard deviations. Double asterisks indicate $p<0.05$ by Student's two-tailed t-test assuming unequal variance.

We next assessed the impact of Dia1 depletion on adhesion formation. Because shDia1 acini failed to form stable protrusions into the collagen matrix, we analyzed acini after 4 hours of HGF stimulation, when acinar rotation and collagen interactions can be observed. Acini were fixed and immunostained for actin, phospho-tyrosine and myosin IIA, and maximum intensity projections at the equatorial plane were analyzed. Phospho-tyrosine was enriched in dense puncta at the basal surface in shControl acini (Figure 3.9C, left). Meanwhile, phospho-tyrosine was diffusely distributed at the basal surface of shDia1 acini (Figure 3.9C, right), and organized into fewer discrete puncta per acinus (Figure 3.10B). This defect was accompanied by a redistribution of phospho-tyrosine away from the basal surface in shDia1 acini (Fig 3.10C), which was paralleled by myosin IIA and paxillin localization (Figure 3.10D). We confirmed these results by immunofluorescence staining for mature focal adhesions in cells scattering on glass coverslips. Consistent with prior reports (Oakes et al., 2012), shDia1 cells formed significantly fewer phospho-FAK-positive focal adhesions relative to shControl cells (Figure 3.10E and 3.10F).

These data demonstrate that a subset of adhesions to collagen fibrils are marked by actin and myosin-rich puncta. Myosin accumulation correlates with force generation against collagen fibrils. We find these adhesions do not form in the absence of Dia1, preventing stabilization of protrusive fronts into the collagen matrix. Dia1 has been previously shown to be essential for focal adhesion maturation on 2D surfaces [170], and we suspect that Dia1 plays a similar role here. Clearly, because Dia1 is not required for planar acini motility, adhesions to collagen are capable of forming, consistent with prior observations [170]. Rather, we hypothesize that Dia1-mediated focal adhesion maturation is necessary to form stable adhesions that facilitate the egress of cells away from the acini into the surrounding collagen.

3.3.7 Dia1 Regulates Actomyosin Organization and Dynamics of the Basal Cortex

Prior reports have demonstrated that formin-dependent stress fibers act as templates for the compositional and morphological maturation of focal adhesions [173, 160, 170]. We hypothesized that Dia1 performs a similar role at the basal actin cortex of acini, and may control focal adhesion maturation through its effects on actin architecture. Indeed, confocal sections of acini stained with phalloidin revealed striking differences in the organization of cortical actin between shControl and shDia1 acini. In the absence of HGF, cortical actin in shControl acini was organized into bundles often emanating from dense puncta in the middle of cells (Figure 3.11A, left). In shDia1 acini, the basal cortex was largely absent of such actin bundles and their associated puncta (Figure3. 11A, right). Instead, actin was diffusely spread across the cortex. These differences in basal actin organization remained after HGF stimulation, and were matched by altered myosin localization (Figure 3.11B). This confirmed an important role for Dia1 in regulating the organization of the basal actomyosin cortex of acini.

To explore changes in dynamics of the actomoysin cortex, we used timelapse fluorescence microcroscopy to image the basal surface of GFP-Lifact/MLC-mCherry acini (Figure 3.11C). We found MLC puncta in shControl remained immobile in cells moving within the plane of the acinus over tens of minutes (Figure 3.11C). By contrast, MLC puncta in shDia1 were more dynamic, undergoing assembly and motion over similar time intervals (Figure 3.11C). Using a threshold of 12 minutes without displacement to distinguish immobile from mobile MLC puncta, we found that shControl acini formed three-fold more immobile MLC puncta relative to shDia1 acini (Figure 3.11D).

How do individual cells adhere to and migrate along collagen fibrils in the midst of ongoing planar motility within the acinus? During acinar rotation, we observed isolated instances of multiple cells forming MLC puncta at the same location on collagen fibrils as they encountered it in sequence (Figure 3.11E). Interestingly, the next cell encountering the

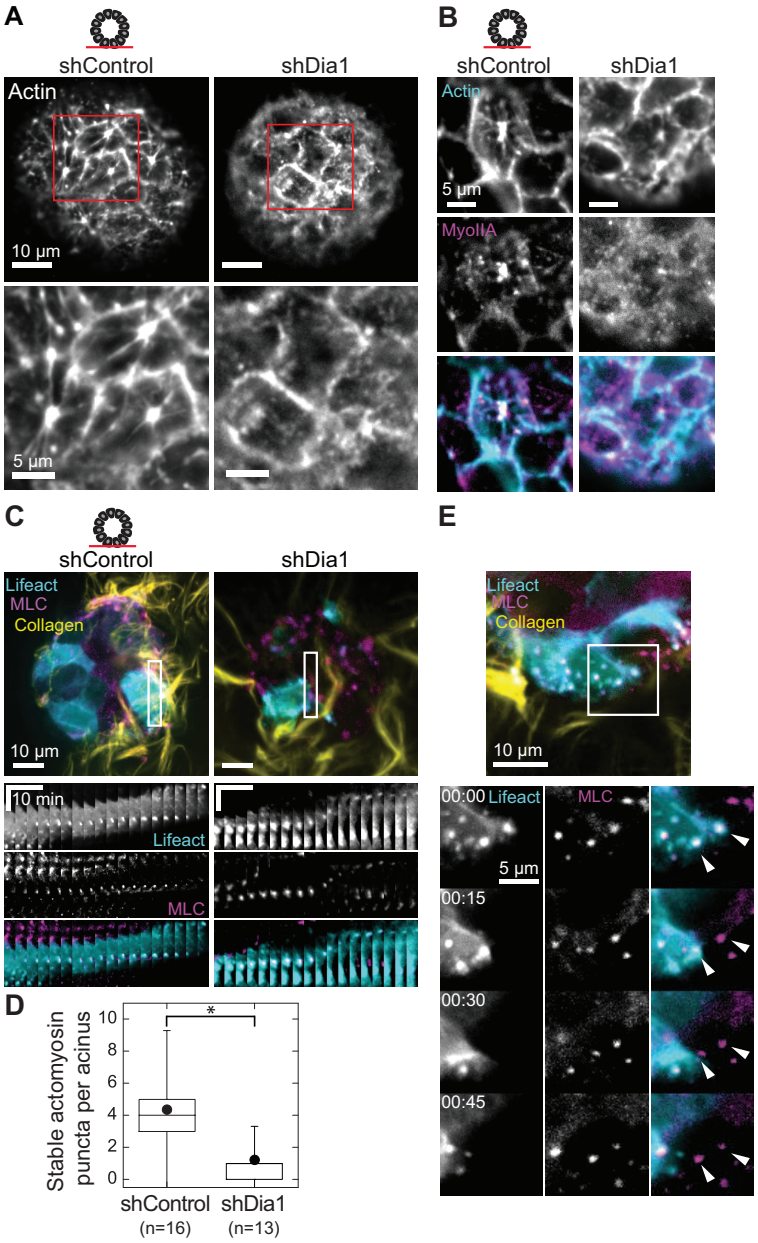

Figure 3.11. Dia1 Regulates Actomyosin Organization and Dynamics of the Basal Cortex. A, F-actin stain of the basal surface of acini prior to HGF addition, with region of interest enlarged below. B, Immunofluorescence of the basal surface of f-actin (cyan) and Myosin IIA (magenta) in shControl and shDia1 acini stimulated with 20 ng/ml HGF for 4 hrs. C, shControl and shDia1 acini coexpressing GFP-Lifeact (cyan) and mCherry-MLC (magenta) were stimulated for 4 hrs with 20 ng/ml HGF and fluorescence images were taken every 3 min at the basal surface. Kymographs show representative MLC and actin puncta, time scale bar represents 10 min and distance scale is 10 μm. D, Box plot of the number of stable actomyosin puncta per field of view observed over 3 hr window, with total organoids imaged indicated below. E, Images of GFP-Lifeact (cyan) and mCherry-MLC (magenta) and Alexa-647 labelled collagen (yellow) in shControl acinus. Montage shows movement of a cell with high expression of GFP-Lifeact, followed by a low-expressing cell. As the first cell moves to the left, MLC and Lifeact puncta remain stationary (arrowheads). Once the cell moves past this region, the next cell forms puncta at the same location. Box plot shows the 25th and 75th percentiles and the median, circle indicates mean, and whiskers mark 1.5 standard deviations. Asterisk indicates $p<0.01$ by a Student's two tailed t-test assuming unequal variance.

same region of collagen assembled a puncta in the same location. This example illustrates that certain locations within the collagen matrix are primed for repeated adhesion assembly in subsequent cells during planar acinar motility.

3.4 Discussion

The suite of molecular mechanisms governing cell motility through 3D environments has enjoyed much attention, as these form the basis for profound tissue shape changes during development and cancer invasion [69]. Detailed models exist to describe how cytoskeletal organelles control the motility of single cells [116], but how these organelles are regulated in space and time to effect tissue shape changes is less clear. Data presented here suggest a previously unappreciated mechanism by which focal adhesion maturation regulates branching morphogenesis in a model epithelial tissue.

Our results suggest that focal adhesions in MDCK acini embedded in collagen matrices share key features with focal adhesions in cells on 2D substrata. We and others have previously reported that maturation of focal adhesions during 2D cell motility requires a stress fiber template, through the activities of alpha-actinin, septins and formins such as Dia1 [157, 173, 170, 172]. HGF signaling in MDCK cells activates Rho, which regulates Dia1 and myosin activity [240]. These effectors play critical roles during branching morphogenesis. When an MDCK cell initially contacts a collagen fibril, formation of a nascent adhesion causes a burst of actin polymerization and myosin recruitment (Figure 12A). Our data indicate that actin and myosin concentrate at the adhesion in a Dia1-dependent manner and promote its maturation, marked by phospho-tyrosine rich proteins such as Focal Adhesion Kinase (FAK) and Paxillin [162, 241]. Mature adhesions are resistant to disassembly as cells change shape and move within the acinus. In concert with myosin contractility, mature focal adhesions enable cells to pull themselves and their neighbors away from the acinus into the collagen matrix (Figure 3.12A).

This work provides evidence to expand the biological functions of focal adhesion mat-

uration. Despite the exquisite detail with which focal adhesion assembly and maturation has been defined [112], the acute consequences of maturation defects on cell motility and tissue morphogenesis remain poorly defined [189, 183, 184, 242]. Data presented here suggest that tissues may require focal adhesion maturation to carry out complex shape changes in 3D fibrillar environments. This conclusion is supported by a recent report demonstrating that focal adhesion maturation through septins is similarly required for MDCK branching morphogenesis [173]. Our data showing a similar role of formins during migration by mouse tumor explants into collagen matrices suggests this idea could be generalized to other morphogenic processes. For an individual cell within a developing or malignant tissue, it is not clear a priori how its motility within the tissue or into the ECM is determined. Here we present a mechanism by which adhesions to the ECM act as a switch from planar motility to invasive motility (Figure 3.12B). Together, these results suggest an expanded repertoire for the biological functions of focal adhesions and their regulators, and prompt testable predictions about the interplay between adhesion stability, cell motility, and tissue shape.

In contrast to adhesions in 2D contexts, we observed myosin accumulation at sites of adhesion in acini. Our data suggest that adhesions to collagen fibrils are sites of continuous actin polymerization and sustained myosin recruitment. It is possible that Rho is recruited to adhesions, and mediates local Dia1 and myosin activation. Indeed this role is consistent with observations of Rho at the leading edge of migrating cells [148, 149]. Finally, the recruitment of myosin at adhesions is a feature shared with invadosomes [243, 244]. Formation of invadosomes in cancer cells were shown to require formins [245], raising the possibility that adhesions described here also play proteolytic roles during MDCK branching morphogenesis.

The role we identify for Dia1 carries important implications for its primary regulator, Rho. Rho activation is thought to impact cell motility primarily through ROCK and myosin contractility [116]. Prior studies have shown that reducing myosin activity during branching morphogenesis results in increased branching, implicating Rho as a negative regulator of tissue shape changes [246, 95]. Conversely, we show that Dia1 is required for branching

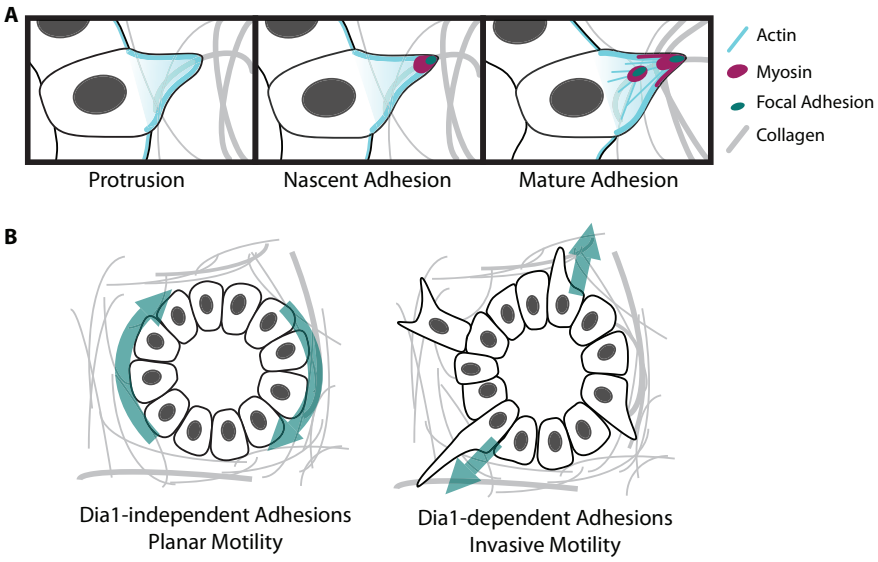

Figure 3.12. Maturation of focal adhesions through Dia1 during tissue shape changes. A, Model for focal adhesion maturation during the onset of MDCK branching morphogenesis. Cells generate actin-rich protrusions from their basal surface into the collagen matrix. Protrusions are initially weakly adhered to collagen fibrils through nascent focal adhesions. Localized actin polymerization through Dia1 and myosin recruitment stabilize focal adhesions and promote their maturation. Mature adhesions resist turnover and allow cells to exert contractile forces against collagen fibrils to enable branching morphogenesis. B, Dia1 may function as a mechanism by which tissues can regulate noninvasive and invasive motility. In the absence of Dia1 activity cells can adhere sufficiently to the collagen matrix to mediate planar motility within the acinus and acinar rotation. Invasive motility into the collagen matrix requires that cells form mature adhesions, dependent on Dia1.

morphogenesis through stabilizing focal adhesions to collagen fibrils. Together these observations suggest competing effects of Rho signaling during complex tissue shape changes: one as a negative regulator via ROCK-mediated contractility and one as a positive-regulator via Dia1-mediated focal adhesion maturation. In the absence of ROCK-mediated contractility, focal adhesion maturation is not needed to facilitate migration of cells away from the acinus due to the overall low levels of contractile tension within the tissue. In the presence of ROCK-mediated contractility, Dia1-mediated focal adhesion maturation is not required for weak adhesion to collagen fibrils and planar cell motility to support rotation. However, it is required to assemble adhesions that are sufficiently stable to withstand physiological contractile tension as cells migrate away from the acinus and drive tissue shape change. Future studies may delineate these apparent opposing roles of Rho effectors, and whether they indeed converge on focal adhesion stability and spatial regulation of contractility during tissue morphogenesis.

3.5 Methods

Cell culture and reagents

Manin-Darby Canine Kidney (MDCK) type II/G cells (American Type Culture Collection) were cultured in a humidified incubator with 5% CO2 using Dulbeccos Minimal Essential Medium (Corning) supplemented with 5% fetal bovine serum (FBS) (Corning), 2 mM l-Glutamine, and penicillin-streptomycin (Corning). Selection media was supplemented with 5 μg/ml puromycin (Gibco). The MDCK cell line expressing GFP-Lifeact was a gift from Thorsten Wittman (University of California, San Francisco). The following antibodies were used: Rat anti-Ecadherin DECMA (Santa Cruz Biotechnologies), mouse anti-Podocalyxin (gift from the Keith Mostov Laboratory, University of California, San Francisco), rabbit anti-Laminin 511 (Sigma), rabbit anti-Myosin IIA heavy chain (Covance), mouse anti-Paxillin 5H11 (Millipore), rabbit anti-FAK-pY397 (Life Technologies), Alexa fluor 488 goat anti-mouse secondary (Life Technologies), Alexa fluor 568 goat anti-mouse secondary (Life Technologies), Alexa fluor 568 goat anti-rat secondary (Life Technologies), rabbit anti-Diaph1 (ProteinTech), rabbit anti-Diaph2 (Cell Signaling), rabbit anti-FHOD1 (Abcam), rabbit anti-GAPDH. For immunofluorescence, all primary antibodies were used at 1:200 and all secondary antibodies were used at 1:500. The formin inhibitor SMIFH2 (gift from David Kovar, University of Chicago) was dissolved in DMSO and used at 30 μM. The Arp2/3 inhibitor (Calbiochem) was dissolved in DMSO and used at 50 μM.

DNA constructs and gene knockdown

Knockdown cell lines were generated using shRNA constructs against canine Dia1 (gatccccgccacagatgagagagacattcaagagatgtctctctcatctgtggcttttta), Dia2 (gatccccgcaaccttacagcaatggattcaagagatccattgctgtaaggttgcttttta), FHOD1 (gatccccgaagacgaggacatactgattcaagagatcagtatgtcctcgtcttcttttta), or a nontargeting control (OligoEngine). These were annealed and cloned into the HindIIII and BglII sites of the pSuper retroviral vector (OligoEngine). Retrovirus was produced using the Phoenix cell line (Nolan Lab, Stanford University) using Fugene 6 transfection reagent (Roche) to transfect the retroviral vector and a VSV-G psuedotyping

plasmid (gift from Marsha Rosner, University of Chicago). Viral supernatant was collected, filtered, and incubated with target MDCK cells for 12 hours in the presence of 8 μg/ml polybrene (Millipore).Following viral transfection and selection, knockdown was confirmed by western blot. For nuclear tracking, shControl and shDia1 cells were transfected using a pQCXIX retrovirus construct encoding H2B-mCherry (gift from Mark Burkard, University of Wisconsin). Cells were purified using flow cytometry (University of Chicago Flow Cytometry Core). The lentiviral vector encoding MLC-mCherry was generated by cloning MLC-mCherry sequence into pWPT lentiviral backbone (Addgene plasmid 12255) with the aid of SnapGene Software (GSL Biotech LLC; www.snapgene.com). Virus was produced in 293T cells (gift from Geof Green, University of Chicago) using a pHR1-8.2-deltaR packaging plasmid and a VSV-G psuedotyping plasmid (gifts from Marsha Rosner, University of Chicago). Following viral transfection cells were isolated by flow cytometry at the University of Chicago Flow Cytometry Core to purify mCherry and GFP positive cells.

Culture and manipulation of acini

Matrigel (Corning) from a single lot containing 9.1 mg/ml protein was used for all 3D culture experiments. To generate acini, the lower surface of wells in a 24-well plate were coated with 30 μl Matrigel and allowed to gel at 37 C. MDCK cells were trypsinized, pipetted vigorously to break up cell clusters, and 10,000 cells were added to 800 μl of a 1:1 solution of growth media and Matrigel, which was kept on ice to prevent gelation. The resulting cell suspension was immediately pipetting up and down to disperse cells and added to the Matrigel-coated well The Matrigel-cell suspension was immediately placed in a 37 C incubator and allowed to gel for 30 minutes before 800 μl growth media was gently added to each well. Media was changed every 3 days for 6-7 days until acini formed lumens. To isolate acini, a modified protocol by Rubashkin et al [181] was used to melt Matrigel by incubation at low temperatures. Briefly, media was aspirated and Matrigel was disrupted by pipetting up and down with 5 ml of warm PBS with Ca/Mg (Corning) per well. The PBS-Matrigel solution was pelleted at 500 x g for 3 minutes and resuspended in 10 ml fresh

PBS was added. Acini were incubated in a bucket of salted ice with rocking at maximum speed for 40 minutes. Acini were pelleted at 500 x g, yielding a 50 μl slurry of residual Matrigel and acini which were kept on ice to prevent gelation. Collagen gels were prepared 30 minutes before use and kept on ice. To prepare collagen gels, 1 M HEPES and 7.5% NaHCO3 were combined with media to achieve final ratios of 1:50 and 1:23.5, respectively. Rat tail collagen 1 (Corning) was gently added to a final concentration of 2 mg/ml. Collagen was fluorescently labeled using Alexa Fluor 647 NHS ester (Life Technologies), dissolved at 10 μg/μl in DMSO and incubated with Rat tail collagen at a ratio of 1:1000 and stored at 4 C. The resulting Alexa-647-labelled collagen was included in a ratio of 1:4 with unlabelled collagen. Acini were added to the collagen solution, mixed by pipetting, and plated in either 4 or 8-well Ibidi chambers (Ibidi) or in 4-well Labtek chamber slides (Nunc), in volumes of 40 or 100 μl. All chambers were precoated with 10 or 30 μl collagen solution for 10 minutes prior to plating acini. Collagen was allowed to gel for at least 30 minutes before growth media was gently added to the sides of wells.

Mouse tumor explants

One female day 70 mouse of the Mouse Mammary Tumor Virus-Polyoma Middle T Antigen strain (MMTV-PyMT, Jackson Laboratories) was sacrificed and the largest mammary tumor from each inguinal mammary gland was surgically excised. Each tumor was manually minced with a razorblade and tumor tissue was digested by shaking for 30 minutes at 37 C in a conical tube containing 40 ml of DMEM/F12/50:50 (Corning) with 3 mg/ml Collagenase A, 1 mg/ml hyaluronidase (Worthington) and 2 U/ml DNase 1 (Fisher). 5 ml of FBS was added to halt digestion, and tumor tissue suspension was pelleted at 500x g for 3 minutes and resuspended. Tumor organoids were placed in a 1:1 mixture of Matrigel and DMEM/F12/50:50 supplemented with 10% Fetal Bovine Serum (Corning), 10 μg/ml human Insulin (PromoCell), 5 μg/ml human Transferrin, and penecilin/streptomycin (Corning). The bottom wells of a 24-well plate (Corning) were coated with Matrigel and allowed to gel before adding 800 μl of organoid-Matrigel suspension per well. Matrigel was allowed to

gel for 30 minutes and 800 μl growth media was gently added. Organoids were cultured in Matrigel for 24-48 hours prior to replating into 2mg/ml Collagen 1 gels in 4-well Ibidi chambers as described above, with the ice incubation step reduced to 20 minutes. Following replating in collagen, fresh media containing DMSO, 30 μM SMIFH2, or 50 μM CK666 was added and chambers were placed on a heated microscope stage. Images were collected every 30 minutes for 72 hours.

Western blot analysis

For Western blotting, cells were lysed in Laemmli buffer (4% sodium dodecyl sulfate, 20% glycerol, 120 mM Tris-Cl pH 6.8, 0.02% bromophenol blue). Lysates were separated by SDS-PAGE gel and electrotransferred to a nitrocellulose membrane. Blots were blocked in PBS with 5% nonfat dry milk and incubated with primary antibodies at 1:1000 overnight at 4 C. Blots were incubated in secondary antibodies at 1:10000 for 1 hour at room temperature and developed with ECL Western blotting substrate (Thermo Fisher Scientific). Blots were scanned as film negatives on a photo scanner (Perfection v700; Epson) and analyzed using the gel analysis tool in ImageJ (National Institutes of Health). The intensity of the protein bands was normalized through comparison with the loading control bands.

Microscopy

All fluorescence images were acquired on an inverted microscope (Ti-E; Nikon) with a confocal scanhead (CSUX; Yokogawa Electric Corporation), laser merge module containing 491, 561, and 642 laser lines (Spectral Applied Research), a stage controller (Prior), and a cooled charge-coupled device camera (HQ2; Roper Scientific). Images were acquired using either a 20x 0.75 NA Plan Fluor multi-immersion objective (Nikon) or a 40x 1.15 NA Plan Apo water immersion extra long working distance objective (Nikon). Immunostained acini or organoids were imaged by acquiring z-stacks with either 500 nm or 1 m z spacing. All transmitted light images were acquired on an inverted microscope (Ti-E; Nikon), a stage controller (Prior), and a cooled charge-coupled device camera (HQ2; Roper Scientific). Images were acquired using a 20x 0.45 NA air extra long working distance objective (Nikon). All

hardware was controlled via MetaMorph acquisition software (Molecular Devices). Bright-field images of acini were acquired on a Nikon Eclipse TS100 (Nikon) with an iPhone 6S (Apple) and a SnapZoom adaptor (SnapZoom).

Live cell imaging

All live cell imaging was performed with a stage incubator for temperature, humidity, and CO2 control (Chamlide TC and FC-5N; Quorum Technologies). The stage adaptor, stage cover, and objective were maintained at 37 C, while humidified 5% CO2 air was maintained at 50 C at its source to prevent condensation within its tubing. Acini were transferred to collagen gels in 4- or 8-well plastic chambers (Ibidi) at least 1 day prior to imaging. Imaging media was identical to growth media except phenol red-free DMEM was used. Imaging media containing 20 ng/ml HGF was added to chambers immediately before transfer to the pre-warmed microscope stage, where they equilibrated for 30 minutes prior to imaging. Image sequences were corrected for drift using the Stackreg plugin in ImageJ (National Institutes of Health), and a custom Matlab script. Fluorescence imaging of cells expressing H2B-mCherry was performed by collecting z-stacks of 21 planes at 3 μm intervals every 10 minutes. For fluorescence imaging of GFP-Lifeact, mCherry-MLC, and Alexa Fluor 647-collagen, 20 ng/ml HGF was added to phenol red-free media 4 or 24 hours prior to imaging. For each acinus, images were acquired at 6 planes separated by 3 m every 3 minutes for 3 hours. Only the lower surface of each acinus was imaged, to capture collagen fibrils and cells simultaneously. Alexa Fluor 647-collagen images were bleach corrected in ImageJ.

Immunofluorescence

For immunofluorescence staining of acini, a 1.5 U/ml solution of Clostridium Collagenase (Sigma) in PBS was added to culture media prior to fixation and acini were replaced in the incubator for 10 minutes. Acini were fixed in a solution of 4% paraformaldehyde with 0.1% Triton X-100 in Phosphate Buffered Saline solution (PBS, Corning). Fixation solution was gently added to each well while simultaneously aspirating culture media, and incubated for 20 minutes. Collagen autofluorescence was quenched with 3 rinses of 0.1 M glycine in PBS

for 20 minutes each. Acini were permeabolized in 0.5% Triton X-100 for 10 minutes, and blocked with 2.5% Bovine Serum Albumin and 0.1% Triton X-100 in PBS for 1 hour. Acini were incubated with primary antibody at 1:200 in blocking solution overnight at 4 C, washed 3 times in 0.1% Triton X-100 for 20 minutes each, and secondary antibody at 1:500 or Alexa fluor 647 phalloidin at 1:1000 (Life Technologies) was incubated in blocking solution for 1 hour. After another 3 20 minute washes with 0.1% Triton X-100, chamber walls were removed and 20 μl Prolong Gold (Life Technologies) was added per well. A clean coverslip had blobs of clear nail polish applied to its corners and allowed to dry, and placed over the chamber slide. Slides were allowed to dry, sealed with nail polish, and stored at 4 C. All incubations were performed on a rotary shaker. Immunofluorescence staining of cells in 2D culture was performed as above but without glycine rinses.

Branching morphogenesis assays

Acini plated in collagen gels were cultured for at least 1 day prior to inducing branching morphogenesis. Briefly, growth media was removed and replaced with media containing 20 ng/ml human recombinant Hepatocyte Growth Factor (HGF) (Sigma-Aldrich), with DMSO or inhibitors as indicated. Fresh HGF with inhibitors was added after 24 hours. After 48 hours, acini were fixed and stained with phalloidin.

Scattering assays

MDCK cells were plated sparsely in 4-well plastic chambers (Ibidi) or on glass coverslips and allowed to form islands. Cells were serum starved by replacing growth media with phenol red-free media supplemented with 0.5% FBS, and culturing for 12 hours. For timelapse microscopy, chambers were placed on a heated microscope stage and 20 ng/ml HGF was added to low-serum media to stimulate scattering. Cells were imaged in brightfield at 10 minute intervals for 12 hours. For immunofluorescence, cells were plated on glass coverslips and allowed to form islands, then serum starved for 12 hours, incubated in HGF for 6 hours, and fixed for immunofluorescence staining.

Image Analysis

For branching morphogenesis assays, z-stacks of each acinus were collected at 0.5 or 1 μm intervals and the entire volume was scored for protrusions. These were scored as single- or multi-cellular extensions at least 5 μm in length emanating from acini into the collagen gel. Protrusion length was measured as a straight line from the basal surface of the cell or cells to the tip of the cellular extension. Protrusions extending in the z direction were measured by counting the confocal sections they spanned. For nuclear tracking, image sequences for analysis were generated by combining lower z-planes from each acinus into maximum projections. Cells were tracked manually in ImageJ (National Institutes of Health) and tracks were analyzed using custom Matlab scripts. For cell tracking during scattering, cells were tracked manually using ImageJ (National Institutes of Health) and tracks were analyzed using custom Matlab scripts. Time of initial of cell-cell contact rupture was scored by the first cell to contract and completely dissociate from its neighbors. Quantification of phospho-Tyrosine puncta was performed on maximum intensity projections combining 3 μm at the acinar equator. The resulting images were background subtracted and binarized, and puncta were counted using the Analyze Particles feature of ImageJ (National Institutes of Health), set to a pixel range of 30-1000 pixels2. Maximum intensity projections were also analyzed with linescans, each measuring 2 by 15 μm. Quantification of phospho-FAK was performed on background subtracted, binarized images using the Analyze Particles feature of ImageJ (National Institutes of Health), set to a pixel range of 30-1000 pixels^2. Analysis of collagen fibril deformations and MLC puncta mobility was performed on image sequences in which the lower basal surface of cells and the collagen matrix could be resolved in the same imaging plane. This surface ranged from 1500-2100 μm^2, representing approximately 0.19 of the total surface area for a typical acinus 50-60 μm in diameter. To quantify collagen fibril deformations, image sequences were analyzed for fibrils that were deformed by 1-2 μm, independently of their neighbors.

Statistical Tests

To assess statistical significance, we used independent two-sample Students t tests of the

mean to determine the significance with respect to WT or Control. P values were indicated by *, $p<0.01$; **, $p<0.05$.

CHAPTER 4

ANALYSIS OF CELL SHAPE IN 3D TISSUES

4.1 Abstract

Collective cell behaviors orchestrate the movement of tissues in development and cancer. However the underlying mechanical properties that govern these changes are difficult to track or measure directly. A computational model was developed recently to integrate the intracellular mechanical properties and cell shape in a packed epithelial monolayer. Using information on cell shape, the model can accurately predict cell motility within the monolayer and describes a tissue jamming and unjamming transition in the tissue. It is unclear whether this model can also describe epithelial monolayers in 3D. Here we show that this model accurately captures properties of 3D tissues of Madin-Darby Canine Kidney cells. We find that under control conditions, these tissues are jammed and exhibit no motility. Inducing cell motility within tissues corresponds with a transition to the unjammed state. We show that maintenance of the jammed state requires the actin regulator Dia1 as well as cell contractility. Finally we validate cell shape changes caused by these defects by accounting for cells' 3D shapes. These data confirm that biophysical principles relating cell shape and cell motility are conserved between cell culture models in 2D and 3D environments.

4.2 Introduction

Tissues change shape dramatically over the course of organismal development as well as during tumor spreading [62, 48]. Shape changes result from the collective actions of cells, whose individual shapes and motions are coordinated across the tissue to drive tissue elongation, folding, spreading, or other large-scale changes [247, 248]. During some such events tissues motions resemble a liquid, and during other events a solid. For instance, cells appear to flow or stream during convergent extension in the *Drosophila* embryo [249, 250], or during

blastoderm spreading in the Zebrafish embryo [251]. These behaviors resemble viscous liquids. Meanwhile, at the leading edge of an invasive tumor [55] or during tissue folding events such as occur during *Drosophila* apical constriction [252], tissues are better approximated as solids that can bear tension or compression [247, 142]. To date there are few established methods to report on mechanical states of epithelial tissues that would capture these putative liquid-like or solid-like behaviors. Many common measurements of the mechanical properties of living tissues are invasive [253] or difficult to interpret [254]. Computational models can help overcome these challenges by generating testable hypotheses that relate cell mechanical properties with tissue shape changes [255, 256].

Recently, Manning and colleagues developed a computational model to explore the relationship between stiffness transitions in tissues and the shapes of their constituent cells [257, 258]. This model is premised on established mechanical properties of epithelial cells integrated into a tissue, and the motility of cells within them [259, 260, 261]. In an epithelial sheet, each cell maintains adhesions to its neighbors through adherens junctions, which permit tension generated by one cell to propagate across many of its neighbors [262]. The strength of a cell-cell adhesion is equivalent to the force required to separate two cells adhered to each other, and can vary widely across different cell types or different cells within a tissue [263, 264]. For example, adhesion strength can be tuned by isoform and expression level of cadherin proteins [265], as well as the components and dynamic regulation of the adherens junction plaque [266]. While daunting in their complexity, these molecular details confer a measurable magnitude of the adhesive energy of a cells junctions [247].

A related but distinct determinant of cell shape is its intracellular contractility. The actomyosin networks spanning a cells cortex cause contraction against the neighbors to which it is adhered [267]. The total contractile energy a cell exerts on its surroundings is directly related to the activity of myosin, which causes contraction of cortical actin networks [121]. Thus a highly contractile cell within a monolayer will pull more against its neighbors, and deform them in turn. Meanwhile a cell with low contractility will be more easily deformed

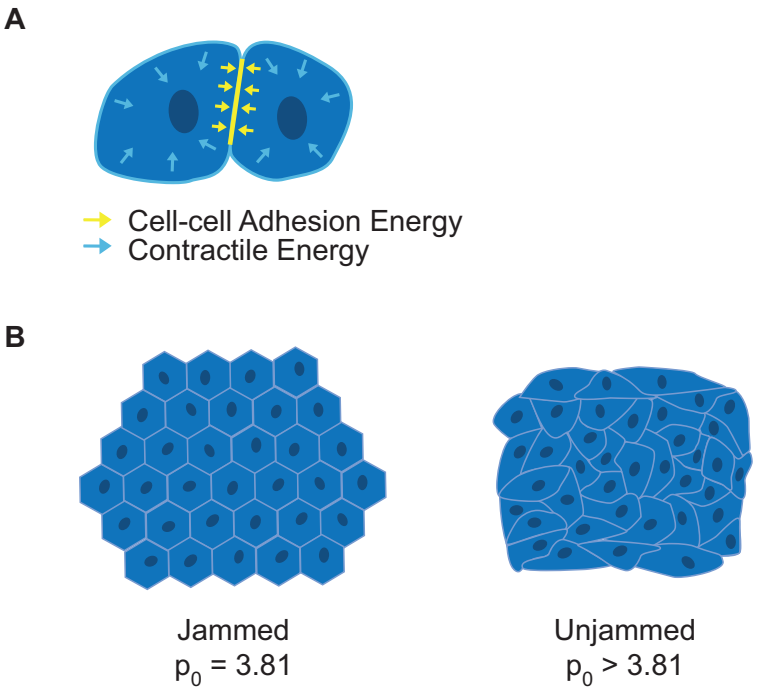

Figure 4.1. Model for jamming transition in epithelial monolayers. A, Diagram showing forces that contribute to epithelial cell shape. Blue arrows represent intracellular contractility, which combine to favor a circular cell shape. Yellow arrows represent intercellular adhesion, which favor maximizing cell-cell junction length at the expense of a circular cell shape. B, Diagram showing cell shape for an epithelial monolayer at either extreme of the jamming transition. In the jammed state, cells are immobile and the shape index p_0 is near or below 3.81. In the unjammed state, cells are mobile and the shape index is above 3.81.

by its neighbors (Figure 4.1). Manning and colleagues have incorporated these quantitative parameters into a vertex model for packed epithelial tissues [257]. This model readily provokes a simple hypothesis: the average shape of cells within a confluent epithelium is a direct consequence of cell-cell adhesion strength and intracellular contractility. Their model predicted that a shape index p_0, equal to the ratio of the cells perimeter to the square root of its area, will capture this relationship. An important condition is assumed by the model: that cell-cell adhesion strength and cell contractility change uniformly across a tissue and do not vary from cell to cell. However, the model is independent of cell absolute size, density, and stiffness of the underlying substrate.

Under these conditions, the model predicts that the balance of these two parameters cell-cell adhesion strength and cell contractility describe two alternate states of a tissue. When intracellular contractility is high, the model predicts that cells will remain immobile within the tissue they appear "caged" by their neighbors. Meanwhile, when cell-cell adhesion is high, cells are predicted to exhibit motility and undergo neighbor exchanges within the monolayer. This trade-off can be expressed by considering the energy that adjacent cells would require to exchange places. Manning and colleagues showed that the energy barrier that cells must overcome in order to undergo rearrangements remains very high at low values of p_0 (e.g. ~3.6), indicative of high cell cortical tension. This energy barrier rapidly disappears as the value of p0 approaches a critical threshold of 3.81. Above this transition point, cells are predicted to freely rearrange within the tissue (Figure 4.1B). Importantly, this measure is dimensionless and can be applied to any epithelial tissue for which the assumptions of this model hold.

Manning et al describe this transition in terms borrowed from granular matter such as sand. Specifically, the model proposes that tissues undergo a transition between liquid-like and solid-like states known as jamming. This transition is analogous to how we experience the bulk properties of sand. Each grain can move independently of its neighbors, thus sand flows out of ones hand when picked up. However, when sufficient external pressure is applied

as when one steps on a pile of sand the individual grains become locked in place, or jammed [268]. The pile will deform up to a point, after which it will support the weight of a person standing atop it.

Unlike this analogy, however, jamming and unjamming in epithelial tissues is proposed as an intrinsic process driven by changes to cell behavior [257]. This model has been successfully applied to biological settings such as the bronchial airway epithelium. In collaboration with Manning, Fredberg and colleagues measured the shape parameter p_0 for primary bronchial epithelia from healthy and asthmatic donors [269]. By time-lapse imaging, they were able to corroborate that p_0 indeed correlates with cell motions within the monolayer. Their results further showed that bronchial airway epithelia from healthy donors were jammed while those from asthmatics were unjammed and cells displayed aberrant motility within the epithelium. This study thereby linked important biomedical states of the epithelium with simple and easily measured physical parameters.

The theoretical implications of jamming transitions have thus far been explored for epithelial monolayers on 2D substrates. Epithelial tissues in 3D culture form spherical acini, which can be thought of as monolayers wrapped around a sphere. Despite a long-standing enthusiasm to explore cell biology using 3D culture techniques [11, 92, 206, 36], few efforts have focused on the shared properties of monolayers in 2D and 3D culture [270]. This has hampered progress in experimentally validating models of epithelial cell biology, as it is often unclear which epithelial cell behaviors are conserved across culture techniques. We address this gap by testing the model elaborated by Manning et al for 2D monolayers using 3D spheroids. We present evidence that this model successfully captures cell shape and motility behaviors within epithelial monolayers cultured in 3D. These results suggest that broadly shared physical principles govern motility within tissues across culture conditions.

4.3 Results

4.3.1 Impairing Cytoskeleton Components causes Unjamming in MDKC Acini

Acini grown from either MDCK shControl or shDia1 cells were transferred to collagen gels (see methods) and cultured for 48 hours prior to fixation. Staining for f-actin using fluorescent phalloidin faithfully revealed cell borders, as virtually all f-actin was cortical (see Chapter 3). Confocal fluorescence microscopy enabled the visualization of individual cell shapes within the epithelium when imaged just above the basal surface (Figure 4.2A and 4.2B). Analysis of cell perimeters and areas across several acini revealed the average p_0 for shControl cells was 3.88 (Figure 4.2C). This suggests these tissues are at or near a jammed state (p_0=3.81).

Meanwhile p_0 measured in acini of shDia1 cells was significantly higher at 4.00. This measurement indicates that, under control conditions, depleting Dia1 is correlated with either lower effective cell cortical tension, or increased effective cell-cell adhesion. Dia1 activity dictates the structure and mechanics of the actin cortex [271, 272] and while Dia1 plays a role at adherens junctions [273], no previous evidence suggests that its loss would strengthen these adhesions.

To confirm the role of cortical tension in determining cell shape, the Rho effector ROCK was inhibited using the compound Y-27632. As a primary regulator of myosin activity, ROCK activity sets cortical stiffness without directly impairing actin network assembly [272, 274]. When wild type MDCK acini plated in collagen gels were incubated with 10 μM y-27632 for 24 hours, the resulting cell shapes had a significantly higher p_0 value than their unperturbed counterparts and were equivalent those measured for shDia1 cells (p_0 = 3.99, Figure 4.2C). These data confirm that tissues become unjammed upon ROCK inhibition and would be predicted to show liquid-like behaviors. These data suggest that directly impairing cortical tension causes similar changes to cell shape as those seen in shDia1 acini.

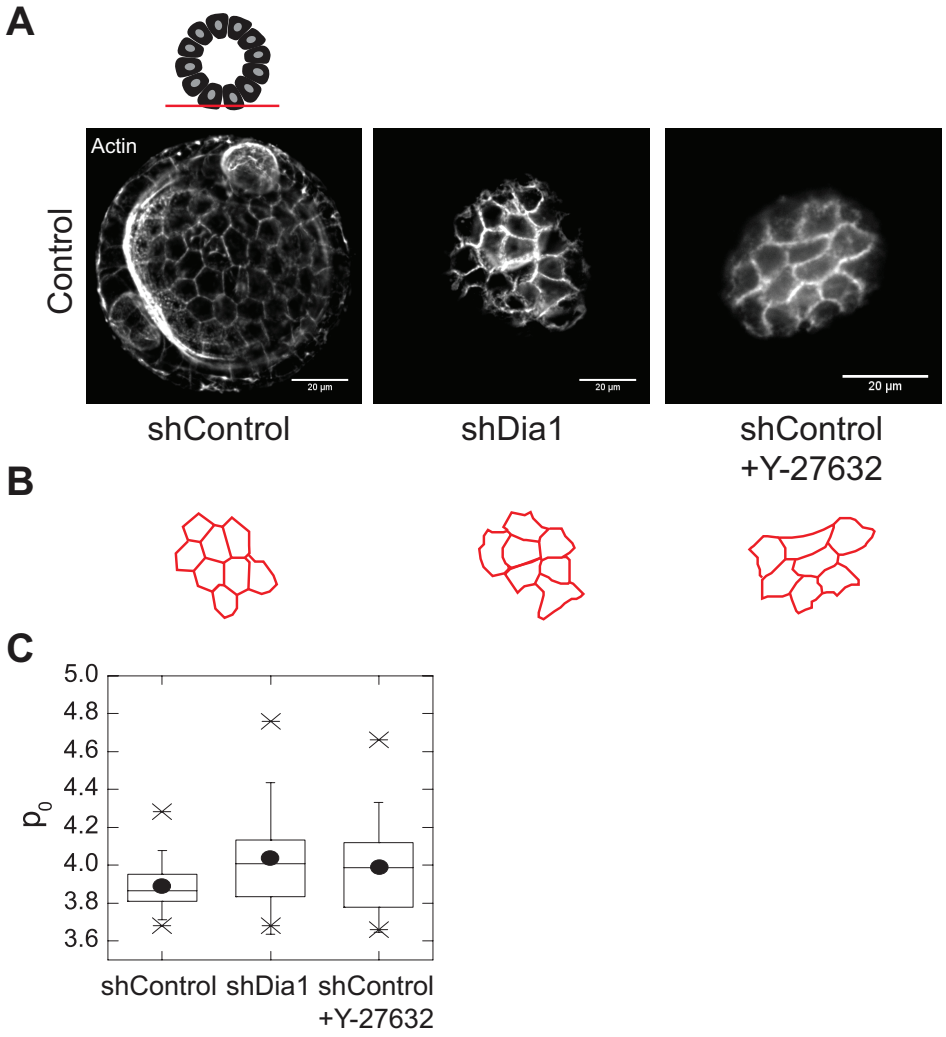

Figure 4.2. Impairing cytoskeletal components causes unjamming in MDCK acini. A, confocal images of acini stained with phalloidin. Imaging plane is indicated by the diagram above, which permits analysis of cell shape within acini. Acini of shControl or shDia1 cells were cultured in collagen gels for 24 hours, with or without 10 μM of the ROCK inhibitor Y-27632 prior to fixation. B, cell shape outlines drawn from each of the acini above showing variation in shape across conditions. C, box plots of measure p_0 values for n>20 cells from at least 6 acini. Box plots show the 25th and 75th percentiles and the median, circle indicates mean, and whiskers mark 1.5 standard deviations. Scale bars, 20 μm.

4.3.2 Stimulation with HGF causes unjamming in MDCK acini

To extend these findings to the execution of tissue shape changes, shControl and shDia1 acini in collagen gels were treated with Hepatocyte Growth Factor (HGF) for 4 hours prior to fixation. As shown previously, at this stage tissues from both cell types undergo rotation and rearrangements, but multicellular branches have not formed in shControl acini. In agreement with their similar behaviors at this state, cell shape analysis revealed that p_0 values for shControl and shDia1 acini were not significantly different (p_0 = 4.15-4.22) (Figure 4.3). In both cell types, p_0 values were consistent with an unjammed state. These data suggest that cell unjamming is an early event during branching morphogenesis, coincident with rotation and in-plane motility of cells prior to collective migration into the collagen gel (see Chapter 3). Given that there was no measurable difference in p_0 between shControl and shDia1 cells, the addition of HGF may induce the maximum p_0 in MDCK cells. In addition, these data show that the increased shape parameter for shDia 1 cells under control conditions is not additive with stimulation by HGF.

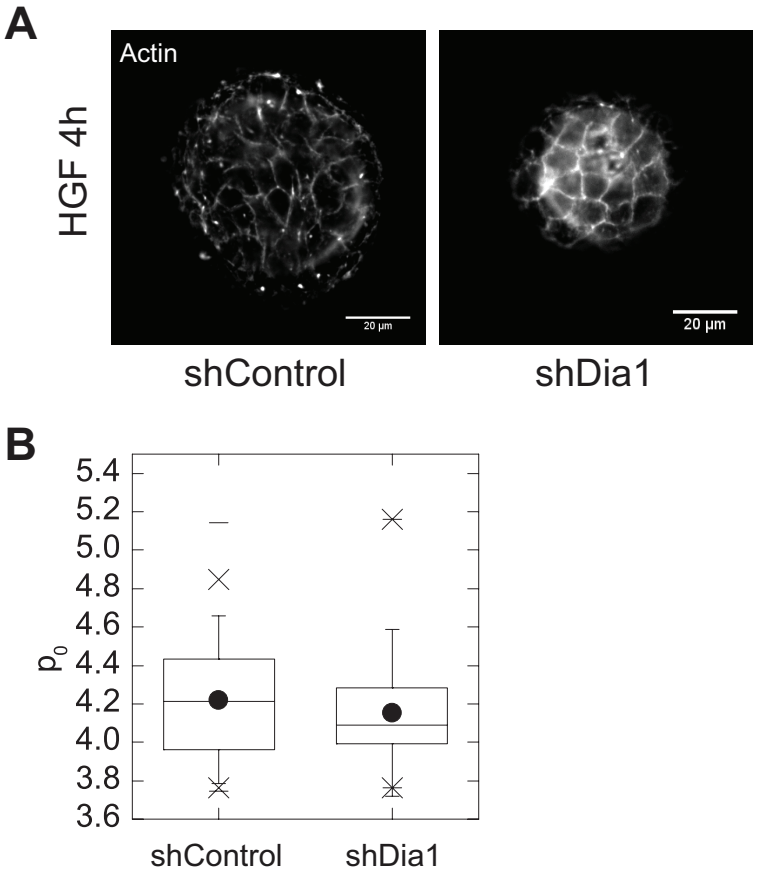

Figure 4.3. Stimulation with HGF causes unjamming in MDCK acini. A, confocal images of acini stained with phalloidin showing cell shapes for shControl and shDia1 acini plated in collagen gels and stimulated for 4 hours with 20 ng/ml Hepatocyte Growth Factor (HGF). B, box plots of measure $p_0 0$ values for n>35 cells from at least 6 acini. Box plots show the 25th and 75th percentiles and the median, circle indicates mean, and whiskers mark 1.5 standard deviations. Scale bars, 20 μm.

4.3.3 Cell motility within acini validates the unjamming transition

Collectively, these measurements suggest that prior to the addition of HGF, wild type MDCK acini are in the jammed, solid-like state. Data presented in the previous chapter shows that upon stimulation with HGF, both shControl and shDia1 acini undergo movements and rotation within the plane of the epithelium. This suggests that these acini are unjammed, in agreement with the cell shape data shown here. We next sought to measure cell motility in wild type acini before and after addition of HGF, to determine whether our measurements of cell shape faithfully report on a an unjamming transition.

Wild type MDCK cells were transfected with a construct encoding the histone H2B tagged with the fluorescent protein mPlum. We cultured these cells to generate acini and placed them in collagen gels, and captured cell positions by time-lapse microscopy at 15 minute intervals with or without the addition of HGF. At each timepoint we collected z-stacks of cell nuclei, then combined these into maximum projections to analyze cell movements within a single x-y plane. We tracked cells manually and calculated the average instantaneous velocity for at least 21 cells across 3 acini per condition. As shown in Figure 4.4A, cells in control conditions undergo little to no motility. Following addition of HGF, as expected, cells rearrange extensively within acini. Cell tracking showed an average instantaneous velocity rose from near 0 microns per minute to 0.16 microns per minute (figure 4.4B). These observations confirm that under control conditions MDCK acini are jammed tissues, with limited cell movement, and undergo unjamming upon the addition of HGF. Overall these data corroborate the model put forth by Manning *et al* [257, 269].

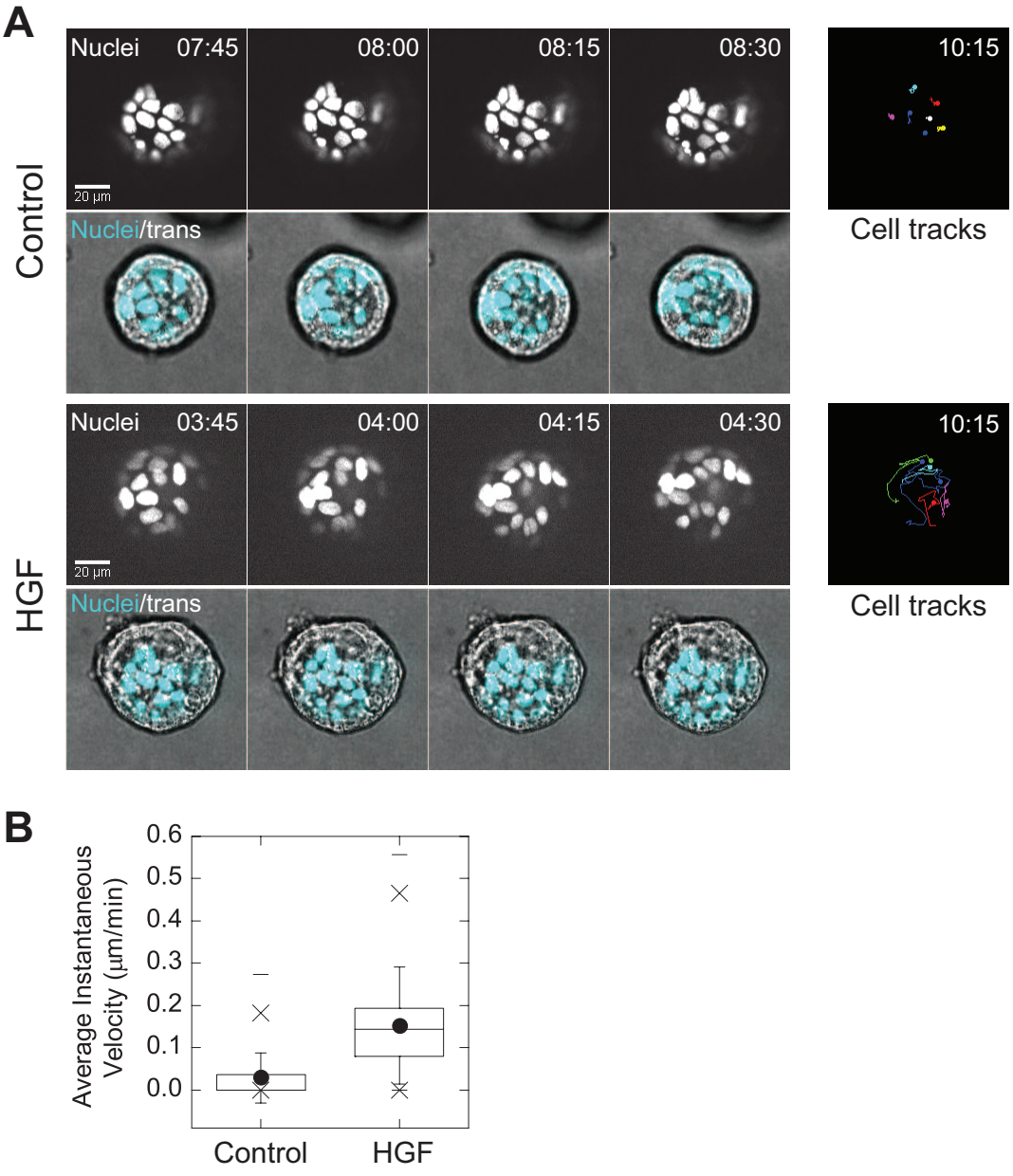

Figure 4.4. Cell motility within acini validates the unjamming transition. A, Confocal and transmitted light images from time-lapse microscopy showing cell positions within acini. MDCK cells expressing H2B-mPlum were cultured to form acini, plated in collagen, and imaged by time-lapse microscopy with or without 20 ng/ml Hepatocyte Growth Factor (HGF). Top montages show control acini, bottom montages show HGF-stimulated acini. Each shows nuclei alone and nucle with transmitted light image overlaid. Time indicated since the start of the imaging. At the right, images show corresponding cell tracks from each acinus. B, box plots of instantaneous cell velocity in um per min for n>21 cells from at least 3 acini. Box plots show the 25th and 75th percentiles and the median, circle indicates mean, and whiskers mark 1.5 standard deviations. Scale bars, 20 μum.

4.3.4 The unjamming transition correlates with altered cell junction orientation

The measurements of cell shapes in Figures 4.2 and 4.3, and the mathematical model to which they refer, offer only an estimation of a cell's 3-dimensional shape. Notably, this method collapses cells along their apical/basal axis to examine the 2-dimensional shape that they occupy within the epithelium. We hypothesized that the cell shape parameter $p_0 0$ might be complemented by an analysis of cell shape along the apical/basal axis. We therefore analyzed cell-cell junctions in images taken at the equatorial plane through the middle of acini. In this plane, cell-cell junctions marked by f-actin extend from the apical surface to the basal surface of a cell and meet the basal surface at right angle to it (Figure 4.5A). As a measure of the orientation of cell-cell junctions, the angle formed by a junction and the basal surface should normally remain near 90 degrees. We hypothesized that deviation from a 90 degree angle would therefore correspond to unjamming and the motility of cells within the acinus. Instances of this junction angle rising above 90 degrees would occur when one cell expands the area of its basal surface, to the exclusion of its neighbors. Conversely, the same geometry would be achieved by one cell contracting at its basal surface and pulling on its neighbors. Both cases would be conceptually consistent with an unjammed tissue state, as defined by fluctuation in cell shape and motility of cells within the tissue. These actions would alter the orientation of cell junctions such that their angle would deviate from 90 degrees relative to the basal surface.

Using this parameter of cell junction angles, the orientation of cell-cell junctions was measured across several cell pairs in multiple shControl and shDia1 acini (Figure 4.5B). For consistency, the angle above 90 degrees was always recorded. The orientation of cell-cell junctions in control cells deviated from the orthogonal by an average of 11 degrees (Figure 4.5C). In shDia1 acini, however, junctional orientation was farther from the orthogonal, by an average of 19 degrees. As above, these results were compared with acini incubated with the ROCK inhibitor Y-27632, which we predicted would cause a deregulation of cell shape.

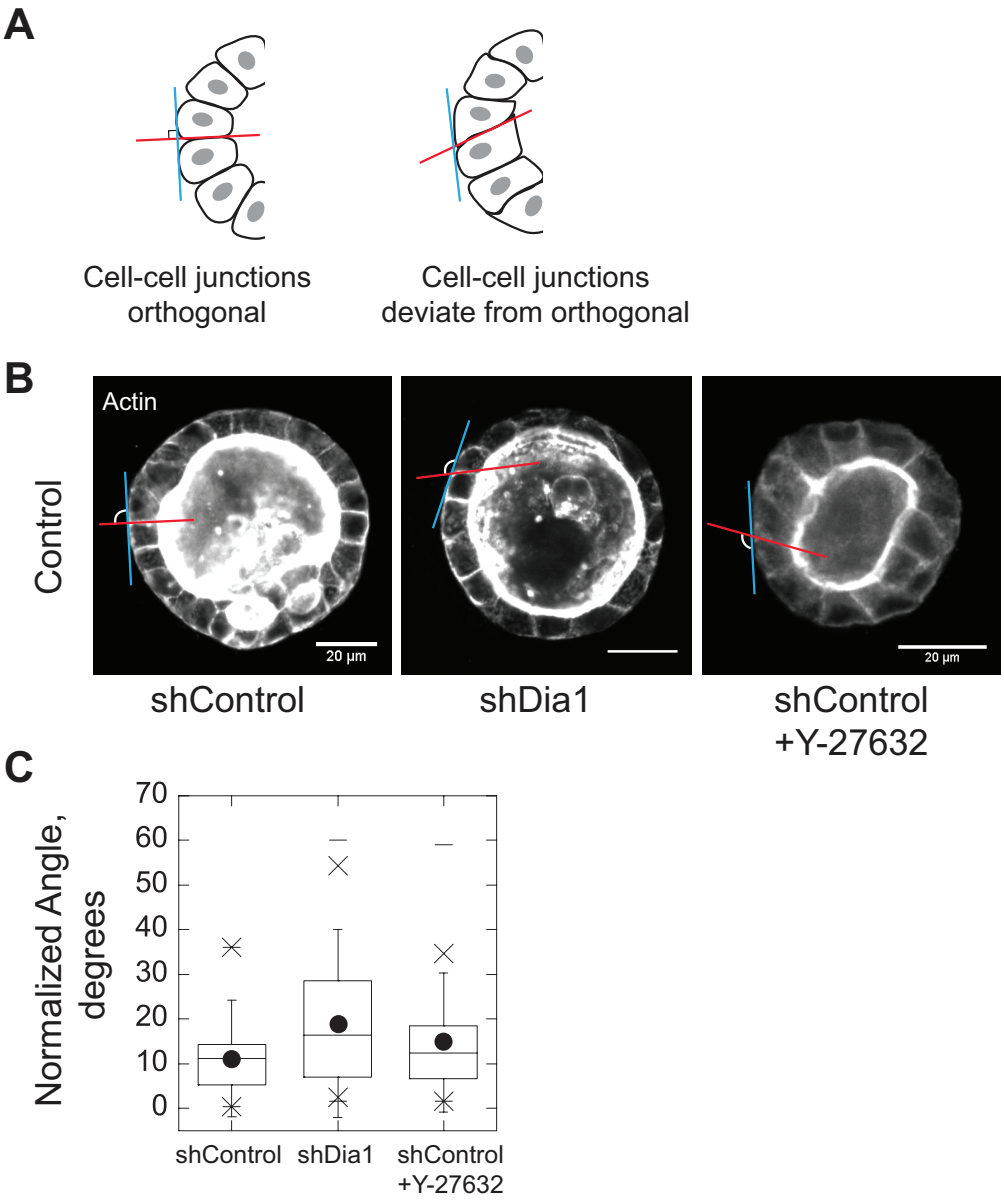

Figure 4.5. The unjamming transition correlates with altered cell junction orientation. A, Diagram showing measurements of cell-cell junction orientation for orthogonal and deviated junctions. Red line indicates orientation of the junction, while the blue line indicates the tangent to the basal surface of the acinus. B, representative confocal images of phalloidin staining in the indicated acini showing junction orientations. Acini of shControl or shDia1 cells were cultured in collagen gels for 24 hours, with or without 10 uM of the ROCK inhibitor Y-27632 prior to fixation. C, box plots of cell-cell junction orientations for n>34 cell pairs from at least 5 acini. Box plots show the 25th and 75th percentiles and the median, circle indicates mean, and whiskers mark 1.5 standard deviations. Scale bars, 20 μum.

Indeed, junction orientation in these acini were more varied than controls, at 14 degrees, although this difference was not statistically significant. Together, these data confirm and extend the conclusions made with the analysis of 2D cell shape above.

4.4 Discussion

Observations described here validate the proposed model by Manning and colleagues that relates cell mechanics with cell motility for epithelial tissues, using a simple index of cell shape [257]. We conclude that quiescent spherical tissues are in the jammed state, which is lost upon either stimulation with HGF to induce cell motility, or upon defects in the actomyosin networks at the cell cortex. These simple observations offer confirmation that the physical determinants of cell motility in monolayers are shared between 2D and 3D culture systems. We expect this correlation could be exploited to further understanding of cytoskeletal determinants of tissue biology that might be conserved across different geometries.

Our results agree with previous reports on Dia1 as a key regulator of cortical actin networks [275, 271, 272]. Fritzsche et al measured actin filaments in the cortex of single cells and found that Dia1 maintains longer actin filaments, which they found allowed actin pools to persist for longer at the cortex [272]. These dynamics were found to directly impact the mechanical properties of the cell cortex, as measured by atomic force microscopy. In light of these observations, we suggest that unjamming in MDKC acini may arise through measurable defects in the actin cortex. Future work could use established methods such as micropipette asipiration to confirm these connections between tissue mechanical properties and cytoskeletal regulators.

An unexplored aspect of this work is the role, if any, of tissue curvature. While a 2D sheet and a 3D shell might be topologically equivalent, a sheet has no curvature while the shell experiences a constant curvature. What are the implications for curvature on jamming in epithelial tissues? We speculate that very high curvature may enforce constitutive unjamming of acini, while low curvature (more closely approximating a 2D sheet) would exhibit

jamming. As curvature increases, we predict cells would be less able to maintain static cell-cell junctions, and cell contractility would be insufficient to restrain cell shape changes. This could be tested by comparing the average shape index of an acinus with its diameter. As diameter increases, $p_0 0$ would approach the jammed state of 3.81. Two reports have measured cell movements within developing acini consisting of just a few cells [237, 276]. Because they are small these structures have a very high curvature and undergo constant motility, consistent with a correlation of curvature and unjamming.

These results also carry implications for the growth and self-organization of cells into tissues. Given that shDia1 cells are capable of forming polarized of acini when cultured in Matrigel, these data suggest that the jamming/unjamming transition may be dispensable for the growth of epithelial tissues. However, shControl acini transition to the jammed state. This transition may relate to cell-ECM interactions and the generation of a basement membrane. Muthuswamy and colleagues investigated movements within acini formed by MCF-10A cells, and found that disruption of the basement membrane stimulated cell motility [276].

Making precise measurements on the actin cortex of living cells is typically an invasive procedure [254, 253], with few models that help interpret such precise measurements to understand their biological significance. Yet it is well-appreciated that mechanical properties of tissues, arising from intracellular actomyosin dynamics, drive many morphogenic events during organismal development [248, 142, 121]. Looking ahead, we suspect that analysis of subcellular actomyosin neworks could help discern how tissue properties arise from cytoskeletal regulators. This work opens new possibilities to explore the how the effects of such cytoskeletal regulators are propagated across tissues.

4.5 Methods

Cell culture and reagents

Manin-Darby Canine Kidney (MDCK) type II/G cells (American Type Culture Col-

lection) were cultured in a humidified incubator with 5% CO2 using Dulbeccos Minimal Essential Medium (Corning) supplemented with 5% fetal bovine serum (FBS) (Corning), 2 mM l-Glutamine, and penicillin-streptomycin (Corning). Y-27632 (Millipore) was diluted to 10 μM in DMSO. MDCK cells stably expressing the nuclear marker H2B-mPlum were kindly provided by W James Nelson (Stanford University).

Culture and manipulation of acini

Matrigel (Corning) from a single lot containing 9.1mg/ml protein was used for all 3D culture experiments. To generate acini, the lower surface of wells in a 24-well plate were coated with 30 μl Matrigel and allowed to gel at 37 C. MDCK cells were trypsinized, pipetted vigorously to break up cell clusters, and 10,000 cells were added to 800 μl of a 1:1 solution of growth media and Matrigel, which was kept on ice to prevent gelation. The resulting cell suspension was immediately pipetting up and down to disperse cells and added to the Matrigel-coated well The Matrigel-cell suspension was immediately placed in a 37 C incubator and allowed to gel for 30 minutes before 800 μl growth media was gently added to each well. Media was changed every 3 days for 6-7 days until acini formed lumens. To isolate acini, a modified protocol by Rubashkin *et al* was used to melt Matrigel by incubation at low temperatures [181]. Briefly, media was aspirated and Matrigel was disrupted by pipetting up and down with 5 ml of warm PBS with Ca/Mg (Corning) per well. The PBS-Matrigel solution was pelleted at 500 x g for 3 minutes and resuspended in 10 ml fresh PBS was added. Acini were incubated in a bucket of salted ice with rocking at maximum speed for 40 minutes. Acini were pelleted at 500 x g, yielding a ˜50 μl slurry of residual Matrigel and acini which were kept on ice to prevent gelation. Collagen gels were prepared 30 minutes before use and kept on ice. To prepare collagen gels, 1 M HEPES and 7.5% NaHCO3 were combined with media to achieve final ratios of 1:50 and 1:23.5, respectively. Rat tail collagen 1 (Corning) was gently added to a final concentration of 2 mg/ml. Acini were added to the collagen solution, mixed by pipetting, and plated in 100 μl onto 25 mm coverslips. Coverslips were sealed in magnetic chambers (Chamlide).

Microscopy

All fluorescence images were acquired on an inverted microscope (Ti-E; Nikon) with a confocal scanhead (CSUX; Yokogawa Electric Corporation), laser merge module containing 491, 561, and 642 laser lines (Spectral Applied Research), a stage controller (Prior), and a cooled charge-coupled device camera (HQ2; Roper Scientific). Images were acquired using either a 20x 0.75 NA Plan Fluor multi-immersion objective (Nikon) or a 40x 1.15 NA Plan Apo water immersion extra long working distance objective (Nikon). Immunostained acini were imaged by acquiring z-stacks with either 500 nm or 1 μm z spacing. All transmitted light images were acquired on an inverted microscope (Ti-E; Nikon), a stage controller (Prior), and a cooled charge-coupled device camera (HQ2; Roper Scientific). Images were acquired using a 20x 0.45 NA air extra long working distance objective (Nikon). All hardware was controlled via MetaMorph acquisition software (Molecular Devices).

Live cell imaging

All live cell imaging was performed with a stage incubator for temperature, humidity, and CO2 control (Chamlide TC and FC-5N; Quorum Technologies). The stage adaptor, stage cover, and objective were maintained at 37 C, while humidified 5% CO2 air was maintained at 50 C at its source to prevent condensation within its tubing. Acini were transferred to collagen gels in magnetic chambers (Chamlide) at least 1 day prior to imaging. Imaging media was identical to growth media except phenol red-free DMEM was used. Imaging media containing 20 ng/ml HGF was added to chambers immediately before transfer to the pre-warmed microscope stage, where they equilibrated for ˜30 minutes prior to imaging. Image sequences were corrected for drift using the Stackreg plugin in ImageJ (National Institutes of Health). Fluorescence imaging of cells expressing H2B-mPlum was performed by collecting z-stacks of 21 planes at 3 μm intervals every 15 minutes.

Immunofluorescence

For immunofluorescence staining of acini, a 1.5 U/ml solution of Clostridium Collagenase (Sigma) in PBS was added to culture media prior to fixation and acini were replaced in the

incubator for 10 minutes. Acini were fixed in a solution of 4% paraformaldehyde with 0.1% Triton X-100 in Phosphate Buffered Saline solution (PBS, Corning). Fixation solution was gently added to each well while simultaneously aspirating culture media, and incubated for 20 minutes. Collagen autofluorescence was quenched with 3 rinses of 0.1 M glycine in PBS for 20 minutes each. Acini were permeabolized in 0.5% Triton X-100 for 10 minutes, and blocked with 2.5% Bovine Serum Albumin and 0.1% Triton X-100 in PBS for 1 hour. Acini were incubated with Alexa fluor 647 phalloidin at 1:1000 (Life Technologies) in blocking solution for 1 hour. After another 3 20 minute washes with 0.1% Triton X-100, chamber walls were removed and 20 l Prolong Gold (Life Technologies) was added per well. A clean coverslip had clear blobs of nail polish applied to its corners and allowed to dry, and placed over the chamber slide. Slides were allowed to dry, sealed with nail polish, and stored at 4 C. All incubations were performed on a rotary shaker.

Image analysis

To trace cell outlines, 2 confocal sections spanning 2 μm in z were combined in maximum projections. This was repeated at the upper and lower surface of each acinus. Acini were only analyzed when cell borders were easily resolved by phalloidin staining. Cell borders were manually drawn and shape analysis was performed using ImageJ (National Institutes of Health). $p_0 0$ for each cell was calculated by dividing its perimeter by the square root of its area, according to the model published by Bi et al (2015). At least 5 cells per acinus were measured. To measure junction orientation, confocal sections of phalloidin staining in the equitorial plane of acini were analyzed. A straight line was drawn from the center of the acinus through a cell junction, orthogonal to the cell's basal surface using ImageJ (National Institutes of Health). Then a straight line was drawn along the cell-cell junction to capture its orientation. The angle between these lines was recorded. For consistency, only the larger angle was recorded for each cell-cell junction. Only junctions that lay within the plane of the confocal section were analyzed. At least 7 junctions were analyzed per acinus. For nuclear tracking, image sequences for analysis were generated by combining lower z-planes from

each acinus into maximum projections. Cells were tracked manually in ImageJ (National Institutes of Health).

Statistical Tests

To assess statistical significance, we used independent two-sample Students t tests of the mean to determine the significance with respect to the Control.

CHAPTER 5

DISCUSSION

5.1 Summary

The preceding chapters have detailed investigations into the biology of epithelial tissues, and how they regulate tissue shape changes in 3D environments. Overall this work links tissue shapes with established regulators of cell adhesion originally defined for cell migration along 2D surfaces. These findings encourage new applications of long-established models for cytoskeletal control of cell motility. They also support an emerging biophysical perspective on the mechanisms of invasion and dissemination by breast cancer cells.

Cells regulate their adhesions to their surroundings through combined biochemical and biophysical mechanisms [112]. Adhesion formation and regulation during cell motility is integrated into the actomyosin networks that span cells [118]. Data presented here shows that cytoskeletal regulators exert dominant effects on cell adhesions to their surroundings during tissue shape changes. The formin Dia1 is required for the morphological and biochemical maturation of focal adhesion plaques, as was shown previously [170]. The present work shows that loss of Dia1 does not prevent the formation of polarized acini in 3D culture, and does not prevent cell movement within acini. Further, Dia1 is dispensable for motility stimulated by the growth factor HGF along 2D substrates. These observations provoke the question: what is the physiologic role of focal adhesion maturation?

Indeed many cell motility behaviors do not require that cells form canonically mature focal adhesions [167]. This question is resolved for tissue shape changes by functionally separating different interactions between MDKC cells and the surrounding collagen matrix, which in turn correspond to different MDCK cell motility behaviors. When stimulated with Hepatocyte Growth Factor (HGF), MDCK cells exhibit two distinct motility phenotypes: cells rearrange and rotate within the plane of the epithelium, after which a few cells initiate out-of-plane motility and extend into the collagen matrix. Current models for cell motil-

ity, whether along 2D surfaces or through 3D matrices, and whether as single cells or cell collectives, did not offer clear predictions on how MDCK acini might control these distinct motility phenotypes. Our observations of cell-collagen interactions establish that Dia1 is critical for stable adhesion to collagen fibrils. Adhesion instability is marked by the inability to deform collagen fibrils as cells contract against them. This adhesion defect prevents MDCK cells depleted of Dia1 from undertaking collective shape changes. A previous report from our group similarly concluded that remodeling of ECM proteins was impaired when focal adhesion maturation was blocked [170]. Together these results suggest that focal adhesion maturation might play a conserved role in the deformation or reorganization of ECM proteins on subcellular scales. Finally, these observations show how multicellular behaviors depend on subcellular cytoskeletal control of adhesions.

The work presented here does not thoroughly address biochemical signaling that might regulate branching morphogenesis. Interestingly, Mostov and colleagues have published a gene expression array study to uncover transcriptional profiles regulating branching morphogenesis [101]. This study notably did not identify formins or their regulators as significantly upregulated genes during branching morphogenesis. There could be several reasons for this. Their gene expression data came from MDCK cells after 72 hours of HGF stimulation. This might be too late to capture expression changes that drive the initial steps of branching morphogenesis, analyzed here. Further, and more importantly, gene expression changes may not be necessary to drive the initial cytoskeletal changes that accomplish cell invasion.

Several cell-intrinsic parameters contribute to the mechanical properties of tissues [247, 142, 262, 260]. Many of these parameters directly impact cell shapes within epithelial monolayers [258]. This prompted our exploration of physical models to help understand and predict tissue properties by analyzing their cellular constituents [257, 277]. We tested a model for tissue jamming transitions predicated on cell shape measurements. Using two different perturbations of the actin cortex – depletion of Dia1 or inhibition of myosin contractility – we could drive MDCK acini from a jammed state into an unjammed, fluid-like state. We

further show that the stimulation of cell motility by HGF also induces unjamming. This work validated the generality for this jamming model in spherical epithelial tissues, which are topologically identical to epithelial monolayers in 2D culture. We therefore confirm that cell shape reports on biologically relevant tissue parameters irrespective of tissue culture as a 2D or a 3D monolayer.

Considered together, this work clarifies the roles for formins as cytoskeletal regulators controlling the mechanical properties and shape changes of epithelial tissues. These expanded roles provoke a reconsideration of how tissues change shape, whether in developmental or pathological contexts. Regulation of formins also offers a mechanism by which tissues could control shape changes downstream of a potent driver of cell motility such as HGF. The turnover of actin networks in the cell cortex might offer a unified mechanism that relates formin activity both to cell shape and to the stability of cell adhesions to collagen. We show that tissue unjamming or fluidization occurs early during HGF-stimulated branching morphogenesis. However, the cell jamming model in its current form does not describe later invasive processes as these involve shape constraints of the tissue as well as inhomogeneities in cell mechanics for which the model cannot account. This model might therefore be helpfully extended by probing whether and how the initial tissue state dictates the course of branching morphogenesis, for example when myosin contractility is inhibited.

The roles we define for Dia1 in controlling adhesion stability during branching morphogenesis encourage a reconsideration of how Dia1 is regulated. In most contexts, Dia1 is activated by binding of Rho [143, 134]. In addition to controlling formins, however, Rho activates myosin contractility through ROCK [143]. As a central regulator of cell motility Rho has been presumed to determine cell shape and motility through myosin contractility. This conflation of myosin with Rho signaling, at the expense of consideration for formins, has contributed to simplistic views of focal adhesion maturation and actin network organization [174, 278, 116]. In contrast, data presented here advocates for opposing roles assumed by Rho. Via ROCK and myosin activity, Rho controls cell shape, limits protrusions, and

enforces front-rear polarity [246, 121, 113]. However, myosin contractility is not required for small, unstable adhesions [170]. Through formins, Rho controls the actin network organization of a cell through formation of stress fibers, which are required to form stable focal adhesions [157, 170].

In the case of MDCK acini undergoing branching morphogenesis, these two effects of Rho appear to compete to control cell motility into the collagen gel. Prior to branching, cells undergo rapid rearrangements and move past sites of adhesion on collagen fibrils. Without formin activity, adhesions are easily disassembled in the midst of these cell rearrangements. On the other hand, without myosin contractility cell rearrangements do not propagate tension across the monolayer. Thus weak adhesions can prevail and cells can migrate into the collagen gel, as has been reported upon ROCK inhibition [95]. Together, these data propose a refined role for Rho and emphasize the competing roles of cytoskeletal regulators.

5.2 Future directions

An immediate implication of this work is the role for formins during branching morphogenesis and tumor invasion. To clarify this role, two avenues could be pursued. First, cells overexpressing either full-length Dia1 or a version missing its regulatory domains could be tested for their ability to invade into collagen gels. Using MDCK cells, a corollary study could test whether these constructs interfere with growth and polarization of acini in Matrigel. Both MDCK acini and mouse tumor explants could be employed to test whether Dia1 expression is sufficient to induce collective cell invasion in a dose-dependent manner. This possibility is suggested already by studies showing that an intermediate filament, Cytokeratin 14, promotes invasion by mammary tumor cells [41]. The actin cytoskeleton and the intermediate filament network have been shown to interact, although the details of their interaction are not understood [279, 280]. If their interaction is indeed mechanistically related to invasion, then Dia1 may operate as a cytoskeletal effector of mammary tumor cell lineage as was demonstrated for Cytokeratin 14.

One aspect of this work that has yet to be fully investigated is the relation of the data shown here to the properties of the cell cortex. The control of actin cortex mechanics are a rich area of investigation by biologists as well as physicists [281, 271, 272] yet cortical dynamics in multicellular ensembles are less well studied outside of intact embryos [264, 282]. The present work may therefore present a compelling case for the integration of two distinct but related areas of investigation: actin cortical dynamics and focal adhesion formation and turnover. Acini of MDCK cells present a unique case for the formation of focal adhesions not seen in canonical models of cell motility on 2D substrates [112] or in single cells migrating through 3D environments [190]. This is thanks to the enforcement of a continuous surface formed by the acini, at which individual cells must form adhesions. The context in which such adhesions are formed appears to be highly dependent on the properties of the actin cortex, as shown by this work. This might be most readily apparent by the lattice light sheet imaging shown in Chapter 2.

It is therefore tempting to speculate that focal adhesions in MDCK acini might share common themes with other cell surface assemblies such as immunological signaling complexes [283]. The formation of such complexes is reliant on specific functions of the cortical actin network to which they are tethered. For example, the immunological synapse formed by T-cells with their targets was recently shown to exert centripetal force dependent on actomyosin contractility [284]. There is little reason to suspect that loss of Dia1 would only impair focal adhesion formation, and it might also prevent normal immune receptor function or a range of complexes that require the dynamics of the actin cortex for their formation [275]. Pursuing focal adhesion formation and stability in spherical tissues might benefit from, and contribute to, the body of literature on the acotmyosin cortex, its mechanical properties, and its role in cell surface receptor signaling. This connection is already suggested by lattice light sheet imaging of myosin activity at the cortex of control and Dia1-deficient MDKC acini, detailed in Chapter 2.

The methodologies pursued throughout this work encourage broader experimental con-

siderations of cell motility. Analyzing cytoskeletal regulators of cell shape or motility within model epithelial tissues draws from decades of accrued knowledge of cell motility and its control by the cytoskeleton. Cells do not create or use different protein components, or even very different subcellular organelles, whether moving in simplified 2D or complex 3D environments. What differs substantively across environments is rather the spatial organization of cytoskeletal proteins that regulate cell motility. Cell biologists must therefore carefully choose how to apply the lessons of cell motility studies across varying environments. The observations described here illustrate the shared overall organization and roles of the actin cytoskeleton in forming adhesions and driving cell motility. However, this work also emphasizes that some cytoskeletal proteins, such as myosin, mark cell adhesions to collagen in 3D contexts but not in 2D. Thus while the conclusions reached by this work are shared between cells migrating collectively in 3D and individually in 2D, namely, that actin organization determines adhesion stability, some of the components that mark subcellular organelles differ appreciably across cell culture conditions. As noted previously, the concentration of myosin at adhesions might signify that these share features with sites of ECM proteolysis known as invodosomes. If true, then the distinctions between focal adhesions and invadosomes might be revisited. Yet this work argues that, whatever their specific constituents, these adhesions require formins for their stability.

Overall this work illustrates that cell biology should advance through clear mechanistic models that make predictions across different experimental settings, but retain flexibility in visualizing and interpreting experimental results. Clearly, the internal organization of cells is under no obligation to abide by cell biologists' established classification schemes of, for example, a focal adhesion or an invadosome. This lesson should discourage dogmatic adherence to specific protein markers in order to validate the presence or absence of subcellular structures. Meanwhile this work encourages the application of mechanistic models differently to suit a given experimental context. This flexibility can move cell biology forward and highlight novel areas of overlap between existing subfields. Showing, for example, that

myosin is indeed localized to sites of adhesion permits us to broaden and specify into new contexts the predictions made by established models of cell motility in 2D.

Finally, the conclusions drawn here regarding emphasize the importance of defining functional outcomes when studing of cell motility and the actin cytoskeleton. Focal adhesion stability might best be studied in contexts where cells use focal adhesions to deform or remodel their physical surroundings in measurable ways, rather than in contexts that simply measure cell displacement. In this sense, cell motility, especially through 3D environments, might be more robust to perturbation than is generally appreciated in this field currently. More broadly, one might conclude that cell motility does not meaningfully capture the most critical behaviors of tissues as they develop or during cancer invasion. Tying functional outcomes for tissues more closely to individual cell behaviors may require consistently revisiting assumptions made about how to bridge these scales.

5.3 Outlook

This work describes methods and data that draws from the self-organization and emergent properties of cells and their fruitful investigation by imaging-based methods. These studies bridge 3D cell culture techniques and investigations into cell adhesions rooted in biophysics. Making these connections requires careful techniques for culturing and imaging multicellular structures. Much more can be learned by leveraging the improved resolution and sensitivity of lattice light sheet microscopy, for example. However, the value of creative and ambitious application of conventional microscopy cannot be overstated. Prioritizing resolution to the exclusion of all else risks missing the cell behaviors, albeit imperfectly captured, that might offer greater biological insight.

In this sense, the work described here highlights the importance of considering spatial scales in future advances in cell biology. Reductionist approaches too often to drive proposed biological mechanisms to the smallest conceptual scale. This scale may be that of a single protein domain [285] or as large as a single cell [286]. Bringing explanatory power

to biological phenomena drives many biologists toward simple causative protein-protein interactions, single gene actions, or cell populations. These often succeed in some instances but fail in others with limited understanding of why [287]. On the one hand, biologists have increasing understanding of the molecular mechanisms of protein actions, especially with recent advances of superresolution microscopy and cryo-EM studies [288]. On the other hand, more and more data is available on the bulk behavior of tumors using gene expression data, histology, or animal models [289, 31, 290]. These advances have yet to properly meet in the middle, to establish causal relationships between proteins and the immediate microenvironment of tissues. This scale has gained increasing relevance, for instance, due to mounting evidence for small clusters of tumor cells as seeds of future metastatic outgrowths [53, 54].

Finally, this work owes a significant debt to generations of microscopists. Prior to the theories and technologies that centralized the DNA code, the study of biology was acutely reliant on the ability to visually inspect and describe living systems. From the forms of single cells and the organelles within them, to the steps by which entire organisms attain their final shapes, living systems were investigated through meticulous description. The success of careful observation as a methodology traverses generations of biologists, from hand drawings of embryonic development by Wilhelm His [203], to the structure of mitochondria described by George Palade using electron microscopy [291]. Visual data provides invaluable source material with which biologists test hypotheses or elaborate underlying mechanisms. Technology drives improvements in observation, which could then adjust or disprove theoretical descriptions of biological systems. In many ways this methodology has changed little since the work of Willhelm His or Darcy Thompson. The ability to directly observe biological phenomena persists today as the foundation of understanding across subfields of biology, especially as a means of testing theories and hypotheses. Increasing the breadth and precision of imaging technologies thus pushes forward the boundaries of biological knowledge.

REFERENCES

[1] Mikala Egeblad, Elizabeth S. Nakasone, and Zena Werb. Tumors as organs: complex tissues that interface with the entire organism. *Developmental Cell*, 18(6):884–901, June 2010.

[2] Celeste M. Nelson and Mina J. Bissell. Of Extracellular Matrix, Scaffolds, and Signaling: Tissue Architecture Regulates Development, Homeostasis, and Cancer. *Annual Review of Cell and Developmental Biology*, 22(1):287–309, November 2006.

[3] Siddhartha Mukherjee. *The emperor of all maladies: a biography of cancer*. Scribner, New York, 1st scribner trade paperback ed edition, 2011.

[4] Leslie Foulds. The natural history of cancer. *Journal of Chronic Diseases*, 8(1):2–37, July 1958.

[5] B. Vogelstein, E. R. Fearon, S. R. Hamilton, S. E. Kern, A. C. Preisinger, M. Leppert, Y. Nakamura, R. White, A. M. Smits, and J. L. Bos. Genetic alterations during colorectal-tumor development. *The New England Journal of Medicine*, 319(9):525–532, September 1988.

[6] Douglas Hanahan and RobertA. Weinberg. Hallmarks of Cancer: The Next Generation. *Cell*, 144(5):646–674, March 2011.

[7] Arthur W. Lambert, Diwakar R. Pattabiraman, and Robert A. Weinberg. Emerging Biological Principles of Metastasis. *Cell*, 168(4):670–691, February 2017.

[8] Andrew G Clark and Danijela Matic Vignjevic. Modes of cancer cell invasion and the role of the microenvironment. *Current Opinion in Cell Biology*, 36:13–22, October 2015.

[9] Markus Affolter, Rolf Zeller, and Emmanuel Caussinus. Tissue remodelling through branching morphogenesis. *Nature Reviews Molecular Cell Biology*, 10(12):831–842, December 2009.

[10] B. A. Howard and B. A. Gusterson. Human breast development. *Journal of Mammary Gland Biology and Neoplasia*, 5(2):119–137, April 2000.

[11] Mina J Bissell, Aylin Rizki, and I Saira Mian. Tissue architecture: the ultimate regulator of breast epithelial function. *Current Opinion in Cell Biology*, 15(6):753–762, December 2003.

[12] Kornelia Polyak and Raghu Kalluri. The role of the microenvironment in mammary gland development and cancer. *Cold Spring Harbor Perspectives in Biology*, 2(11):a003244, November 2010.

[13] Mark D. Sternlicht, Hosein Kouros-Mehr, Pengfei Lu, and Zena Werb. Hormonal and local control of mammary branching morphogenesis. *Differentiation*, 74(7):365–381, September 2006.

[14] Sunil R Lakhani and Michael J O'Hare. The mammary myoepithelial cell - Cinderella or ugly sister? *Breast Cancer Research*, 3(1), February 2000.

[15] John Stingl, Connie J. Eaves, Iman Zandieh, and Joanne T. Emerman. Characterization of bipotent mammary epithelial progenitor cells in normal adult human breast tissue. *Breast Cancer Research and Treatment*, 67(2):93–109, May 2001.

[16] Lixing Zhan, Avi Rosenberg, Kenneth C. Bergami, Min Yu, Zhenyu Xuan, Aron B. Jaffe, Craig Allred, and Senthil K. Muthuswamy. Deregulation of Scribble Promotes Mammary Tumorigenesis and Reveals a Role for Cell Polarity in Carcinoma. *Cell*, 135(5):865–878, November 2008.

[17] Mona L. Gauthier, Hal K. Berman, Caroline Miller, Krystyna Kozakeiwicz, Karen Chew, Dan Moore, Joseph Rabban, Yunn Yi Chen, Karla Kerlikowske, and Thea D. Tlsty. Abrogated Response to Cellular Stress Identifies DCIS Associated with Subsequent Tumor Events and Defines Basal-like Breast Tumors. *Cancer Cell*, 12(5):479–491, November 2007.

[18] Marc J. van de Vijver, Yudong D. He, Laura J. van 't Veer, Hongyue Dai, Augustinus A.M. Hart, Dorien W. Voskuil, George J. Schreiber, Johannes L. Peterse, Chris Roberts, Matthew J. Marton, Mark Parrish, Douwe Atsma, Anke Witteveen, Annuska Glas, Leonie Delahaye, Tony van der Velde, Harry Bartelink, Sjoerd Rodenhuis, Emiel T. Rutgers, Stephen H. Friend, and Ren Bernards. A Gene-Expression Signature as a Predictor of Survival in Breast Cancer. *New England Journal of Medicine*, 347(25):1999–2009, December 2002.

[19] Richard M. Neve, Koei Chin, Jane Fridlyand, Jennifer Yeh, Frederick L. Baehner, Tea Fevr, Laura Clark, Nora Bayani, Jean-Philippe Coppe, Frances Tong, Terry Speed, Paul T. Spellman, Sandy DeVries, Anna Lapuk, Nick J. Wang, Wen-Lin Kuo, Jackie L. Stilwell, Daniel Pinkel, Donna G. Albertson, Frederic M. Waldman, Frank McCormick, Robert B. Dickson, Michael D. Johnson, Marc Lippman, Stephen Ethier, Adi Gazdar, and Joe W. Gray. A collection of breast cancer cell lines for the study of functionally distinct cancer subtypes. *Cancer Cell*, 10(6):515–527, December 2006.

[20] Harold J. Burstein, Kornelia Polyak, Julia S. Wong, Susan C. Lester, and Carolyn M. Kaelin. Ductal Carcinoma in Situ of the Breast. *New England Journal of Medicine*, 350(14):1430–1441, April 2004.

[21] Gaorav P. Gupta and Joan Massagu. Cancer Metastasis: Building a Framework. *Cell*, 127(4):679–695, November 2006.

[22] Robert Lesurf, MiriamRagle Aure, HanneHberg Mrk, Valeria Vitelli, Steinar Lundgren, Anne-Lise Brresen-Dale, Vessela Kristensen, Fredrik Wrnberg, Michael Hallett, Therese Srlie, Torill Sauer, Jrgen Geisler, Solveig Hofvind, Elin Borgen, Anne-Lise Brresen-Dale, Olav Engebrten, ystein Fodstad, ystein Garred, GryAarum Geitvik, Rolf Kresen, Bjrn Naume, GunhildMari Mlandsmo, HegeG. Russnes, Ellen Schlichting, Therese Srlie, OleChristian Lingjrde, Vessela Kristensen, KristineKleivi Sahlberg,

HelleKristine Skjerven, and Britt Fritzman. Molecular Features of Subtype-Specific Progression from Ductal Carcinoma In Situ to Invasive Breast Cancer. *Cell Reports*, 16(4):1166–1179, July 2016.

[23] Karla Kerlikowske, Annette Molinaro, Imok Cha, Britt-Marie Ljung, Virginia L. Ernster, Kim Stewart, Karen Chew, Dan H. Moore, and Fred Waldman. Characteristics associated with recurrence among women with ductal carcinoma in situ treated by lumpectomy. *Journal of the National Cancer Institute*, 95(22):1692–1702, November 2003.

[24] Vinay Kumar, Abul K. Abbas, Jon C. Aster, and Stanley L. Robbins, editors. *Robbins basic pathology*. Elsevier/Saunders, Philadelphia, PA, 9th ed edition, 2013.

[25] P. Schedin and P. J. Keely. Mammary Gland ECM Remodeling, Stiffness, and Mechanosignaling in Normal Development and Tumor Progression. *Cold Spring Harbor Perspectives in Biology*, 3(1):a003228–a003228, January 2011.

[26] So Yeon Park, Mithat Gnen, Hee Jung Kim, Franziska Michor, and Kornelia Polyak. Cellular and genetic diversity in the progression of in situ human breast carcinomas to an invasive phenotype. *Journal of Clinical Investigation*, 120(2):636–644, February 2010.

[27] Kornelia Polyak and Min Hu. Do Myoepithelial Cells Hold the Key for Breast Tumor Progression? *Journal of Mammary Gland Biology and Neoplasia*, 10(3):231–247, July 2005.

[28] Thea D. Tlsty and Lisa M. Coussens. Tumor Stroma and Regulation of Cancer Development. *Annual Review of Pathology: Mechanisms of Disease*, 1(1):119–150, February 2006.

[29] Matthew W. Conklin, Jens C. Eickhoff, Kristin M. Riching, Carolyn A. Pehlke, Kevin W. Eliceiri, Paolo P. Provenzano, Andreas Friedl, and Patricia J. Keely. Aligned Collagen Is a Prognostic Signature for Survival in Human Breast Carcinoma. *The American Journal of Pathology*, 178(3):1221–1232, March 2011.

[30] Sridhar Ramaswamy, Ken N. Ross, Eric S. Lander, and Todd R. Golub. A molecular signature of metastasis in primary solid tumors. *Nature Genetics*, 33(1):49–54, December 2002.

[31] Daniel C. Koboldt, Robert S. Fulton, Michael D. McLellan, Heather Schmidt, Joelle Kalicki-Veizer, Joshua F. McMichael, Lucinda L. Fulton, David J. Dooling, Li Ding, Elaine R. Mardis, Richard K. Wilson, Adrian Ally, Miruna Balasundaram, Yaron S. N. Butterfield, Rebecca Carlsen, Candace Carter, Andy Chu, Eric Chuah, Hye-Jung E. Chun, Robin J. N. Coope, Noreen Dhalla, Ranabir Guin, Carrie Hirst, Martin Hirst, Robert A. Holt, Darlene Lee, Haiyan I. Li, Michael Mayo, Richard A. Moore, Andrew J. Mungall, Erin Pleasance, A. Gordon Robertson, Jacqueline E. Schein, Arash Shafiei, Payal Sipahimalani, Jared R. Slobodan, Dominik Stoll, Angela Tam, Nina Thiessen, Richard J. Varhol, Natasja Wye, Thomas Zeng, Yongjun Zhao, Inanc

Birol, Steven J. M. Jones, Marco A. Marra, Andrew D. Cherniack, Gordon Saksena, Robert C. Onofrio, Nam H. Pho, Scott L. Carter, Steven E. Schumacher, Barbara Tabak, Bryan Hernandez, Jeff Gentry, Huy Nguyen, Andrew Crenshaw, Kristin Ardlie, Rameen Beroukhim, Wendy Winckler, Gad Getz, Stacey B. Gabriel, Matthew Meyerson, Lynda Chin, Peter J. Park, Raju Kucherlapati, Katherine A. Hoadley, J. Todd Auman, Cheng Fan, Yidi J. Turman, Yan Shi, Ling Li, Michael D. Topal, Xiaping He, Hann-Hsiang Chao, Aleix Prat, Grace O. Silva, Michael D. Iglesia, Wei Zhao, Jerry Usary, Jonathan S. Berg, Michael Adams, Jessica Booker, Junyuan Wu, Anisha Gulabani, Tom Bodenheimer, Alan P. Hoyle, Janae V. Simons, Matthew G. Soloway, Lisle E. Mose, Stuart R. Jefferys, Saianand Balu, Joel S. Parker, D. Neil Hayes, Charles M. Perou, Simeen Malik, Swapna Mahurkar, Hui Shen, Daniel J. Weisenberger, Timothy Triche Jr, Phillip H. Lai, Moiz S. Bootwalla, Dennis T. Maglinte, Benjamin P. Berman, David J. Van Den Berg, Stephen B. Baylin, Peter W. Laird, Chad J. Creighton, Lawrence A. Donehower, Gad Getz, Michael Noble, Doug Voet, Gordon Saksena, Nils Gehlenborg, Daniel DiCara, Juinhua Zhang, Hailei Zhang, Chang-Jiun Wu, Spring Yingchun Liu, Michael S. Lawrence, Lihua Zou, Andrey Sivachenko, Pei Lin, Petar Stojanov, Rui Jing, Juok Cho, Raktim Sinha, Richard W. Park, Marc-Danie Nazaire, Jim Robinson, Helga Thorvaldsdottir, Jill Mesirov, Peter J. Park, Lynda Chin, Sheila Reynolds, Richard B. Kreisberg, Brady Bernard, Ryan Bressler, Timo Erkkila, Jake Lin, Vesteinn Thorsson, Wei Zhang, Ilya Shmulevich, Giovanni Ciriello, Nils Weinhold, Nikolaus Schultz, Jianjiong Gao, Ethan Cerami, Benjamin Gross, Anders Jacobsen, Rileen Sinha, B. Arman Aksoy, Yevgeniy Antipin, Boris Reva, Ronglai Shen, Barry S. Taylor, Marc Ladanyi, Chris Sander, Pavana Anur, Paul T. Spellman, Yiling Lu, Wenbin Liu, Roel R. G. Verhaak, Gordon B. Mills, Rehan Akbani, Nianxiang Zhang, Bradley M. Broom, Tod D. Casasent, Chris Wakefield, Anna K. Unruh, Keith Baggerly, Kevin Coombes, John N. Weinstein, David Haussler, Christopher C. Benz, Joshua M. Stuart, Stephen C. Benz, Jingchun Zhu, Christopher C. Szeto, Gary K. Scott, Christina Yau, Evan O. Paull, Daniel Carlin, Christopher Wong, Artem Sokolov, Janita Thusberg, Sean Mooney, Sam Ng, Theodore C. Goldstein, Kyle Ellrott, Mia Grifford, Christopher Wilks, Singer Ma, Brian Craft, Chunhua Yan, Ying Hu, Daoud Meerzaman, Julie M. Gastier-Foster, Jay Bowen, Nilsa C. Ramirez, Aaron D. Black, Robert E. XPATH ERROR: unknown variable "tname"., Peter White, Erik J. Zmuda, Jessica Frick, Tara M. Lichtenberg, Robin Brookens, Myra M. George, Mark A. Gerken, Hollie A. Harper, Kristen M. Leraas, Lisa J. Wise, Teresa R. Tabler, Cynthia McAllister, Thomas Barr, Melissa Hart-Kothari, Katie Tarvin, Charles Saller, George Sandusky, Colleen Mitchell, Mary V. Iacocca, Jennifer Brown, Brenda Rabeno, Christine Czerwinski, Nicholas Petrelli, Oleg Dolzhansky, Mikhail Abramov, Olga Voronina, Olga Potapova, Jeffrey R. Marks, Wiktoria M. Suchorska, Dawid Murawa, Witold Kycler, Matthew Ibbs, Konstanty Korski, Arkadiusz Spychaa, Pawe Murawa, Jacek J. Brzeziski, Hanna Perz, Radosaw aniak, Marek Teresiak, Honorata Tatka, Ewa Leporowska, Marta Bogusz-Czerniewicz, Julian Malicki, Andrzej Mackiewicz, Maciej Wiznerowicz, Xuan Van Le, Bernard Kohl, Nguyen Viet Tien, Richard Thorp, Nguyen Van Bang, Howard Sussman, Bui Duc Phu, Richard Hajek, Nguyen Phi Hung, Tran Viet The Phuong, Huynh Quyet Thang, Khurram Zaki Khan, Robert Penny, David Mallery, Erin Curley, Candace Shelton,

Peggy Yena, James N. Ingle, Fergus J. Couch, Wilma L. Lingle, Tari A. King, Ana Maria Gonzalez-Angulo, Gordon B. Mills, Mary D. Dyer, Shuying Liu, Xiaolong Meng, Modesto Patangan, Frederic Waldman, Hubert Stppler, W. Kimryn Rathmell, Leigh Thorne, Mei Huang, Lori Boice, Ashley Hill, Carl Morrison, Carmelo Gaudioso, Wiam Bshara, Kelly Daily, Sophie C. Egea, Mark D. Pegram, Carmen Gomez-Fernandez, Rajiv Dhir, Rohit Bhargava, Adam Brufsky, Craig D. Shriver, Jeffrey A. Hooke, Jamie Leigh Campbell, Richard J. Mural, Hai Hu, Stella Somiari, Caroline Larson, Brenda Deyarmin, Leonid Kvecher, Albert J. Kovatich, Matthew J. Ellis, Tari A. King, Hai Hu, Fergus J. Couch, Richard J. Mural, Tho. Comprehensive molecular portraits of human breast tumours. *Nature*, 490(7418):61–70, September 2012.

[32] T. Sorlie, C. M. Perou, R. Tibshirani, T. Aas, S. Geisler, H. Johnsen, T. Hastie, M. B. Eisen, M. van de Rijn, S. S. Jeffrey, T. Thorsen, H. Quist, J. C. Matese, P. O. Brown, D. Botstein, P. E. Lonning, and A.-L. Borresen-Dale. Gene expression patterns of breast carcinomas distinguish tumor subclasses with clinical implications. *Proceedings of the National Academy of Sciences*, 98(19):10869–10874, September 2001.

[33] S. Lee, S. Stewart, I. Nagtegaal, J. Luo, Y. Wu, G. Colditz, D. Medina, and D. C. Allred. Differentially Expressed Genes Regulating the Progression of Ductal Carcinoma In Situ to Invasive Breast Cancer. *Cancer Research*, 72(17):4574–4586, September 2012.

[34] H. K. Berman, M. L. Gauthier, and T. D. Tlsty. Premalignant Breast Neoplasia: A Paradigm of Interlesional and Intralesional Molecular Heterogeneity and Its Biological and Clinical Ramifications. *Cancer Prevention Research*, 3(5):579–587, May 2010.

[35] Andriy Marusyk and Kornelia Polyak. Tumor heterogeneity: Causes and consequences. *Biochimica et Biophysica Acta (BBA) - Reviews on Cancer*, 1805(1):105–117, January 2010.

[36] Eliah R. Shamir and Andrew J. Ewald. Three-dimensional organotypic culture: experimental models of mammalian biology and disease. *Nature Reviews Molecular Cell Biology*, 15(10):647–664, September 2014.

[37] A. J. Ewald. Practical Considerations for Long-Term Time-Lapse Imaging of Epithelial Morphogenesis in Three-Dimensional Organotypic Cultures. *Cold Spring Harbor Protocols*, 2013(2):pdb.top072884–pdb.top072884, February 2013.

[38] Eliah R. Shamir, Elisa Pappalardo, Danielle M. Jorgens, Kester Coutinho, Wen-Ting Tsai, Khaled Aziz, Manfred Auer, Phuoc T. Tran, Joel S. Bader, and Andrew J. Ewald. Twist1-induced dissemination preserves epithelial identity and requires E-cadherin. *The Journal of Cell Biology*, 204(5):839–856, March 2014.

[39] K.-V. Nguyen-Ngoc and A.J. Ewald. Mammary ductal elongation and myoepithelial migration are regulated by the composition of the extracellular matrix: EXTRACELLULAR MATRIX REGULATION OF BRANCHING MORPHOGENESIS. *Journal of Microscopy*, 251(3):212–223, September 2013.

[40] Mina J. Bissell and Mark A. LaBarge. Context, tissue plasticity, and cancer. *Cancer Cell*, 7(1):17–23, January 2005.

[41] KevinJ. Cheung, Edward Gabrielson, Zena Werb, and AndrewJ. Ewald. Collective Invasion in Breast Cancer Requires a Conserved Basal Epithelial Program. *Cell*, 155(7):1639–1651, December 2013.

[42] Robert J. Huebner and Andrew J. Ewald. Cellular foundations of mammary tubulogenesis. *Seminars in Cell & Developmental Biology*, 31:124–131, July 2014.

[43] K.-V. Nguyen-Ngoc, K. J. Cheung, A. Brenot, E. R. Shamir, R. S. Gray, W. C. Hines, P. Yaswen, Z. Werb, and A. J. Ewald. ECM microenvironment regulates collective migration and local dissemination in normal and malignant mammary epithelium. *Proceedings of the National Academy of Sciences*, 109(39):E2595–E2604, September 2012.

[44] Anna Labernadie, Takuya Kato, Agust Brugus, Xavier Serra-Picamal, Stefanie Derzsi, Esther Arwert, Anne Weston, Victor Gonzlez-Tarrag, Alberto Elosegui-Artola, Lorenzo Albertazzi, Jordi Alcaraz, Pere Roca-Cusachs, Erik Sahai, and Xavier Trepat. A mechanically active heterotypic E-cadherin/N-cadherin adhesion enables fibroblasts to drive cancer cell invasion. *Nature Cell Biology*, 19(3):224–237, February 2017.

[45] J. B. Wyckoff, Y. Wang, E. Y. Lin, J.-f. Li, S. Goswami, E. R. Stanley, J. E. Segall, J. W. Pollard, and J. Condeelis. Direct Visualization of Macrophage-Assisted Tumor Cell Intravasation in Mammary Tumors. *Cancer Research*, 67(6):2649–2656, March 2007.

[46] John Condeelis and Jeffrey W. Pollard. Macrophages: Obligate Partners for Tumor Cell Migration, Invasion, and Metastasis. *Cell*, 124(2):263–266, January 2006.

[47] P Bronsert, K Enderle-Ammour, M Bader, S Timme, M Kuehs, A Csanadi, G Kayser, I Kohler, D Bausch, J Hoeppner, Ut Hopt, T Keck, E Stickeler, B Passlick, O Schilling, Cp Reiss, Y Vashist, T Brabletz, J Berger, J Lotz, J Olesch, M Werner, and Uf Wellner. Cancer cell invasion and EMT marker expression: a three-dimensional study of the human cancer-host interface: 3d cancer-host interface. *The Journal of Pathology*, 234(3):410–422, November 2014.

[48] Peter Friedl, Joseph Locker, Erik Sahai, and Jeffrey E. Segall. Classifying collective cancer cell invasion. *Nature cell biology*, 14(8):777–783, 2012.

[49] Patricia J. Keely. Mechanisms by Which the Extracellular Matrix and Integrin Signaling Act to Regulate the Switch Between Tumor Suppression and Tumor Promotion. *Journal of Mammary Gland Biology and Neoplasia*, 16(3):205–219, September 2011.

[50] Christopher C. DuFort, Matthew J. Paszek, and Valerie M. Weaver. Balancing forces: architectural control of mechanotransduction. *Nature Reviews Molecular Cell Biology*, 12(5):308–319, May 2011.

[51] Kandice R. Levental, Hongmei Yu, Laura Kass, Johnathon N. Lakins, Mikala Egeblad, Janine T. Erler, Sheri F.T. Fong, Katalin Csiszar, Amato Giaccia, Wolfgang Weninger, Mitsuo Yamauchi, David L. Gasser, and Valerie M. Weaver. Matrix Crosslinking Forces Tumor Progression by Enhancing Integrin Signaling. *Cell*, 139(5):891–906, November 2009.

[52] I. Zeidman and J. M. Buss. Transpulmonary passage of tumor cell emboli. *Cancer Research*, 12(10):731–733, October 1952.

[53] Nicola Aceto, Aditya Bardia, DavidT. Miyamoto, MariaC. Donaldson, BenS. Wittner, JoelA. Spencer, Min Yu, Adam Pely, Amanda Engstrom, Huili Zhu, BrianW. Brannigan, Ravi Kapur, ShannonL. Stott, Toshi Shioda, Sridhar Ramaswamy, DavidT. Ting, CharlesP. Lin, Mehmet Toner, DanielA. Haber, and Shyamala Maheswaran. Circulating Tumor Cell Clusters Are Oligoclonal Precursors of Breast Cancer Metastasis. *Cell*, 158(5):1110–1122, August 2014.

[54] K. J. Cheung and A. J. Ewald. A collective route to metastasis: Seeding by tumor cell clusters. *Science*, 352(6282):167–169, April 2016.

[55] Sanjay Kumar and Valerie M. Weaver. Mechanics, malignancy, and metastasis: The force journey of a tumor cell. *Cancer and Metastasis Reviews*, 28(1-2):113–127, June 2009.

[56] Xavier Bichat. *General Anatomy, Applied to Physiology and Medicine*. Richardson and Lord, 1822.

[57] Keith L. Moore, Arthur F. Dalley, and A. M. R. Agur. *Clinically oriented anatomy*. Wolters Kluwer/Lippincott Williams & Wilkins Health, Philadelphia, 7th ed edition, 2014.

[58] Michael H. Ross and Wojciech Pawlina. *Histology: a text and atlas: with correlated cell and molecular biology*. Wolters Kluwer/Lippincott Williams & Wilkins Health, Philadelphia, 6th ed edition, 2011. OCLC: ocn548651322.

[59] E. R. Weibel and D. M. Gomez. Architecture of the Human Lung: Use of quantitative methods establishes fundamental relations between size and number of lung structures. *Science*, 137(3530):577–585, August 1962.

[60] L Saxen. *Organogenesis of the Kidney*. Cambridge University Press, 1987.

[61] Mark D Sternlicht. Key stages in mammary gland development: The cues that regulate ductal branching morphogenesis. *Breast Cancer Research*, 8(1), February 2005.

[62] Barry Lubarsky and Mark A. Krasnow. Tube Morphogenesis. *Cell*, 112(1):19–28, January 2003.

[63] Shaohe Wang, Rei Sekiguchi, William P. Daley, and Kenneth M. Yamada. Patterned cell and matrix dynamics in branching morphogenesis. *The Journal of Cell Biology*, page jcb.201610048, February 2017.

[64] Virginie Lecaudey and Darren Gilmour. Organizing moving groups during morphogenesis. *Current Opinion in Cell Biology*, 18(1):102–107, February 2006.

[65] Andrew J. Ewald, Audrey Brenot, Myhanh Duong, Bianca S. Chan, and Zena Werb. Collective Epithelial Migration and Cell Rearrangements Drive Mammary Branching Morphogenesis. *Developmental Cell*, 14(4):570–581, April 2008.

[66] Anne Uv, Rafael Cantera, and Christos Samakovlis. Drosophila tracheal morphogenesis: intricate cellular solutions to basic plumbing problems. *Trends in Cell Biology*, 13(6):301–309, June 2003.

[67] Celeste M. Nelson. Geometric control of tissue morphogenesis. *Biochimica et Biophysica Acta (BBA) - Molecular Cell Research*, 1793(5):903–910, May 2009.

[68] G. B. West, J. H. Brown, and B. J. Enquist. A general model for the origin of allometric scaling laws in biology. *Science (New York, N.Y.)*, 276(5309):122–126, April 1997.

[69] Ryan S Gray, Kevin J Cheung, and Andrew J Ewald. Cellular mechanisms regulating epithelial morphogenesis and cancer invasion. *Current Opinion in Cell Biology*, 22(5):640–650, October 2010.

[70] Markus Affolter, Savrio Bellusci, Nobuyuki Itoh, Benny Shilo, Jean-Paul Thiery, and Zena Werb. Tube or Not Tube. *Developmental Cell*, 4(1):11–18, January 2003.

[71] P. Devreotes. Dictyostelium discoideum: a model system for cell-cell interactions in development. *Science (New York, N.Y.)*, 245(4922):1054–1058, September 1989.

[72] Peter Friedl. Prespecification and plasticity: shifting mechanisms of cell migration. *Current Opinion in Cell Biology*, 16(1):14–23, February 2004.

[73] Tim Lmmermann and Michael Sixt. Mechanical modes of amoeboid cell migration. *Current Opinion in Cell Biology*, 21(5):636–644, October 2009.

[74] Amin S. Ghabrial and Mark A. Krasnow. Social interactions among epithelial cells during tracheal branching morphogenesis. *Nature*, 441(7094):746–749, June 2006.

[75] Lucy Erin O'Brien, Mirjam MP Zegers, and Keith E. Mostov. Building epithelial architecture: insights from three-dimensional culture models. *Nature Reviews Molecular Cell Biology*, 3(7):531–537, 2002.

[76] Andrew J. Ewald, R. J. Huebner, H. Palsdottir, J. K. Lee, M. J. Perez, D. M. Jorgens, A. N. Tauscher, K. J. Cheung, Z. Werb, and M. Auer. Mammary collective cell migration involves transient loss of epithelial features and individual cell migration within the epithelium. *Journal of Cell Science*, 125(11):2638–2654, June 2012.

[77] R. J. Huebner, N. M. Neumann, and A. J. Ewald. Mammary epithelial tubes elongate through MAPK-dependent coordination of cell migration. *Development*, 143(6):983–993, March 2016.

[78] A. D. Lander. How Cells Know Where They Are. *Science*, 339(6122):923–927, February 2013.

[79] Celeste M. Nelson, Martijn M. VanDuijn, Jamie L. Inman, Daniel A. Fletcher, and Mina J. Bissell. Tissue geometry determines sites of mammary branching morphogenesis in organotypic cultures. *Science*, 314(5797):298–300, 2006.

[80] AmyE. Shyer, TylerR. Huycke, ChangHee Lee, L. Mahadevan, and CliffordJ. Tabin. Bending Gradients: How the Intestinal Stem Cell Gets Its Home. *Cell*, 161(3):569–580, April 2015.

[81] Joseph Leighton, Larry W. Estes, Sunder Mansukhani, and Zbynek Brada. A cell line derived from normal dog kidney (MDCK) exhibiting qualities of papillary adenocarcinoma and of renal tubular epithelium. *Cancer*, 26(5):1022–1028, November 1970.

[82] H. G. Hall, D. A. Farson, and M. J. Bissell. Lumen formation by epithelial cell lines in response to collagen overlay: a morphogenetic model in culture. *Proceedings of the National Academy of Sciences of the United States of America*, 79(15):4672–4676, August 1982.

[83] James A. McAteer, Andrew P. Evan, and Kenneth D. Gardner. Morphogenetic clonal growth of kidney epithelial cell line MDCK. *The Anatomical Record*, 217(3):229–239, March 1987.

[84] M. Stoker and M. Perryman. An epithelial scatter factor released by embryo fibroblasts. *Journal of Cell Science*, 77:209–223, August 1985.

[85] Michael Stoker, Ermanno Gherardi, Marion Perryman, and Julia Gray. Scatter factor is a fibroblast-derived modulator of epithelial cell mobility. *Nature*, 327(6119):239–242, May 1987.

[86] Michael Stoker, Ermanno Gherardi, Marion Perryman, and Julia Gray. Scatter factor is a fibroblast-derived modulator of epithelial cell mobility. *Nature*, 327(6119):239–242, May 1987.

[87] J. Behrens, W. Birchmeier, S. L. Goodman, and B. A. Imhof. Dissociation of Madin-Darby canine kidney epithelial cells by the monoclonal antibody anti-arc-1: mechanistic aspects and identification of the antigen as a component related to uvomorulin. *The Journal of Cell Biology*, 101(4):1307–1315, October 1985.

[88] Beat A. Imhof, H. Peter Vollmers, Simon L. Goodman, and Walter Birchmeier. Cell-cell interaction and polarity of epithelial cells: Specific perturbation using a monoclonal antibody. *Cell*, 35(3):667–675, December 1983.

[89] J. Behrens. Dissecting tumor cell invasion: epithelial cells acquire invasive properties after the loss of uvomorulin-mediated cell-cell adhesion. *The Journal of Cell Biology*, 108(6):2435–2447, June 1989.

[90] R. Montesano, G. Schaller, and L. Orci. Induction of epithelial tubular morphogenesis in vitro by fibroblast-derived soluble factors. *Cell*, 66(4):697–711.

[91] K. M. Weidner, N. Arakaki, G. Hartmann, J. Vandekerckhove, S. Weingart, H. Rieder, C. Fonatsch, H. Tsubouchi, T. Hishida, and Y. Daikuhara. Evidence for the identity of human scatter factor and human hepatocyte growth factor. *Proceedings of the National Academy of Sciences*, 88(16):7001–7005, August 1991.

[92] David M. Bryant and Keith E. Mostov. From cells to organs: building polarized tissue. *Nature Reviews Molecular Cell Biology*, 9(11):887–901, November 2008.

[93] Fernando Martin-Belmonte, Ama Gassama, Anirban Datta, Wei Yu, Ursula Rescher, Volker Gerke, and Keith Mostov. PTEN-Mediated Apical Segregation of Phosphoinositides Controls Epithelial Morphogenesis through Cdc42. *Cell*, 128(2):383–397, January 2007.

[94] DavidM. Bryant, Julie Roignot, Anirban Datta, ArendW. Overeem, Minji Kim, Wei Yu, Xiao Peng, DennisJ. Eastburn, AndrewJ. Ewald, Zena Werb, and KeithE. Mostov. A Molecular Switch for the Orientation of Epithelial Cell Polarization. *Developmental Cell*, 31(2):171–187, October 2014.

[95] Wei Yu, Lucy E. O'Brien, Fei Wang, Henry Bourne, Keith E. Mostov, and Mirjam MP Zegers. Hepatocyte growth factor switches orientation of polarity and mode of movement during morphogenesis of multicellular epithelial structures. *Molecular biology of the cell*, 14(2):748–763, 2003.

[96] Mirjam M.P. Zegers, Lucy E. O'Brien, Wei Yu, Anirban Datta, and Keith E. Mostov. Epithelial polarity and tubulogenesis in vitro. *Trends in Cell Biology*, 13(4):169–176, April 2003.

[97] Jean Paul Thiery, Herv Acloque, Ruby Y.J. Huang, and M. Angela Nieto. Epithelial-Mesenchymal Transitions in Development and Disease. *Cell*, 139(5):871–890, November 2009.

[98] Elzbieta Janda, Kerstin Lehmann, Iris Killisch, Martin Jechlinger, Michaela Herzig, Julian Downward, Hartmut Beug, and Stefan Grnert. Ras and TGF cooperatively regulate epithelial cell plasticity and metastasis: dissection of Ras signaling pathways. *The Journal of Cell Biology*, 156(2):299–314, January 2002.

[99] Raghu Kalluri and Eric G. Neilson. Epithelial-mesenchymal transition and its implications for fibrosis. *Journal of Clinical Investigation*, 112(12):1776–1784, December 2003.

[100] M. Kim, A. M. Shewan, A. J. Ewald, Z. Werb, and K. E. Mostov. p114rhogef governs cell motility and lumen formation during tubulogenesis through a ROCK-myosin-II pathway. *Journal of Cell Science*, 128(23):4317–4327, December 2015.

[101] Lucy Erin O'Brien, Kitty Tang, Ellen S Kats, Amy Schutz-Geschwender, Joshua H Lipschutz, and Keith E Mostov. ERK and MMPs Sequentially Regulate Distinct Stages of Epithelial Tubule Development. *Developmental Cell*, 7(1):21–32, July 2004.

[102] Emmanuel Vial, Erik Sahai, and Christopher J. Marshall. ERK-MAPK signaling coordinately regulates activity of Rac1 and RhoA for tumor cell motility. *Cancer Cell*, 4(1):67–79, July 2003.

[103] Wei Yu, Annette M Shewan, Paul Brakeman, Dennis J Eastburn, Anirban Datta, David M Bryant, Qi-Wen Fan, William A Weiss, Mirjam M P Zegers, and Keith E Mostov. Involvement of RhoA, ROCK I and myosin II in inverted orientation of epithelial polarity. *EMBO reports*, 9(9):923–929, September 2008.

[104] M. P. Hunter and M. M. Zegers. Pak1 regulates branching morphogenesis in 3d MDCK cell culture by a PIX and 1-integrin-dependent mechanism. *AJP: Cell Physiology*, 299(1):C21–C32, July 2010.

[105] Si-Tse Jiang, Sue-Jean Chiu, Hong-Chen Chen, Woei-Jer Chuang, and Ming-Jer Tang. Role of 31 integrin in tubulogenesis of Madin-Darby canine kidney cells. *Kidney International*, 59(5):1770–1778, May 2001.

[106] Wei-Chun Wei, Anna K Kopec, and Ming-Jer Tang. Requirement of focal adhesion kinase in branching tubulogenesis. *Journal of Biomedical Science*, 16(1):5, 2009.

[107] Sarah Gierke and Torsten Wittmann. EB1-Recruited Microtubule +TIP Complexes Coordinate Protrusion Dynamics during 3d Epithelial Remodeling. *Current Biology*, 22(9):753–762, May 2012.

[108] M. Abercrombie. The Croonian Lecture, 1978: The Crawling Movement of Metazoan Cells. *Proceedings of the Royal Society B: Biological Sciences*, 207(1167):129–147, February 1980.

[109] Douglas A. Lauffenburger and Alan F. Horwitz. Cell migration: a physically integrated molecular process. *Cell*, 84(3):359–369, 1996.

[110] A. Mogilner and G. Oster. Cell motility driven by actin polymerization. *Biophysical Journal*, 71(6):3030–3045, December 1996.

[111] Heath E. Johnson, Samantha J. King, Sreeja B. Asokan, Jeremy D. Rotty, James E. Bear, and Jason M. Haugh. F-actin bundles direct the initiation and orientation of lamellipodia through adhesion-based signaling. *The Journal of Cell Biology*, 208(4):443–455, February 2015.

[112] B. Geiger and K. M. Yamada. Molecular Architecture and Function of Matrix Adhesions. *Cold Spring Harbor Perspectives in Biology*, 3(5):a005033–a005033, May 2011.

[113] A. J. Ridley. Cell Migration: Integrating Signals from Front to Back. *Science*, 302(5651):1704–1709, December 2003.

[114] A. J. Ridley. Rho GTPases and cell migration. *Journal of Cell Science*, 114(Pt 15):2713–2722, August 2001.

[115] Guillaume Charras and Erik Sahai. Physical influences of the extracellular environment on cell migration. *Nature Reviews Molecular Cell Biology*, 15(12):813–824, October 2014.

[116] Ryan J. Petrie and Kenneth M. Yamada. At the leading edge of three-dimensional cell migration. *Journal of Cell Science*, 125(24):5917–5926, December 2012.

[117] Thomas D. Pollard. Regulation of Actin Filament Assembly by Arp2/3 Complex and Formins. *Annual Review of Biophysics and Biomolecular Structure*, 36(1):451–477, June 2007.

[118] Margaret L. Gardel, Ian C. Schneider, Yvonne Aratyn-Schaus, and Clare M. Waterman. Mechanical Integration of Actin and Adhesion Dynamics in Cell Migration. *Annual Review of Cell and Developmental Biology*, 26(1):315–333, November 2010.

[119] Thomas D. Pollard and Gary G. Borisy. Cellular motility driven by assembly and disassembly of actin filaments. *Cell*, 112(4):453–465, February 2003.

[120] Miguel Vicente-Manzanares, Xuefei Ma, Robert S. Adelstein, and Alan Rick Horwitz. Non-muscle myosin II takes centre stage in cell adhesion and migration. *Nature Reviews Molecular Cell Biology*, 10(11):778–790, November 2009.

[121] Michael Murrell, Patrick W. Oakes, Martin Lenz, and Margaret L. Gardel. Forcing cells into shape: the mechanics of actomyosin contractility. *Nature Reviews Molecular Cell Biology*, 16(8):486–498, July 2015.

[122] Marie-France Carlier and Dominique Pantaloni. Control of actin dynamics in cell motility. *Journal of Molecular Biology*, 269(4):459–467, June 1997.

[123] Julie A. Theriot and Timothy J. Mitchison. Actin microfilament dynamics in locomoting cells. *Nature*, 352(6331):126–131, July 1991.

[124] J.Victor Small, Theresia Stradal, Emmanuel Vignal, and Klemens Rottner. The lamellipodium: where motility begins. *Trends in Cell Biology*, 12(3):112–120, March 2002.

[125] R. D. Mullins, J. A. Heuser, and T. D. Pollard. The interaction of Arp2/3 complex with actin: nucleation, high affinity pointed end capping, and formation of branching networks of filaments. *Proceedings of the National Academy of Sciences of the United States of America*, 95(11):6181–6186, May 1998.

[126] Laurent Blanchoin, Thomas D. Pollard, and R.Dyche Mullins. Interactions of ADF/cofilin, Arp2/3 complex, capping protein and profilin in remodeling of branched actin filament networks. *Current Biology*, 10(20):1273–1282, October 2000.

[127] Ursula Euteneuer and Manfred Schliwa. Persistent, directional motility of cells and cytoplasmic fragments in the absence of microtubules. *Nature*, 310(5972):58–61, July 1984.

[128] B. J. Nolen, N. Tomasevic, A. Russell, D. W. Pierce, Z. Jia, C. D. McCormick, J. Hartman, R. Sakowicz, and T. D. Pollard. Characterization of two classes of small molecule inhibitors of Arp2/3 complex. *Nature*, 460(7258):1031–1034, August 2009.

[129] Yvonne Beckham, Robert J. Vasquez, Jonathan Stricker, Kareem Sayegh, Clement Campillo, and Margaret L. Gardel. Arp2/3 Inhibition Induces Amoeboid-Like Protrusions in MCF10a Epithelial Cells by Reduced Cytoskeletal-Membrane Coupling and Focal Adhesion Assembly. *PLoS ONE*, 9(6):e100943, June 2014.

[130] Congying Wu, SreejaB. Asokan, MatthewE. Berginski, ElizabethM. Haynes, NormanE. Sharpless, JackD. Griffith, ShawnM. Gomez, and JamesE. Bear. Arp2/3 Is Critical for Lamellipodia and Response to Extracellular Matrix Cues but Is Dispensable for Chemotaxis. *Cell*, 148(5):973–987, March 2012.

[131] Bruce L. Goode and Michael J. Eck. Mechanism and Function of Formins in the Control of Actin Assembly. *Annual Review of Biochemistry*, 76(1):593–627, June 2007.

[132] David R Kovar. Molecular details of formin-mediated actin assembly. *Current Opinion in Cell Biology*, 18(1):11–17, February 2006.

[133] David R. Kovar, Andrew J. Bestul, Yujie Li, and Bonnie J. Scott. Formin-Mediated Actin Assembly. In Marie-France Carlier, editor, *Actin-based Motility*, pages 279–316. Springer Netherlands, Dordrecht, 2010.

[134] David R. Kovar, Elizabeth S. Harris, Rachel Mahaffy, Henry N. Higgs, and Thomas D. Pollard. Control of the Assembly of ATP- and ADP-Actin by Formins and Profilin. *Cell*, 124(2):423–435, January 2006.

[135] Melissa A. Chesarone, Amy Grace DuPage, and Bruce L. Goode. Unleashing formins to remodel the actin and microtubule cytoskeletons. *Nature Reviews Molecular Cell Biology*, 11(1):62–74, January 2010.

[136] Tomoko Tominaga, Erik Sahai, Pierre Chardin, Frank McCormick, Sara A. Courtneidge, and Arthur S. Alberts. Diaphanous-Related Formins Bridge Rho GTPase and Src Tyrosine Kinase Signaling. *Molecular Cell*, 5(1):13–25, January 2000.

[137] Judith E. Gasteier, Ricardo Madrid, Ellen Krautkrmer, Sebastian Schrder, Walter Muranyi, Serge Benichou, and Oliver T. Fackler. Activation of the Rac-binding Partner FHOD1 Induces Actin Stress Fibers via a ROCK-dependent Mechanism. *Journal of Biological Chemistry*, 278(40):38902–38912, October 2003.

[138] R. Niederman and T. D. Pollard. Human platelet myosin. II. In vitro assembly and structure of myosin filaments. *The Journal of Cell Biology*, 67(1):72–92, October 1975.

[139] H. E. Huxley. Muscular Contraction and Cell Motility. *Nature*, 243(5408):445–449, June 1973.

[140] E. D. Korn and J. A. Hammer. Myosins of nonmuscle cells. *Annual Review of Biophysics and Biophysical Chemistry*, 17:23–45, 1988.

[141] Miguel Vicente-Manzanares, Jessica Zareno, Leanna Whitmore, Colin K. Choi, and Alan F. Horwitz. Regulation of protrusion, adhesion dynamics, and polarity by myosins IIA and IIB in migrating cells. *The Journal of Cell Biology*, 176(5):573–580, February 2007.

[142] Thomas Lecuit, Pierre-Franois Lenne, and Edwin Munro. Force Generation, Transmission, and Integration during Cell and Tissue Morphogenesis. *Annual Review of Cell and Developmental Biology*, 27(1):157–184, November 2011.

[143] Aron B. Jaffe and Alan Hall. RHO GTPASES: Biochemistry and Biology. *Annual Review of Cell and Developmental Biology*, 21(1):247–269, November 2005.

[144] Ryu Takeya, Kenichiro Taniguchi, Shuh Narumiya, and Hideki Sumimoto. The mammalian formin FHOD1 is activated through phosphorylation by ROCK and mediates thrombin-induced stress fibre formation in endothelial cells. *The EMBO Journal*, 27(4):618–628, February 2008.

[145] Catherine D Nobes and Alan Hall. Rho, Rac, and Cdc42 GTPases regulate the assembly of multimolecular focal complexes associated with actin stress fibers, lamellipodia, and filopodia. *Cell*, 81(1):53–62, April 1995.

[146] M. Maekawa. Signaling from Rho to the Actin Cytoskeleton Through Protein Kinases ROCK and LIM-kinase. *Science*, 285(5429):895–898, August 1999.

[147] Christophe Guilluy, Rafael Garcia-Mata, and Keith Burridge. Rho protein crosstalk: another social network? *Trends in Cell Biology*, 21(12):718–726, December 2011.

[148] R. D. Fritz, M. Letzelter, A. Reimann, K. Martin, L. Fusco, L. Ritsma, B. Ponsioen, E. Fluri, S. Schulte-Merker, J. van Rheenen, and O. Pertz. A Versatile Toolkit to Produce Sensitive FRET Biosensors to Visualize Signaling in Time and Space. *Science Signaling*, 6(285):rs12–rs12, July 2013.

[149] Matthias Machacek, Louis Hodgson, Christopher Welch, Hunter Elliott, Olivier Pertz, Perihan Nalbant, Amy Abell, Gary L. Johnson, Klaus M. Hahn, and Gaudenz Danuser. Coordination of Rho GTPase activities during cell protrusion. *Nature*, 461(7260):99–103, September 2009.

[150] C. S. Izzard and L. R. Lochner. Cell-to-substrate contacts in living fibroblasts: an interference reflexion study with an evaluation of the technique. *Journal of Cell Science*, 21(1):129–159, June 1976.

[151] C. S. Izzard and L. R. Lochner. Formation of cell-to-substrate contacts during fibroblast motility: an interference-reflexion study. *Journal of Cell Science*, 42:81–116, April 1980.

[152] J. Thomas Parsons, Alan Rick Horwitz, and Martin A. Schwartz. Cell adhesion: integrating cytoskeletal dynamics and cellular tension. *Nature Reviews Molecular Cell Biology*, 11(9):633–643, September 2010.

[153] Richard O. Hynes. Integrins. *Cell*, 110(6):673–687, September 2002.

[154] Masatoshi Morimatsu, Armen H. Mekhdjian, Arjun S. Adhikari, and Alexander R. Dunn. Molecular Tension Sensors Report Forces Generated by Single Integrin Molecules in Living Cells. *Nano Letters*, 13(9):3985–3989, September 2013.

[155] Yun Zhang, Chenghao Ge, Cheng Zhu, and Khalid Salaita. DNA-based digital tension probes reveal integrin forces during early cell adhesion. *Nature Communications*, 5:5167, October 2014.

[156] M. Vicente-Manzanares, C. K. Choi, and A. R. Horwitz. Integrins in cell migration - the actin connection. *Journal of Cell Science*, 122(2):199–206, January 2009.

[157] Colin K. Choi, Miguel Vicente-Manzanares, Jessica Zareno, Leanna A. Whitmore, Alex Mogilner, and Alan Rick Horwitz. Actin and -actinin orchestrate the assembly and maturation of nascent adhesions in a myosin II motor-independent manner. *Nature Cell Biology*, 10(9):1039–1050, September 2008.

[158] Ronen Zaidel-Bar, Christoph Ballestrem, Zvi Kam, and Benjamin Geiger. Early molecular events in the assembly of matrix adhesions at the leading edge of migrating cells. *Journal of Cell Science*, 116(Pt 22):4605–4613, November 2003.

[159] Pirta Hotulainen and Pekka Lappalainen. Stress fibers are generated by two distinct actin assembly mechanisms in motile cells. *The Journal of Cell Biology*, 173(3):383–394, May 2006.

[160] Thomas Iskratsch, Cheng-Han Yu, Anurag Mathur, Shuaimin Liu, Virginie Stvenin, Joseph Dwyer, James Hone, Elisabeth Ehler, and Michael Sheetz. FHOD1 Is Needed for Directed Forces and Adhesion Maturation during Cell Spreading and Migration. *Developmental Cell*, 27(5):545–559, December 2013.

[161] L. A. Cary, J. F. Chang, and J. L. Guan. Stimulation of cell migration by overexpression of focal adhesion kinase and its association with Src and Fyn. *Journal of Cell Science*, 109 (Pt 7):1787–1794, July 1996.

[162] Satyajit K. Mitra, Daniel A. Hanson, and David D. Schlaepfer. Focal adhesion kinase: in command and control of cell motility. *Nature Reviews Molecular Cell Biology*, 6(1):56–68, January 2005.

[163] Yvonne Aratyn-Schaus and Margaret L. Gardel. Transient Frictional Slip between Integrin and the ECM in Focal Adhesions under Myosin II Tension. *Current Biology*, 20(13):1145–1153, July 2010.

[164] James I. Lim, Mohsen Sabouri-Ghomi, Matthias Machacek, Clare M. Waterman, and Gaudenz Danuser. Protrusion and actin assembly are coupled to the organization of lamellar contractile structures. *Experimental Cell Research*, 316(13):2027–2041, August 2010.

[165] A. K. Harris. Cell surface movements related to cell locomotion. *Ciba Foundation Symposium*, 14:3–26, 1973.

[166] J. P. Heath. Behaviour and structure of the leading lamella in moving fibroblasts. I. Occurrence and centripetal movement of arc-shaped microfilament bundles beneath the dorsal cell surface. *Journal of Cell Science*, 60:331–354, March 1983.

[167] Patrick W Oakes and Margaret L Gardel. Stressing the limits of focal adhesion mechanosensitivity. *Current Opinion in Cell Biology*, 30:68–73, October 2014.

[168] A. Ponti, M. Machacek, S. L. Gupton, C. M. Waterman-Storer, and G. Danuser. Two distinct actin networks drive the protrusion of migrating cells. *Science (New York, N.Y.)*, 305(5691):1782–1786, September 2004.

[169] Bryan Serrels, Alan Serrels, Valerie G. Brunton, Mark Holt, Gordon W. McLean, Christopher H. Gray, Gareth E. Jones, and Margaret C. Frame. Focal adhesion kinase controls actin assembly via a FERM-mediated interaction with the Arp2/3 complex. *Nature Cell Biology*, 9(9):1046–1056, September 2007.

[170] Patrick W. Oakes, Yvonne Beckham, Jonathan Stricker, and Margaret L. Gardel. Tension is required but not sufficient for focal adhesion maturation without a stress fiber template. *The Journal of Cell Biology*, 196(3):363–374, February 2012.

[171] Nicholas P. J. Brindle, Mark R. Holt, Joanna E Davies, Caroline J Price, and David R. Critchley. The focal-adhesion vasodilator-stimulated phosphoprotein (VASP) binds to the proline-rich domain in vinculin. *Biochemical Journal*, 318(3):753–757, September 1996.

[172] S. L. Gupton, K. Eisenmann, A. S. Alberts, and C. M. Waterman-Storer. mDia2 regulates actin and focal adhesion dynamics and organization in the lamella for efficient epithelial cell migration. *Journal of Cell Science*, 120(19):3475–3487, October 2007.

[173] Lee Dolat, John L. Hunyara, Jonathan R. Bowen, Eva Pauline Karasmanis, Maha Elgawly, Vitold E. Galkin, and Elias T. Spiliotis. Septins promote stress fibermediated maturation of focal adhesions and renal epithelial motility. *The Journal of Cell Biology*, 207(2):225–235, October 2014.

[174] M. Chrzanowska-Wodnicka and K. Burridge. Rho-stimulated contractility drives the formation of stress fibers and focal adhesions. *The Journal of Cell Biology*, 133(6):1403–1415, June 1996.

[175] Benjamin Geiger, Joachim P. Spatz, and Alexander D. Bershadsky. Environmental sensing through focal adhesions. *Nature Reviews Molecular Cell Biology*, 10(1):21–33, January 2009.

[176] Daniel Riveline, Eli Zamir, Nathalie Q. Balaban, Ulrich S. Schwarz, Toshimasa Ishizaki, Shuh Narumiya, Zvi Kam, Benjamin Geiger, and Alexander D. Bershadsky. Focal Contacts as Mechanosensors: Externally Applied Local Mechanical Force Induces Growth

of Focal Contacts by an Mdia1-Dependent and Rock-Independent Mechanism. *The Journal of Cell Biology*, 153(6):1175–1186, June 2001.

[177] Lindsay B. Case and Clare M. Waterman. Integration of actin dynamics and cell adhesion by a three-dimensional, mechanosensitive molecular clutch. *Nature Cell Biology*, June 2015.

[178] Yunfei Cai and Michael P Sheetz. Force propagation across cells: mechanical coherence of dynamic cytoskeletons. *Current Opinion in Cell Biology*, 21(1):47–50, February 2009.

[179] Boon Chuan Low, Catherine Qiurong Pan, G.V. Shivashankar, Alexander Bershadsky, Marius Sudol, and Michael Sheetz. YAP/TAZ as mechanosensors and mechanotransducers in regulating organ size and tumor growth. *FEBS Letters*, 588(16):2663–2670, August 2014.

[180] Beth L. Pruitt, Alexander R. Dunn, William I. Weis, and W. James Nelson. Mechano-Transduction: From Molecules to Tissues. *PLoS Biology*, 12(11):e1001996, November 2014.

[181] M. G. Rubashkin, L. Cassereau, R. Bainer, C. C. DuFort, Y. Yui, G. Ou, M. J. Paszek, M. W. Davidson, Y.-Y. Chen, and V. M. Weaver. Force Engages Vinculin and Promotes Tumor Progression by Enhancing PI3k Activation of Phosphatidylinositol (3,4,5)-Triphosphate. *Cancer Research*, 74(17):4597–4611, September 2014.

[182] Patrick W Oakes, Elizabeth Wagner, Christoph A Brand, Dimitri Probst, Marco Linke, Ulrich S Schwarz, Michael Glotzer, and Margaret L Gardel. Optogenetic Control of RhoA Reveals Zyxin-mediated Elasticity of Stress Fibers. *bioRxiv*, April 2017.

[183] Laura M. Hoffman, Christopher C. Jensen, Susanne Kloeker, C.-L. Albert Wang, Masaaki Yoshigi, and Mary C. Beckerle. Genetic ablation of zyxin causes Mena/VASP mislocalization, increased motility, and deficits in actin remodeling. *The Journal of Cell Biology*, 172(5):771–782, February 2006.

[184] Ingo Thievessen, Peter M. Thompson, Sylvain Berlemont, Karen M. Plevock, Sergey V. Plotnikov, Alice Zemljic-Harpf, Robert S. Ross, Michael W. Davidson, Gaudenz Danuser, Sharon L. Campbell, and Clare M. Waterman. Vinculinactin interaction couples actin retrograde flow to focal adhesions, but is dispensable for focal adhesion growth. *The Journal of Cell Biology*, 202(1):163–177, July 2013.

[185] A. Rahman, S. P. Carey, C. M. Kraning-Rush, Z. E. Goldblatt, F. Bordeleau, M. C. Lampi, D. Y. Lin, A. J. Garcia, and C. A. Reinhart-King. Vinculin regulates directionality and cell polarity in two- and three-dimensional matrix and three-dimensional microtrack migration. *Molecular Biology of the Cell*, 27(9):1431–1441, May 2016.

[186] Edward R. Horton, Jonathan D. Humphries, Ben Stutchbury, Guillaume Jacquemet, Christoph Ballestrem, Simon T. Barry, and Martin J. Humphries. Modulation of FAK and Src adhesion signaling occurs independently of adhesion complex composition. *The Journal of Cell Biology*, 212(3):349–364, February 2016.

[187] Andrew D Doyle, Ryan J Petrie, Matthew L Kutys, and Kenneth M Yamada. Dimensions in cell migration. *Current Opinion in Cell Biology*, 25(5):642–649, October 2013.

[188] Michael F. Olson and Erik Sahai. The actin cytoskeleton in cancer cell motility. *Clinical & Experimental Metastasis*, 26(4):273–287, April 2009.

[189] Stephanie I. Fraley, Yunfeng Feng, Ranjini Krishnamurthy, Dong-Hwee Kim, Alfredo Celedon, Gregory D. Longmore, and Denis Wirtz. A distinctive role for focal adhesion proteins in three-dimensional cell motility. *Nature Cell Biology*, 12(6):598–604, June 2010.

[190] Jill S. Harunaga and Kenneth M. Yamada. Cell-matrix adhesions in 3d. *Matrix Biology*, 30(7-8):363–368, September 2011.

[191] Matthew L. Kutys and Kenneth M. Yamada. An extracellular-matrix-specific GEF-GAP interaction regulates Rho GTPase crosstalk for 3d collagen migration. *Nature Cell Biology*, 16(9):909–917, August 2014.

[192] Andrew D. Doyle, Nicole Carvajal, Albert Jin, Kazue Matsumoto, and Kenneth M. Yamada. Local 3d matrix microenvironment regulates cell migration through spatiotemporal dynamics of contractility-dependent adhesions. *Nature Communications*, 6:8720, November 2015.

[193] KristopherE. Kubow, SarahK. Conrad, and A.Rick Horwitz. Matrix Microarchitecture and Myosin II Determine Adhesion in 3d Matrices. *Current Biology*, 23(17):1607–1619, September 2013.

[194] Andrew D. Doyle, Francis W. Wang, Kazue Matsumoto, and Kenneth M. Yamada. One-dimensional topography underlies three-dimensional fibrillar cell migration. *The Journal of Cell Biology*, 184(4):481–490, February 2009.

[195] Katarina Wolf, Mariska te Lindert, Marina Krause, Stephanie Alexander, Joost te Riet, Amanda L. Willis, Robert M. Hoffman, Carl G. Figdor, Stephen J. Weiss, and Peter Friedl. Physical limits of cell migration: Control by ECM space and nuclear deformation and tuning by proteolysis and traction force. *The Journal of Cell Biology*, 201(7):1069–1084, June 2013.

[196] Erik Sahai and Christopher J. Marshall. Differing modes of tumour cell invasion have distinct requirements for Rho/ROCK signalling and extracellular proteolysis. *Nature Cell Biology*, 5(8):711–719, August 2003.

[197] Victoria Sanz-Moreno, Gilles Gadea, Jessica Ahn, Hugh Paterson, Pierfrancesco Marra, Sophie Pinner, Erik Sahai, and Christopher J. Marshall. Rac Activation and Inactivation Control Plasticity of Tumor Cell Movement. *Cell*, 135(3):510–523, October 2008.

[198] Stacey Lee and Sanjay Kumar. Actomyosin stress fiber mechanosensing in 2d and 3d. *F1000Research*, 5:2261, September 2016.

[199] Peter Friedl and Stephanie Alexander. Cancer Invasion and the Microenvironment: Plasticity and Reciprocity. *Cell*, 147(5):992–1009, November 2011.

[200] J.-F. Lai. Involvement of Focal Adhesion Kinase in Hepatocyte Growth Factor-induced Scatter of Madin-Darby Canine Kidney Cells. *Journal of Biological Chemistry*, 275(11):7474–7480, March 2000.

[201] Wei Yu, Anirban Datta, Pascale Leroy, Lucy Erin O'Brien, Grace Mak, Tzuu-Shuh Jou, Karl S. Matlin, Keith E. Mostov, and Mirjam M. P. Zegers. Beta1-integrin orients epithelial polarity via Rac1 and laminin. *Molecular Biology of the Cell*, 16(2):433–445, February 2005.

[202] Andrew J. Ewald. 3d cell biology the expanding frontier. *Journal of Cell Science*, 130(1):1–1, January 2017.

[203] Wilhelm His. *Unsere Krperform und das physiologische Problem ihrer Enstehung: Briefe an einen Befreundeten Naturforscher*. FCW Vogel, 1874.

[204] E. B. Lewis. A gene complex controlling segmentation in Drosophila. *Nature*, 276(5688):565–570, December 1978.

[205] J. E. Sulston, E. Schierenberg, J. G. White, and J. N. Thomson. The embryonic cell lineage of the nematode Caenorhabditis elegans. *Developmental Biology*, 100(1):64–119, November 1983.

[206] Jayanta Debnath and Joan S. Brugge. Modelling glandular epithelial cancers in three-dimensional cultures. *Nature Reviews Cancer*, 5(9):675–688, September 2005.

[207] Genee Y Lee, Paraic A Kenny, Eva H Lee, and Mina J Bissell. Three-dimensional culture models of normal and malignant breast epithelial cells. *Nature Methods*, 4(4):359–365, April 2007.

[208] Hongmei Yu, Janna Kay Mouw, and Valerie M. Weaver. Forcing form and function: biomechanical regulation of tumor evolution. *Trends in Cell Biology*, 21(1):47–56, January 2011.

[209] Hynda K. Kleinman and George R. Martin. Matrigel: Basement membrane matrix with biological activity. *Seminars in Cancer Biology*, 15(5):378–386, October 2005.

[210] Grace Z. Mak, Gina M. Kavanaugh, Mary M. Buschmann, Shaun M. Stickley, Manuel Koch, Kathleen Heppner Goss, Holly Waechter, Anna Zuk, and Karl S. Matlin. Regulated synthesis and functions of laminin 5 in polarized madin-darby canine kidney epithelial cells. *Molecular Biology of the Cell*, 17(8):3664–3677, August 2006.

[211] D. J. Prockop and K. I. Kivirikko. Collagens: molecular biology, diseases, and potentials for therapy. *Annual Review of Biochemistry*, 64:403–434, 1995.

[212] Christopher B. Raub, Vinod Suresh, Tatiana Krasieva, Julia Lyubovitsky, Justin D. Mih, Andrew J. Putnam, Bruce J. Tromberg, and Steven C. George. Noninvasive assessment of collagen gel microstructure and mechanics using multiphoton microscopy. *Biophysical Journal*, 92(6):2212–2222, March 2007.

[213] Cheuk T. Leung and Joan S. Brugge. Outgrowth of single oncogene-expressing cells from suppressive epithelial environments. *Nature*, 482(7385):410–413, February 2012.

[214] C. A. Schoenenberger, A. Zuk, G. M. Zinkl, D. Kendall, and K. S. Matlin. Integrin expression and localization in normal MDCK cells and transformed MDCK cells lacking apical polarity. *Journal of Cell Science*, 107 (Pt 2):527–541, February 1994.

[215] Matthew J. Paszek, Nastaran Zahir, Kandice R. Johnson, Johnathon N. Lakins, Gabriela I. Rozenberg, Amit Gefen, Cynthia A. Reinhart-King, Susan S. Margulies, Micah Dembo, David Boettiger, Daniel A. Hammer, and Valerie M. Weaver. Tensional homeostasis and the malignant phenotype. *Cancer Cell*, 8(3):241–254, September 2005.

[216] Y. Huang, P. Arora, C. A. McCulloch, and W. F. Vogel. The collagen receptor DDR1 regulates cell spreading and motility by associating with myosin IIA. *Journal of Cell Science*, 122(10):1637–1646, May 2009.

[217] D. J. Stephens. Light Microscopy Techniques for Live Cell Imaging. *Science*, 300(5616):82–86, April 2003.

[218] J. Nunnari, W. F. Marshall, A. Straight, A. Murray, J. W. Sedat, and P. Walter. Mitochondrial transmission during mating in Saccharomyces cerevisiae is determined by mitochondrial fusion and fission and the intramitochondrial segregation of mitochondrial DNA. *Molecular Biology of the Cell*, 8(7):1233–1242, July 1997.

[219] J. Nixon-Abell, C. J. Obara, A. V. Weigel, D. Li, W. R. Legant, C. S. Xu, H. A. Pasolli, K. Harvey, H. F. Hess, E. Betzig, C. Blackstone, and J. Lippincott-Schwartz. Increased spatiotemporal resolution reveals highly dynamic dense tubular matrices in the peripheral ER. *Science*, 354(6311):aaf3928–aaf3928, October 2016.

[220] Michael Weber and Jan Huisken. Light sheet microscopy for real-time developmental biology. *Current Opinion in Genetics & Development*, 21(5):566–572, October 2011.

[221] A. H. Voie, D. H. Burns, and F. A. Spelman. Orthogonal-plane fluorescence optical sectioning: Three-dimensional imaging of macroscopic biological specimens. *Journal of Microscopy*, 170(3):229–236, June 1993.

[222] P. J. Keller and E. H. K. Stelzer. Digital Scanned Laser Light Sheet Fluorescence Microscopy. *Cold Spring Harbor Protocols*, 2010(5):pdb.top78–pdb.top78, May 2010.

[223] M. Roh-Johnson, G. Shemer, C. D. Higgins, J. H. McClellan, A. D. Werts, U. S. Tulu, L. Gao, E. Betzig, D. P. Kiehart, and B. Goldstein. Triggering a Cell Shape Change by Exploiting Preexisting Actomyosin Contractions. *Science*, 335(6073):1232–1235, March 2012.

[224] B.-C. Chen, W. R. Legant, K. Wang, L. Shao, D. E. Milkie, M. W. Davidson, C. Janetopoulos, X. S. Wu, J. A. Hammer, Z. Liu, B. P. English, Y. Mimori-Kiyosue, D. P. Romero, A. T. Ritter, J. Lippincott-Schwartz, L. Fritz-Laylin, R. D. Mullins, D. M. Mitchell, J. N. Bembenek, A.-C. Reymann, R. Bohme, S. W. Grill, J. T. Wang, G. Seydoux, U. S. Tulu, D. P. Kiehart, and E. Betzig. Lattice light-sheet microscopy: Imaging molecules to embryos at high spatiotemporal resolution. *Science*, 346(6208):1257998–1257998, October 2014.

[225] Julia Riedl, Alvaro H Crevenna, Kai Kessenbrock, Jerry Haochen Yu, Dorothee Neukirchen, Michal Bista, Frank Bradke, Dieter Jenne, Tad A Holak, Zena Werb, Michael Sixt, and Roland Wedlich-Soldner. Lifeact: a versatile marker to visualize F-actin. *Nature Methods*, 5(7):605–607, July 2008.

[226] Naomi Courtemanche, Thomas D. Pollard, and Qian Chen. Avoiding artefacts when counting polymerized actin in live cells with LifeAct fused to fluorescent proteins. *Nature Cell Biology*, 18(6):676–683, May 2016.

[227] Paul J Kowalski, Mark A Rubin, and Celina G Kleer. E-cadherin expression in primary carcinomas of the breast and its distant metastases. *Breast Cancer Research*, 5(6), December 2003.

[228] J. J. Christiansen. Reassessing Epithelial to Mesenchymal Transition as a Prerequisite for Carcinoma Invasion and Metastasis. *Cancer Research*, 66(17):8319–8326, September 2006.

[229] Cline Revenu and Darren Gilmour. EMT 2.0: shaping epithelia through collective migration. *Current Opinion in Genetics & Development*, 19(4):338–342, August 2009.

[230] Saori L. Haigo and David Bilder. Global tissue revolutions in a morphogenetic movement controlling elongation. *Science (New York, N.Y.)*, 331(6020):1071–1074, February 2011.

[231] AdamJ. Isabella and Sally Horne-Badovinac. Rab10-Mediated Secretion Synergizes with Tissue Movement to Build a Polarized Basement Membrane Architecture for Organ Morphogenesis. *Developmental Cell*, 38(1):47–60, July 2016.

[232] Syed A. Rizvi, Erin M. Neidt, Jiayue Cui, Zach Feiger, Colleen T. Skau, Margaret L. Gardel, Sergey A. Kozmin, and David R. Kovar. Identification and Characterization of a Small Molecule Inhibitor of Formin-Mediated Actin Assembly. *Chemistry & Biology*, 16(11):1158–1168, November 2009.

[233] Elaine Y. Lin, Joan G. Jones, Ping Li, Liyin Zhu, Kathleen D. Whitney, William J. Muller, and Jeffrey W. Pollard. Progression to Malignancy in the Polyoma Middle T Oncoprotein Mouse Breast Cancer Model Provides a Reliable Model for Human Diseases. *The American Journal of Pathology*, 163(5):2113–2126, November 2003.

[234] Thomas D Pollard. Mechanics of cytokinesis in eukaryotes. *Current Opinion in Cell Biology*, 22(1):50–56, February 2010.

[235] T. Isogai, R. van der Kammen, D. Leyton-Puig, K. M. Kedziora, K. Jalink, and M. Innocenti. Initiation of lamellipodia and ruffles involves cooperation between mDia1 and the Arp2/3 complex. *Journal of Cell Science*, 128(20):3796–3810, October 2015.

[236] Gray W. Pearson and Tony Hunter. Real-time imaging reveals that noninvasive mammary epithelial acini can contain motile cells. *The Journal of Cell Biology*, 179(7):1555–1567, December 2007.

[237] K. Tanner, H. Mori, R. Mroue, A. Bruni-Cardoso, and M. J. Bissell. Coherent angular motion in the establishment of multicellular architecture of glandular tissues. *Proceedings of the National Academy of Sciences*, 109(6):1973–1978, February 2012.

[238] AnaM. Pasapera, SergeyV. Plotnikov, RobertS. Fischer, LindsayB. Case, ThomasT. Egelhoff, and ClareM. Waterman. Rac1-Dependent Phosphorylation and Focal Adhesion Recruitment of Myosin IIA Regulates Migration and Mechanosensing. *Current Biology*, 25(2):175–186, January 2015.

[239] Jeffrey B. Wyckoff, Sophie E. Pinner, Steve Gschmeissner, John S. Condeelis, and Erik Sahai. ROCK- and Myosin-Dependent Matrix Deformation Enables Protease-Independent Tumor-Cell Invasion In Vivo. *Current Biology*, 16(15):1515–1523, August 2006.

[240] A J Ridley, P M Comoglio, and A Hall. Regulation of scatter factor/hepatocyte growth factor responses by Ras, Rac, and Rho in MDCK cells. *Molecular and Cellular Biology*, 15(2):1110–1122, February 1995.

[241] Ronen Zaidel-Bar, R. Milo, Z. Kam, and B. Geiger. A paxillin tyrosine phosphorylation switch regulates the assembly and form of cell-matrix adhesions. *Journal of Cell Science*, 120(1):137–148, December 2006.

[242] D. J. Sieg, C. R. Hauck, D. Ilic, C. K. Klingbeil, E. Schaefer, C. H. Damsky, and D. D. Schlaepfer. FAK integrates growth-factor and integrin signals to promote cell migration. *Nature Cell Biology*, 2(5):249–256, May 2000.

[243] Olivier Collin, Sungsoo Na, Farhan Chowdhury, Michael Hong, Myung Eun Shin, Fei Wang, and Ning Wang. Self-Organized Podosomes Are Dynamic Mechanosensors. *Current Biology*, 18(17):1288–1294, September 2008.

[244] Aron Parekh and Alissa M. Weaver. Regulation of invadopodia by mechanical signaling. *Experimental Cell Research*, 343(1):89–95, April 2016.

[245] F. Lizarraga, R. Poincloux, M. Romao, G. Montagnac, G. Le Dez, I. Bonne, G. Rigaill, G. Raposo, and P. Chavrier. Diaphanous-Related Formins Are Required for Invadopodia Formation and Invasion of Breast Tumor Cells. *Cancer Research*, 69(7):2792–2800, March 2009.

[246] Robert S. Fischer, Margaret Gardel, Xuefei Ma, Robert S. Adelstein, and Clare M. Waterman. Local Cortical Tension by Myosin II Guides 3d Endothelial Cell Branching. *Current Biology*, 19(3):260–265, February 2009.

[247] Carl-Philipp Heisenberg and Yohanns Bellache. Forces in Tissue Morphogenesis and Patterning. *Cell*, 153(5):948–962, May 2013.

[248] Thomas Lecuit and Pierre-Franois Lenne. Cell surface mechanics and the control of cell shape, tissue patterns and morphogenesis. *Nature Reviews Molecular Cell Biology*, 8(8):633–644, August 2007.

[249] Lucy C. Butler, Guy B. Blanchard, Alexandre J. Kabla, Nicola J. Lawrence, David P. Welchman, L. Mahadevan, Richard J. Adams, and Benedicte Sanson. Cell shape changes indicate a role for extrinsic tensile forces in Drosophila germ-band extension. *Nature Cell Biology*, 11(7):859–864, July 2009.

[250] John B Wallingford, Scott E Fraser, and Richard M Harland. Convergent Extension. *Developmental Cell*, 2(6):695–706, June 2002.

[251] Hitoshi Morita, Silvia Grigolon, Martin Bock, S.F. Gabriel Krens, Guillaume Salbreux, and Carl-Philipp Heisenberg. The Physical Basis of Coordinated Tissue Spreading in Zebrafish Gastrulation. *Developmental Cell*, 40(4):354–366.e4, February 2017.

[252] Adam C. Martin, Michael Gelbart, Rodrigo Fernandez-Gonzalez, Matthias Kaschube, and Eric F. Wieschaus. Integration of contractile forces during tissue invagination. *The Journal of Cell Biology*, 188(5):735–749, March 2010.

[253] M. S. Hutson. Forces for Morphogenesis Investigated with Laser Microsurgery and Quantitative Modeling. *Science*, 300(5616):145–149, April 2003.

[254] Otger Camps, Tadanori Mammoto, Sean Hasso, Ralph A Sperling, Daniel O'Connell, Ashley G Bischof, Richard Maas, David A Weitz, L Mahadevan, and Donald E Ingber. Quantifying cell-generated mechanical forces within living embryonic tissues. *Nature Methods*, 11(2):183–189, December 2013.

[255] G. Wayne Brodland. How computational models can help unlock biological systems. *Seminars in Cell & Developmental Biology*, 47-48:62–73, December 2015.

[256] Margaret L. Gardel. Moving beyond molecular mechanisms. *The Journal of Cell Biology*, 208(2):143–145, January 2015.

[257] Dapeng Bi, J. H. Lopez, J. M. Schwarz, and M. Lisa Manning. A density-independent rigidity transition in biological tissues. *Nature Physics*, 11(12):1074–1079, September 2015.

[258] Matthias Merkel and M. Lisa Manning. Using cell deformation and motion to predict forces and collective behavior in morphogenesis. *Seminars in Cell & Developmental Biology*, August 2016.

[259] Karen E Kasza, Amy C Rowat, Jiayu Liu, Thomas E Angelini, Clifford P Brangwynne, Gijsje H Koenderink, and David A Weitz. The cell as a material. *Current Opinion in Cell Biology*, 19(1):101–107, February 2007.

[260] T. E. Angelini, E. Hannezo, X. Trepat, M. Marquez, J. J. Fredberg, and D. A. Weitz. Glass-like dynamics of collective cell migration. *Proceedings of the National Academy of Sciences*, 108(12):4714–4719, March 2011.

[261] D. B. Staple, R. Farhadifar, J.-C. Rper, B. Aigouy, S. Eaton, and F. Jlicher. Mechanics and remodelling of cell packings in epithelia. *The European Physical Journal. E, Soft Matter*, 33(2):117–127, October 2010.

[262] Xavier Trepat, Michael R. Wasserman, Thomas E. Angelini, Emil Millet, David A. Weitz, James P. Butler, and Jeffrey J. Fredberg. Physical forces during collective cell migration. *Nature Physics*, 5(6):426–430, June 2009.

[263] J.-L. Maitre, H. Berthoumieux, S. F. G. Krens, G. Salbreux, F. Julicher, E. Paluch, and C.-P. Heisenberg. Adhesion Functions in Cell Sorting by Mechanically Coupling the Cortices of Adhering Cells. *Science*, 338(6104):253–256, October 2012.

[264] M. Lisa Manning, Ramsey A. Foty, Malcolm S. Steinberg, and Eva-Maria Schoetz. Coaction of intercellular adhesion and cortical tension specifies tissue surface tension. *Proceedings of the National Academy of Sciences*, 107(28):12517–12522, 2010.

[265] Barry M. Gumbiner. Regulation of cadherin-mediated adhesion in morphogenesis. *Nature Reviews Molecular Cell Biology*, 6(8):622–634, July 2005.

[266] Cristina Bertocchi, Yilin Wang, Andrea Ravasio, Yusuke Hara, Yao Wu, Talgat Sailov, Michelle A. Baird, Michael W. Davidson, Ronen Zaidel-Bar, Yusuke Toyama, Benoit Ladoux, Rene-Marc Mege, and Pakorn Kanchanawong. Nanoscale architecture of cadherin-based cell adhesions. *Nature Cell Biology*, 19(1):28–37, December 2016.

[267] Venkat Maruthamuthu, Benedikt Sabass, Ulrich S. Schwarz, and Margaret L. Gardel. Cell-ECM traction force modulates endogenous tension at cellcell contacts. *Proceedings of the National Academy of Sciences*, 108(12):4708–4713, 2011.

[268] M. E. Cates, J. P. Wittmer, J.-P. Bouchaud, and P. Claudin. Jamming, Force Chains, and Fragile Matter. *Physical Review Letters*, 81(9):1841–1844, August 1998.

[269] Jin-Ah Park, Jae Hun Kim, Dapeng Bi, Jennifer A. Mitchel, Nader Taheri Qazvini, Kelan Tantisira, Chan Young Park, Maureen McGill, Sae-Hoon Kim, Bomi Gweon, Jacob Notbohm, Robert Steward Jr, Stephanie Burger, Scott H. Randell, Alvin T. Kho, Dhananjay T. Tambe, Corey Hardin, Stephanie A. Shore, Elliot Israel, David A. Weitz, Daniel J. Tschumperlin, ElizabethP. Henske, Scott T. Weiss, M. Lisa Manning, James P. Butler, Jeffrey M. Drazen, and Jeffrey J. Fredberg. Unjamming and cell shape in the asthmatic airway epithelium. *Nature Materials*, 14(10):1040–1048, August 2015.

[270] Paraic A. Kenny, Genee Y. Lee, Connie A. Myers, Richard M. Neve, Jeremy R. Semeiks, Paul T. Spellman, Katrin Lorenz, Eva H. Lee, Mary Helen Barcellos-Hoff, Ole W. Petersen, Joe W. Gray, and Mina J. Bissell. The morphologies of breast cancer cell lines in three-dimensional assays correlate with their profiles of gene expression. *Molecular Oncology*, 1(1):84–96, June 2007.

[271] Miia Bovellan, Yves Romeo, Mat Biro, Annett Boden, Priyamvada Chugh, Amina Yonis, Malti Vaghela, Marco Fritzsche, Dale Moulding, Richard Thorogate, Antoine Jgou, AdrianJ. Thrasher, Guillaume Romet-Lemonne, PhilippeP. Roux, EwaK. Paluch, and Guillaume Charras. Cellular Control of Cortical Actin Nucleation. *Current Biology*, 24(14):1628–1635, July 2014.

[272] M. Fritzsche, C. Erlenkamper, E. Moeendarbary, G. Charras, and K. Kruse. Actin kinetics shapes cortical network structure and mechanics. *Science Advances*, 2(4):e1501337–e1501337, April 2016.

[273] Bipul R. Acharya, Selwin K. Wu, Zi Zhao Lieu, Robert G. Parton, Stephan W. Grill, Alexander D. Bershadsky, Guillermo A. Gomez, and Alpha S. Yap. Mammalian Diaphanous 1 Mediates a Pathway for E-cadherin to Stabilize Epithelial Barriers through Junctional Contractility. *Cell Reports*, 18(12):2854–2867, March 2017.

[274] Ewa Paluch, Matthieu Piel, Jacques Prost, Michel Bornens, and Ccile Sykes. Cortical Actomyosin Breakage Triggers Shape Oscillations in Cells and Cell Fragments. *Biophysical Journal*, 89(1):724–733, July 2005.

[275] Magdalena Bezanilla, Amy S. Gladfelter, David R. Kovar, and Wei-Lih Lee. Cytoskeletal dynamics: A view from the membrane. *The Journal of Cell Biology*, 209(3):329–337, May 2015.

[276] H. Wang, S. Lacoche, L. Huang, B. Xue, and S. K. Muthuswamy. Rotational motion during three-dimensional morphogenesis of mammary epithelial acini relates to laminin matrix assembly. *Proceedings of the National Academy of Sciences*, 110(1):163–168, January 2013.

[277] G. Wayne Brodland, Jim H. Veldhuis, Steven Kim, Matthew Perrone, David Mashburn, and M. Shane Hutson. CellFIT: A Cellular Force-Inference Toolkit Using Curvilinear Cell Boundaries. *PLoS ONE*, 9(6):e99116, June 2014.

[278] Alexis J. Lomakin, Kun-Chun Lee, Sangyoon J. Han, Duyen A. Bui, Michael Davidson, Alex Mogilner, and Gaudenz Danuser. Competition for actin between two distinct F-actin networks defines a bistable switch for cell polarization. *Nature Cell Biology*, 17(11):1435–1445, September 2015.

[279] Heather A. Long, Veronika Boczonadi, Lorna McInroy, Martin Goldberg, and Arto Mtt. Periplakin-dependent re-organisation of keratin cytoskeleton and loss of collective migration in keratin-8-downregulated epithelial sheets. *Journal of Cell Science*, 119(Pt 24):5147–5159, December 2006.

[280] Kari L. Weber and William M. Bement. F-actin serves as a template for cytokeratin organization in cell free extracts. *Journal of Cell Science*, 115(Pt 7):1373–1382, April 2002.

[281] M. Bergert, S. D. Chandradoss, R. A. Desai, and E. Paluch. Cell mechanics control rapid transitions between blebs and lamellipodia during migration. *Proceedings of the National Academy of Sciences*, 109(36):14434–14439, September 2012.

[282] Guillaume Salbreux, Guillaume Charras, and Ewa Paluch. Actin cortex mechanics and cellular morphogenesis. *Trends in Cell Biology*, 22(10):536–545, October 2012.

[283] Pieta K. Mattila, Facundo D. Batista, and Bebhinn Treanor. Dynamics of the actin cytoskeleton mediates receptor cross talk: An emerging concept in tuning receptor signaling. *The Journal of Cell Biology*, 212(3):267–280, February 2016.

[284] Roshni Basu, Benjamin M. Whitlock, Julien Husson, Audrey Le Floch, Weiyang Jin, Alon Oyler-Yaniv, Farokh Dotiwala, Gregory Giannone, Claire Hivroz, Nicolas Biais, Judy Lieberman, Lance C. Kam, and Morgan Huse. Cytotoxic T Cells Use Mechanical Force to Potentiate Target Cell Killing. *Cell*, 165(1):100–110, March 2016.

[285] Ramin Nazarian, Hubing Shi, Qi Wang, Xiangju Kong, Richard C. Koya, Hane Lee, Zugen Chen, Mi-Kyung Lee, Narsis Attar, Hooman Sazegar, Thinle Chodon, Stanley F. Nelson, Grant McArthur, Jeffrey A. Sosman, Antoni Ribas, and Roger S. Lo. Melanomas acquire resistance to B-RAF(V600e) inhibition by RTK or N-RAS upregulation. *Nature*, 468(7326):973–977, November 2010.

[286] Mark Shackleton, Franois Vaillant, Kaylene J. Simpson, John Stingl, Gordon K. Smyth, Marie-Liesse Asselin-Labat, Li Wu, Geoffrey J. Lindeman, and Jane E. Visvader. Generation of a functional mammary gland from a single stem cell. *Nature*, 439(7072):84–88, January 2006.

[287] Vinay Prasad. Perspective: The precision-oncology illusion. *Nature*, 537(7619):S63–S63, September 2016.

[288] Bo Huang, Mark Bates, and Xiaowei Zhuang. Super-Resolution Fluorescence Microscopy. *Annual Review of Biochemistry*, 78(1):993–1016, June 2009.

[289] Juha Kononen, Lukas Bubendorf, Anne Kallionimeni, Maarit Brlund, Peter Schraml, Stephen Leighton, Joachim Torhorst, Michael J Mihatsch, Guido Sauter, and Olli-P. Kallionimeni. Tissue microarrays for high-throughput molecular profiling of tumor specimens. *Nature Medicine*, 4(7):844–847, July 1998.

[290] John J. Tentler, Aik Choon Tan, Colin D. Weekes, Antonio Jimeno, Stephen Leong, Todd M. Pitts, John J. Arcaroli, Wells A. Messersmith, and S. Gail Eckhardt. Patient-derived tumour xenografts as models for oncology drug development. *Nature Reviews Clinical Oncology*, 9(6):338–350, April 2012.

[291] George E. Palade. An Electron Microscopy Study of the Mitochondrial Structure. *Journal of Histochemistry & Cytochemistry*, 1(4):188–211, July 1953.